In-plane dynamics of high-speed rotating rings on elastic foundation

Lu, T.

DOI
10.4233/uuid:77784d7c-8f01-4222-bb83-87ee1de52930

Publication date
2019

Document Version
Final published version

Citation (APA)
Lu, T. (2019). *In-plane dynamics of high-speed rotating rings on elastic foundation*. [Dissertation (TU Delft), Delft University of Technology]. https://doi.org/10.4233/uuid:77784d7c-8f01-4222-bb83-87ee1de52930

IN-PLANE DYNAMICS OF HIGH-SPEED ROTATING RINGS ON ELASTIC FOUNDATION

IN-PLANE DYNAMICS OF HIGH-SPEED ROTATING RINGS ON ELASTIC FOUNDATION

Proefschrift

ter verkrijging van de graad van doctor
aan de Technische Universiteit Delft,
op gezag van de Rector Magnificus prof. dr. ir. T.H.J.J. van der Hagen,
voorzitter van het College voor Promoties,
in het openbaar te verdedigen op dinsdag 29 oktober 2019 om 10.00 uur

door

Tao LU

Bachelor of Engineering in Civil Engineering, Beijing Jiaotong University, China
geboren te Sichuan, China.

Dit proefschrift is goedgekeurd door de promotoren.

Samenstelling promotiecommissie:

Rector Magnificus,	voorzitter
Prof. dr. A.V. Metrikine,	Technische Universiteit Delft, promotor
Dr. ir. A. Tsouvalas,	Technische Universiteit Delft, copromotor
Onafhankelijke leden:	
Prof. dr. H. Ouyang,	University of Liverpool, United Kingdom
Prof. dr. E. Carrera,	Politecnico di Torino, Italy
Prof. dr. ing. T. Mazilu,	Universitatea Politehnica din București, Romania
Prof. dr. ir. A.R.M. Wolfert,	Technische Universiteit Delft
Dr. ir. W.T. van Horssen,	Technische Universiteit Delft

Keywords: high-speed, rotating rings, elastic foundation, in-plane vibration, stability, high-order theory, traction boundary effects, critical speeds, steady-state response, ring-oscillator system

Printed by: Gildeprint

Cover design: Zahid Hossain

ISBN 978-94-6323-850-2

An electronic version of this dissertation is available at
http://repository.tudelft.nl/.

CONTENTS

SUMMARY

Rotating ring-like structures are very commonly used in civil, mechanical and aerospace engineering. Typical examples of such structures are components in turbomachinery, compliant gears, rolling tyres and flexible train wheels. At the micro-scale, rotating ring models find their applications in the field of ring gyroscopes, in which high accuracy of modelling is required. The in-plane vibrations of rotating rings are of particular interest since such structural components are usually subject to in-plane loads. The focus in this thesis is therefore placed on the in-plane dynamics of rotating rings.

While the radial and circumferential motions of a stationary ring are coupled due to curvature, a steadily rotating ring, as any gyroscopic system, is subject to two additional fictitious forces induced by the gyroscopic coupling due to rotation, i.e. the Coriolis and centrifugal forces. Among them the centrifugal force associated with the steady rotation of the ring (quasi-static force) introduces an axi-symmetric radial expansion and a hoop stress; the latter has the tendency to stiffen the ring. In contrast, the dynamic part of the centrifugal force has the tendency to soften the system. Next to that, the Coriolis force bifurcates the natural frequencies of the ring. The proper consideration of the rotation effects is essential to determine the dynamic behaviour of rotating rings, such as stability of free vibrations and resonance of rotating rings under stationary loads.

Although various models exist, the considerations of rotation effects are not always in agreement, resulting in distinct theoretical predictions of critical speeds associated with instability and resonance of rotating rings. In addition, in all the existing rotating ring models, the equations of motion were derived assuming the inner and outer surfaces of the ring to be traction-free. However, when one considers a ring whose inner surface is elastically restrained by distributed springs, this assumption is violated. The traction at the inner surface can significantly influence the stress distribution along the thickness of the ring and this effect has to be properly accounted for since the internal stresses may show a strong gradient from the inner surface to the outer surface, especially in the case of rings rotating at high speeds or when the latter are supported by stiff foundation.

The primary aim of this thesis is to develop a highly accurate rotating ring model that properly accounts for both the rotation and boundary effects with rigorous mathematical derivation to fill the gap regarding the modelling and prediction of the dynamic behaviour of high-speed rotating rings. To achieve this aim, the following four objectives are set: (i) identify the reasons of disagreements between various existing rotating ring models and clarify the mathematically sound derivations of governing equations; (ii) develop a high-order rotating ring model which properly accounts for the rotation effects, as well as the non-zero tractions at boundaries; (iii) close the debate on the prediction of critical speeds associated with instability of free vibrations and resonance of forced vibrations; and (iv) apply the developed high-order model to predict the steady-state response of rotating rings under stationary loads and the stability of rotating ring-stationary oscillator system.

With regard to the first objective, the most widely used existing rotating thin ring models are reviewed, covering aspects of the derivation procedure, assumptions upon which different models are based and the geometrical nonlinearity. The consequences of the employment of different derivation procedures, assumptions and geometrical nonlinearities are analysed in terms of the resulting governing equations and predictions of the dynamic behaviour. The reasonable mathematical treatment of obtaining governing equations is pointed out. The analysis of the existing models serves a dual purpose. First, it results at a comprehensive source of reference for existing rotating thin ring models. Second, it highlights limitations of existing thin ring models in application to high speed rotating rings; an analysis which is essential for the establishment of the new ring model in this thesis.

Based on the analysis above, a new rotating ring model is developed which properly accounts for the rotation and the boundary effects. The new model overcomes the deficiencies of previously developed models and expands the range of applicability to high speeds of rotation and stiff foundation. To take the rotation effects into account, geometrical nonlinear governing equations are first derived and the static equilibrium is obtained accordingly. To consider the tractions at boundaries and the through-thickness variation of the internal stresses, nonlinear through-thickness displacement distributions are introduced both in the radial and the circumferential directions. The accuracy of the developed model can be adjusted by choosing different orders of the displacement polynomials. Furthermore, the model can deal with both plane strain and plane stress configurations. The developed high-order model (upon linearisation) is verified by comparing the frequency spectra predicted by the proposed model with those resulting from linear elasticity for the corresponding stationary ring case. It is shown that the model is superior to all existing classical thin ring models and the Timoshenko-type ring model.

Regarding the third objective, the existence of critical speeds for rotating rings, namely the one corresponding to the onset of instability and the one associated with resonances of a rotating ring subjected to a stationary constant load, is investigated using the developed model. In most known to the author papers, instability of free vibration of a rotating ring is not mentioned, or the in-plane vibrations of a rotating thin ring are reported to be stable. In contrast, instability of free in-plane vibrations of high-speed rotating rings is predicted in this study. It is shown that the divergence instability of mode $n = 0$ always occurs at a lower rotational speed than those correspond to instability of higher order modes. Contrary to the most commonly used Endo-Huang-Soedel model, results in this thesis show the existence of resonance of the rotating ring subject to a stationary load of constant magnitude. This resonance occurs only for a specific range of the ring parameters.

With respect to the fourth objective, the steady-state response of a rotating ring subjected to a constant stationary load is investigated using the developed high-order model which confirms the existence of resonance speeds. A wave-like stationary deformation pattern occurs in a rotating ring under a stationary load when the ring rotates at speeds higher than the minimum resonance speed. The predictions are theoretical and further experimental confirmation of the predictions is needed. Finally, the stability of vibrations of a stationary oscillator in contact with a rotating ring is studied. Such a ring-oscillator system can be used to model the contact problems between flexible train

wheel and railway track, calenders of paper machines, etc.. The ring-oscillator system is shown to be unstable for certain system parameters when the ring rotates at speeds higher than the minimum resonance speed. However, the vibration of the stationary oscillator-rotating ring system is always stable if the ring is rotating sub-critically.

SAMENVATTING

Roterende ringachtige structuren worden vaak gebruikt in de civiele techniek, werktuigbouwkunde en in de lucht- en ruimtevaart. Voorbeelden van dergelijke structuren zijn componenten in turbomachines, rollende banden, en flexibele tand- en treinwielen. Op de microschaal vinden roterende ringmodellen hun toepassingen op het gebied van ringgyroscopen, wat een hoge accuraatheid vereist qua modellering. De trillingen in het vlak van roterende ringen zijn van bijzonder belang, omdat dergelijke structurele componenten gewoonlijk onderhevig zijn aan belastingen in het vlak. De focus in dit proefschrift ligt daarom op het dynamisch gedrag van roterende ringen in het vlak.

Terwijl de radiale en circumferentiële bewegingen van een stationaire ring zijn gekoppeld vanwege kromming, is een gestaag roterende ring, zoals elk gyroscopisch systeem, onderhevig aan twee fictieve krachten geïnduceerd door de rotatie, namelijk Coriolis en centrifugale krachten. De centrifugale kracht die is geassocieerd met de gelijkmatige rotatie van de ring (quasi-statische kracht) introduceert een axi-symmetrische radiale uitzetting en een ringspanning, welke de de neiging heeft om de ring te verstijven. Daarentegen heeft het dynamische deel van de centrifugale kracht de neiging om het systeem te verzachten. Daarnaast veroorzaakt de Coriolis-kracht een bifurcatie van de natuurlijke frequenties van de ring. Rotatie-effecten zijn essentieel om het dynamische gedrag van roterende ringen te bepalen, zoals de stabiliteit van vrije trillingen en resonantie van roterende ringen onder stationaire belastingen.

Hoewel er verschillende modellen bestaan, zijn de aannames qua rotatie-effecten niet altijd in overeenstemming, wat resulteert in verschillende theoretische voorspellingen van kritische snelheden die samenhangen met instabiliteit en resonantie van roterende ringen. Bovendien zijn in alle bestaande roterende ringmodellen de bewegingsvergelijkingen afgeleid ervan uitgaande dat de binnen- en buitenoppervlakken van de ring tractievrij zijn. Wanneer men echter een ring beschouwt waarvan het binnenoppervlak elastisch wordt tegengehouden door verdeelde veren, wordt deze aanname geschonden. De tractie aan het binnenoppervlak kan de spanningsverdeling over de dikte van de ring aanzienlijk beïnvloeden en moet meegenomen worden omdat de inwendige spanningen een sterke gradiënt van het binnenoppervlak naar het buitenoppervlak kunnen vertonen, vooral in het geval van ringen die draaien op hoge snelheden of wanneer deze worden ondersteund door een stijve fundering.

Het primaire doel van dit proefschrift is om een zeer nauwkeurig roterend ringmodel te ontwikkelen dat rekening houdt met zowel de rotatie- als de effecten van de randvoorwaarden met rigoureuze mathematische afleiding om de opening te vullen met betrekking tot de modellering en voorspelling van het dynamische gedrag van roterende ringen met hoge snelheid. Om dit doel te bereiken, worden de volgende vier doelen vastgesteld: (i) identificeren van de redenen van meningsverschillen tussen verschillende bestaande roterende ringmodellen en verduidelijken van de wiskundig afleidingen van bestaande vergelijkingen; (ii) een rotatie-ringmodel van hoge orde ontwikkelen dat op

de juiste wijze rekening houdt met de rotatie-effecten, evenals de niet-nul-tracties bij de randen; (iii) het debat afsluiten over de voorspelling van kritische snelheden die samenhangen met de instabiliteit van vrije trillingen en resonantie van geforceerde trillingen; en (iv) het ontwikkelde hoge orde model toepassen om de stationaire respons van roterende ringen onder stationaire belastingen en de stabiliteit van roterend ring-stationair oscillatorsysteem te voorspellen.

Met betrekking tot de eerste doelstelling worden de meest gebruikte bestaande roterende dunne-ringsmodellen besproken, waarbij wordt gelet op de afleidingsprocedure, de veronderstellingen waarop verschillende modellen zijn gebaseerd en de geometrische niet-lineariteit. De consequenties van het gebruik van verschillende afleidingsprocedures, aannames en geometrische niet-lineariteiten worden geanalyseerd op de resulterende vergelijkingen en de voorspellingen van het dynamische gedrag. De wiskundige behandeling om de vergelijkende vergelijkingen te verkrijgen, wordt aangegeven. De analyse van de bestaande modellen dient een tweeledig doel. Ten eerste resulteert het in een uitgebreide referentiebron voor bestaande roterende dunne ringmodellen. Ten tweede benadrukt het beperkingen van bestaande dunne ringmodellen toegepast op roterende ringen met hoge snelheid; een analyse die essentieel is voor het vaststellen van het nieuwe ringmodel in dit proefschrift.

Op basis van de bovenstaande analyse is een nieuw roterend ringmodel ontwikkeld dat de rotatie en de effecten van de randvoorwaarden goed verwerkt. Het nieuwe model verbetert de tekortkomingen van eerder ontwikkelde modellen en breidt het bereik van toepasbaarheid tot hoge snelheden van rotatie en stijve fundering uit. Om rekening te houden met de rotatie-effecten, worden eerst geometrische niet-lineaire vergelijkingen afgeleid en wordt het statische evenwicht verkregen. Om de tracties bij de randen en de verdeling van de inwendige spanningen over de dikte van de ring te beschouwen, worden niet-lineaire verdelingen over de dikte van de verplaatsen geïntroduceerd in zowel de radiale als in de omtreksrichtingen. De nauwkeurigheid van het ontwikkelde model kan worden aangepast door verschillende volgordes van de verplaatsingspolynomen te kiezen. Bovendien kan het model zowel plane strain en plane stress configuraties aan. Het ontwikkelde hoogorde-model wordt, na linearisatie, geverifieerd door de frequentiespectra te vergelijken met die welke resulteren uit lineaire elasticiteit voor het overeenkomstige stationaire ringbehuizing. Het is aangetoond dat het model superieur is aan alle bestaande klassieke dunne ringmodellen en het ringmodel van het Timoshenko-type.

Met betrekking tot het derde doel, wordt het bestaan van kritieke snelheden voor roterende ringen, namelijk degene die corresponderen met het begin van instabiliteit en degene die geassocieerd zijn met resonanties van een roterende ring onderworpen aan een stationaire constante belasting, onderzocht met behulp van het ontwikkelde model. In de meest documenten waarmee de auteur bekend is, wordt de instabiliteit van de vrije trilling van een roterende ring niet genoemd, of worden geconstateerd dat de trillingen in het vlak van een draaiende dunne ring stabiel zijn. Daarentegen wordt instabiliteit van vrije trillingen in het vlak van roterende ringen met hoge snelheid wel voorspeld in deze studie. Er wordt aangetoond dat de divergentie-instabiliteit van modus $n = 0$ altijd optreedt bij een lagere rotatiesnelheid dan die correspondeert met instabiliteit van hogere orde modi. In tegenstelling tot het meest gebruikte Endo-Huang-Soedel-model,

laten de resultaten van dit proefschrift het bestaan zien van resonantie van de roterende ring afhankelijk van een stationaire belasting van constante grootte. Deze resonantie treedt alleen op voor een specifiek bereik van de parameters van de ring.

Met betrekking tot het vierde objectief wordt de stationaire respons van een roterende ring onderworpen aan een constante stationaire belasting onderzocht met behulp van het ontwikkelde hoogordermodel dat het bestaan van resonantiesnelheden bevestigt. Een golfachtig stationair vervormingspatroon treedt op in een roterende ring onder een stationaire belasting wanneer de ring roteert met snelheden hoger dan de minimale resonantiesnelheid. De voorspellingen zijn theoretisch en verdere experimentele bevestiging van de voorspellingen is nodig. Tenslotte wordt de stabiliteit van trillingen van een stationaire oscillator in contact met een roterende ring bestudeerd. Een dergelijk ring-oscillatorsysteem kan worden gebruikt om de contactproblemen tussen flexibel treinwiel en spoor, kalenders van papiermachines, enz. te modelleren. Het ringoscillatorsysteem is onstabiel gebleken voor bepaalde systeemparameters wanneer de ring draait met snelheden hoger dan de minimale resonantiesnelheid. De trilling van het stationaire oscillator-roterende ringsysteem is echter altijd stabiel als de ring subkritisch roteert.

1

INTRODUCTION

1.1. BACKGROUND AND MOTIVATION

Ring-like structures are very commonly used in civil, mechanical and aerospace engineering. An excellent review by Chidamparam and Leissa on vibrations of rings can be found in [1]. Because of the broad applications in engineering, rotating rings have attracted much attention since the first study by Bryan [2] in 1890 who investigated the dynamics of a rotating wine glass. The studies on the rotating ring dynamics thrived in the field of tyre research approximately half a century ago when such models were widely used to describe the in-plane vibrations of the pneumatic tyres. A comprehensive overview of the early studies devoted to rotating thin rings in application to rolling tyres can be found in [3]. Instead of describing the sidewall of the tyre in detail, the support from the sidewall and inflation is roughly treated as an elastic foundation. Consequently, analytical expressions for natural frequencies can be obtained for a rotating thin ring. The research on tyres using rotating rings is still ongoing despite the availability of detailed finite element models due to the ability of rotating thin ring models to determine the vibrational characteristics of tyres in a fast and reasonably accurate manner [4]. Besides the conventional pneumatic tyres, the major tyre manufacturers are developing the so-called "airless tyre" which can be modelled as a rotating ring as well [5]. One example is the Michelin TWEEL that is shown in Fig. 1.1(a). At the micro scale, rotating ring models find their applications in the field of ring gyroscopes [6] (Fig. 1.1(b)). Other applications of rotating rings include flywheel storage systems [7], flexible train wheels [8], compliant gears [9], and energy harvesting devices [10], to name only a few.

The vibration of rotating rings is a classic problem in solid mechanics. The radial and circumferential motions of a stationary ring are coupled due to curvature. Rotating rings are additionally subject to gyroscopic coupling due to rotation. In Figure 1.2(a), the accelerations of a point P on a rotating ring are shown. The ring shown in this figure rotates at an angular speed Ω and is resting on an elastic foundation (distributed springs) with radial stiffness k_r and circumferential stiffness k_c. The distributed springs are connected to an immovable hub. The radial and circumferential displacements are denoted

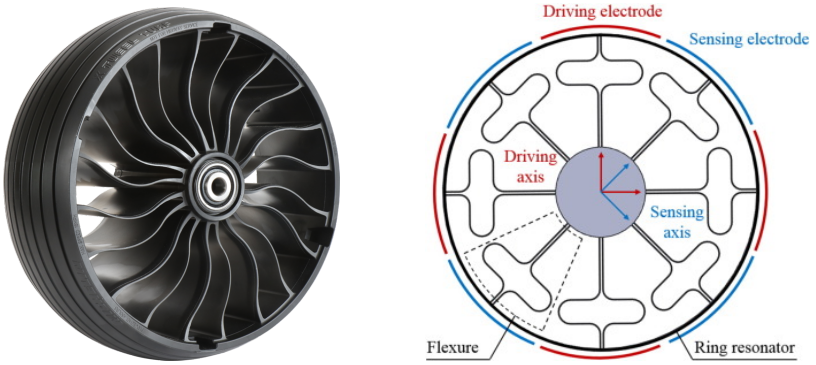

Figure 1.1: (a) Michelin TWEEL; (b) A ring gyroscope [6].

as w and u respectively, whereas r is the radial position of a point on the ring. Taking the radial direction as an example, as shown in Figure 1.2(a), an arbitrary point P on the ring experiences vibrational acceleration $\ddot{w}$, Coriolis acceleration $2\Omega\dot{w}$ and centripetal acceleration $(r+w)\Omega^2$ simultaneously. The same holds in the circumferential direction. The centripetal acceleration generally causes a softening effect on the ring. Meanwhile, the uniform centrifugal force along the ring caused by rotation induces an axi-symmetric radial expansion of the ring (Figure 1.2(b)) and consequently results in hoop stress in the ring. The hoop stress has a stiffening effect on the ring. The spin-softening associated with the centripetal acceleration and the stress-stiffening effect due to the tensile hoop stress all increase with the speed of rotation.

Interesting dynamic phenomena exhibited by the rotating rings are related to the Coriolis and centrifugal forces and the hoop tension caused by rotation. The Coriolis and centrifugal forces were considered in most of the earlier studies on the rotating rings. The effect of the tensile hoop stress caused by rotation was addressed less frequently [11, 12]. The likely reason for this is that in order to capture this effect a relatively sophisticated nonlinear strain-displacement relation needs to be employed. Endo et al. [13] derived equations of motion for a rotating thin ring accounting for the pretension (the static component of the tensile hoop stresses) due to rotation. Experiments were conducted to verify the model predictions and comparisons were made between the model in [13] and other existing models in the literature. It was shown that the pretension must not be overlooked since it influences the ring dynamics significantly. Huang and Soedel [14] presented essentially the same model and systematically analysed the free and forced vibrations of rotating thin rings and shells on elastic foundation [14–16] accounting for the ring extensibility. It is rarely mentioned by researchers, except in [17, 18], that the Endo-Huang-Soedel model gives an erroneous result when the steady-state response of the ring is considered to a stationary constant load. The result is that the response is independent of the speed of rotation in the absence of damping. This erroneous result is a consequence of the chosen strain-displacement relation and of the applied linearisation procedure, which led to a so-called cancellation of rotation effect. The latter implies that the Coriolis and centrifugal forces totally neutralise the pretension effect in this model. Obviously, this result calls for a critical review of the Endo-Huang-

Soedel model. It is interesting to mention that in the late monograph [19] by Soedel, the pretension is neglected.

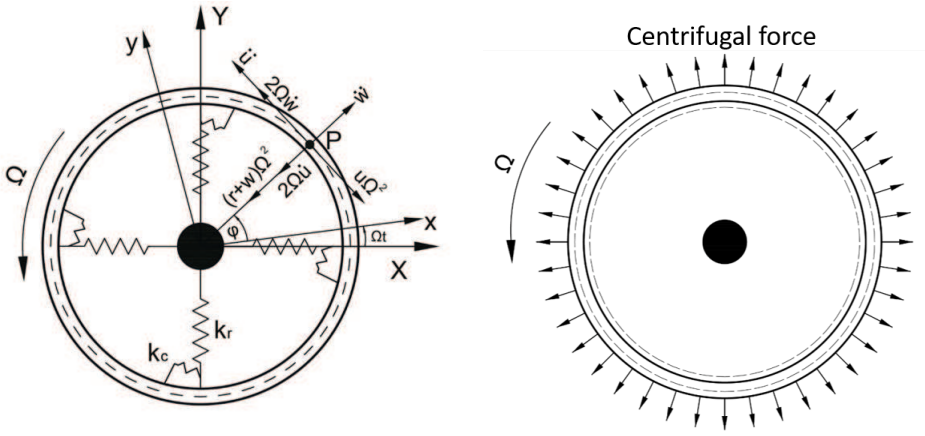

Figure 1.2: (a): Accelerations of a point on a rotating ring on elastic foundation; (b) Ring expansion due to rotation.

Several other studies exist, in which the effect of pretension on the dynamics of rings was addressed. In the early 1990s, Gong [20] developed a rotating thin ring model for pneumatic tyres in which the engineering nonlinear strain was employed to capture the pretension. Kim and Bolton [21] derived a model for rotating shells in which the term representing the pretension is similar to that of a tensioned beam resulting from the implementation of the Donnell's nonlinear shell theory. This model was modified to a rotating ring model by neglecting the axial displacement to study the dynamics of rolling tyres by Saeedi [22]. It must be realised though that the expressions for the rotation-associated pretension used in the aforementioned papers are approximate and do not account for the centrifugal force associated with the radial expansion of the ring due to rotation. The latter force is indeed negligible at relatively low rotation speeds. However, it should be taken into account when the dynamics of the rings rotating at high speeds is focused upon.

To accurately derive the static equilibrium of a ring rotating at a high speed the geometrically nonlinear equations of motion have to be formulated first. This was first accomplished by Zadoks and Krousgrill [23] who used the nonlinear strain-displacement relation given by Stein [24]. Later, Kim and Chung [25] considered the effect of different strain-displacement relations on the free, small-amplitude vibration of the ring about the static equilibrium. Elastic foundation was not included in their model and the rigid-body modes were not studied. Subsequently, Cooley and Parker [9] derived new governing equations applicable to the rings rotating at high speeds to study the dynamics of compliant gears. The method of derivation was similar to that of Kim and Chung [25], however, the static equilibrium and the linearised equations of motion were different because of the different nonlinear strain-displacement relations employed in their paper. Using the same model, Cooley and Parker [26] investigated the influence of the inextensibility assumption on the in-plane vibrations of rotating rings, and concluded

that this assumption “works poorly at high rotation speeds". Recently, the model in [9] is further improved by Ding et al. [27] in which the transverse shear and rotary inertia are included. They concluded that the Timoshenko-type theory is necessary for analysing the free vibrations of rotating rings.

In the literature, numerous studies focus on free vibrations of rotating rings [7, 9, 14, 17, 18, 20, 21, 25, 27–33]. A simple formula for predicting the in-plane flexural natural frequencies of rotating rings is proposed in [34]. Due to the existence of the Coriolis force, the characteristic equation of a rotating ring is a general polynomial of frequency with non-zero coefficients. As a consequence, the backward and forward travelling waves have different frequencies even for the same mode number and the same type of motion (e.g. the bending dominant backward and forward traveling waves of mode n have different frequencies for a rotating ring, but they have same frequencies for a stationary ring). Modal analysis is widely employed to investigate the free vibrations of rotating rings. Meanwhile, other techniques, such as the wave method [32] and spectral element method [33] are also used to investigate free vibrations. The forced vibrations are emphasized in [11, 12, 14, 15, 20, 35, 36] using classical mode superposition, except [37], in which the authors employed a new modal analysis method proposed by Meirovitch in [38, 39] for linear gyroscopic systems to obtain the transient response of a rotating ring subjected to a point excitation.

Most studies on rotating rings in the literature deal with thin rings, which utilise the Euler-Bernoulli hypothesis. Rotating thick rings are studied by various authors [7, 17, 27, 29, 36] by employing improvement analogous to that proposed by Timoshenko for straight beams. One can also be referred to a dissertation dedicated to vibrations of rotating thick rings by Lin [40]. The in-plane motions of rings attract more attention, nonetheless there is no lack of interest for the study of the out-of-plane vibrations, e.g. in [7, 25, 30, 41–43]. Nonlinear vibrations of rotating rings are studied in [44–50]. Other relevant studies regarding varying spin speeds, parametric instability of a rotating ring with moving springs, rotating rings under internal or external pressure, influences of properties of radial supports and size-dependent dynamic behaviour of rotating micro-rings can be found in [51–57].

Although various models exist, the theoretical predictions of critical speeds of rotating rings are in striking disagreement. There are two kinds of critical speeds of interest in the case of a rotating ring. One corresponds to the instability of the divergence or flutter type (the corresponding ring displacements increase exponentially when applying a set of initial conditions) [58], whereas the other one corresponds to resonances of a rotating ring subjected to a stationary load of constant magnitude. To the author’s knowledge, the onset of instability was not properly addressed in the scientific literature prior to a recent publication [58] in which the existence of divergence instability of high-speed rotating ring is thoroughly addressed. Recently, instability of a similar type is theoretically predicted in magnetically levitated rotating rings by Arena and Lacarbonara [59]. The condition of resonance of a stationary ring subject to a uniformly moving load is well-known [60, 61]. In contrast, the existence of resonances in the reciprocal problem, namely in a rotating ring subject to a stationary load of constant magnitude, is still debated. The most commonly used Endo-Huang-Soedel model [13–15] does not predict resonance for a rotating ring subjected to a constant stationary load. Lin and Soedel [17, 18] ar-

gued that the incapability of predicting resonance speeds is due to the employment of the Green-Lagrange strain-displacement relation, which causes cancellation of rotation effects. The resonance speeds were investigated including shear deformation and rotatory inertia by Lin and Soedel [18]. However the linearisation procedure adopted in [18] is discussable. A most recent contribution to the discussion on the existence of resonance speeds can be found in [62–64].

In all the aforementioned studies, the equations of motion were derived assuming the inner and outer surfaces of the ring to be traction-free, regardless of whether the types of models used, i.e. classical lower order theories [9, 13, 14] or improved Timoshenko-type theories [27, 29]. However, when one considers a ring whose inner surface is elastically restrained by distributed springs, this assumption is violated. The traction at the inner surface can significantly influence the stress distribution in the ring and affect its dynamics. The stress effects at the boundaries are especially important in the case of rings rotating at high speeds and supported by stiff foundation.

1.2. AIM AND SCOPE

THIS study presents a theoretical investigation into the in-plane dynamics of rotating rings resting on elastic foundation (distributed springs) using new high-order theories. The first goal of this thesis is to develop a high-order model which can account for the tractions at the boundaries, which are comparable in magnitude with the internal stresses, and for the through-thickness variation of stresses. The models available in the literature, e.g. [9, 13, 14, 18, 20, 27], which only include the low-order terms in the description of the through-thickness stress variation cannot deal with the boundary effects in question. This goal is achieved by introducing nonlinear displacement distributions along the thickness of the ring. The influence of stresses at the inner and outer surfaces (boundaries) on the internal stresses in the ring is investigated. The lower order theories are first reviewed and limitations thereof are pointed out. The developed high-order model (upon linearisation) is verified by comparing the frequency spectra predicted by the proposed model with those resulting from linear elasticity for the corresponding stationary ring case. It is shown that the model, as expected, is superior to the existing classical thin ring models [9, 14] and the Timoshenko-type ring model [27].

The second goal of this thesis is to study the existence of critical speeds for rotating rings, namely the one corresponding to the onset of instability of a rotating ring and the one associated with resonances of a rotating ring subjected to a stationary constant load. In most known to the author papers, instability of free vibration of a rotating ring is not mentioned, or the in-plane vibrations of a rotating thin ring are reported to be stable [13]. In several studies, the occurrence of instability is associated with the velocity at which the natural frequency of a specific mode becomes zero [65, 66]. However, this conclusion is debatable; it is questionable whether this situation will lead to the exponential increase of the ring displacement upon application of a set of initial conditions. Instability of free in-plane vibrations of high-speed rotating rings is predicted in this study. Contrary to the most commonly used Endo-Huang-Soedel model [13–15], results in this thesis do show the existence of resonance of the rotating ring subject to

a stationary load of constant magnitude, as well as instability of free vibrations. This conclusion is based on rigorous analysis and is considered as a novel contribution of this study. The existence of resonance speeds is further confirmed by investigating the steady-state response of a rotating ring subjected to a constant stationary load.

The third goal is to determine the stability of vibrations of a stationary oscillator in relative motion with a rotating ring. This issue has not been investigated earlier even thought it is of practical importance, e.g. for compliant gears.

1.3. OUTLINE

MODES of and wave dispersion in thin rings are reviewed in Chapter 2 for both stationary and rotating rings using classical thin ring theory in which the motions of a ring are uniquely described by the radial and circumferential displacements of the middle surface of the ring. The influence of an elastic foundation is addressed. The differences between various existing rotating thin ring models and the reasons resulting in these differences are clarified. The assumptions and simplifications employed before and during derivations of governing equations are pointed out. The consequences of these assumptions and simplifications are examined. The review provides a comprehensive source of reference to existing classical rotating ring models covering derivation procedures, assumptions and simplifications, as well as geometrically nonlinearity.

A first attempt to develop a rotating thin ring model which accounts for the through-thickness variation of the radial stress is described in Chapter 3. Nonlinear equations of motion, which account for geometrical nonlinearity, are first derived. Linearisation of the nonlinear equations is conducted to obtain the linear equations which govern small vibrations about the static equilibrium. Non-zero tractions at the inner and outer surfaces are imposed. These considerations significantly change the theoretical predictions compared to existing models, especially when the ring rests on stiff foundation or when it rotates at high speeds. Using this model, stability of in-plane free vibration is revisited, and divergence instability is found. The influence of various ring parameters on the instability is investigated.

A more general high-order rotating ring model, which allows one to consider properly the effects of tractions on the ring surfaces, as well as through-thickness variation of stresses is developed in Chapter 4. Using the high-order model proposed in Chapter 4, the critical speeds of a rotating ring are investigated in Chapter 5. Two types of critical speeds are discussed. One is the speed after which instability of free vibrations occurs and the other is resonance speed of a rotating ring subjected to a stationary load of constant magnitude. To address the effect of higher order corrections and through-thickness variation of stresses on critical speeds, predictions of the proposed model are compared with those obtained using the other existing models. The resonance speed of a rotating ring and its inverted problem, namely the case of a circumferentially moving constant load on a stationary ring are compared in Chapter 5.

Chapter 6 deals with the steady-state response of a rotating ring on an elastic foundation subjected to a constant stationary point load implementing the high-order rotating ring model developed in Chapter 4. Wave-like steady-state responses are predicted, and

the existence of resonances (resonance speeds) is confirmed. The dynamic response of a rotating ring subjected to a harmonic load is analysed as well.

In Chapter 7, the stability of a stationary oscillator interacting with a rotating ring is studied. It is found that the vibration of the oscillator can become unstable when the ring rotates super-critically.

Finally, Chapter 8 summarises the main conclusions of the thesis and gives suggestions for future studies.

2

CLASSICAL THEORY OF THIN RINGS AND ITS LIMITATIONS

Rings can be considered as curved beams or cylindrical shells without the longitudinal dimension. Regarding thin rings, only the radial and circumferential displacements at the middle surface of the ring are retained. In this chapter, modes and wave dispersion are reviewed for both stationary and rotating thin rings. The classical low order theories are employed since thin rings are discussed in this chapter. Apart from the purpose of reviewing, this chapter aims to extend understanding of the effect of an elastic foundation on both stationary and rotating thin rings. The significant influence on the ring dynamics of the adopted nonlinear strain-displacement relations is also addressed with examples to raise awareness about this seldom discussed effect. The most widely used existing rotating thin ring models are discussed, covering the derivation procedure, assumptions, geometrical nonlinearity, limitations of the models, etc. Thus, this chapter serves a dual purpose. First, it is a comprehensive source of reference for existing rotating thin ring models. Second, it highlights limitations of existing thin ring models in application to high speed rotating rings.

In this chapter, modes and wave dispersion of stationary rings are first reviewed in section 2.1 whereas a review of rotating rings follows in section 2.2. The differences between various existing rotating ring models are discussed in section 2.2 with the focus on the derivation procedures and the adopted assumptions. In section 2.3, applicability and limitations of the classical low order models for both stationary and rotating rings are addressed. Conclusions are drawn in section 2.4.

2.1. REVIEWS OF STATIONARY THIN RING MODELS

In this section, modes and wave dispersion of stationary rings are discussed based on the classical thin ring theory.

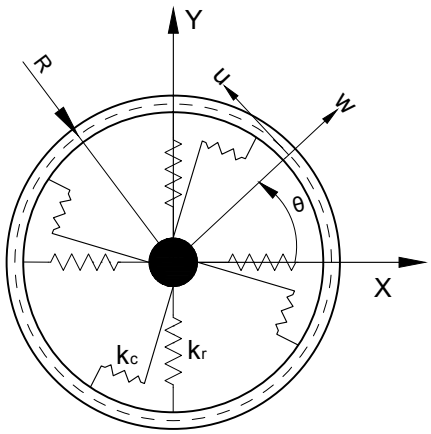

Figure 2.1: A thin ring on an elastic foundation

2.1.1. MODES OF STATIONARY THIN RINGS

In Fig. 2.1 the side view is shown of a thin ring resting on an elastic foundation (distributed springs). It is assumed that the mean radius of the ring is R and r is the radial coordinate. The radial and circumferential displacements of the middle surface of the ring with respect to the undeformed configuration are designated by $w(\theta,t)$ and $u(\theta,t)$, respectively. The stiffnesses of the radial and circumferential springs per unit length are designated as k_r and k_c (unit N/m^2), respectively. Furthermore, ρ is the mass density of the ring, E is the Young's modulus, A is the cross-sectional area and I is the cross-sectional moment of inertia.

In the literature, the thin ring models are based on Love's thin shell theory [19]. Only the displacements at the middle surface are considered, namely

$$\begin{aligned} w(r,\theta,t) &= w(\theta,t), \\ u(r,\theta,t) &= u(\theta,t) + \frac{(r-R)}{R}\left((u(\theta,t) - \frac{\partial w(\theta,t)}{\partial\theta}\right). \end{aligned} \tag{2.1}$$

The classical equations of motion of a stationary thin ring on elastic foundation read [19, 60]:

$$\begin{aligned} \rho A\ddot{w} + \frac{EI}{R^4}(w'''' - u''') + \frac{EA}{R^2}(w+u') + k_r w = 0, \\ \rho A\ddot{u} + \frac{EI}{R^4}(w''' - u'') - \frac{EA}{R^2}(w'+u'') + k_c u = 0, \end{aligned} \tag{2.2}$$

in which the prime stands for the partial derivative with respect to a circumferential coordinate θ and the overdot represents time derivative. Due to periodicity in the circumferential direction θ, the following solution is assumed to obtain the mode shapes:

$$w(\theta,t) = C_{wn}\cos\left(n(\theta-\theta^*)\right)e^{i\omega_n t},\ u(\theta,t) = C_{un}\sin\left(n(\theta-\theta^*)\right)e^{i\omega_n t} \tag{2.3}$$

where i is the imaginary unit. θ^* is an arbitrary phase angle that signifies the fact that the ring does not show a preference for the orientation of its modes [19]. By substituting Eq. (2.3) into the governing equations (2.2), one obtains

$$\begin{bmatrix} L_{11} & L_{12} \\ L_{21} & L_{22} \end{bmatrix} \begin{bmatrix} C_{wn} \\ C_{un} \end{bmatrix} = \mathbf{0} \tag{2.4}$$

where

$$\begin{aligned} L_{11} &= \frac{EIn^4}{R^4} + \frac{EA}{R^2} + k_r - \rho A {\omega_n}^2,\ L_{12} = (\frac{EIn^3}{R^4} + \frac{EAn}{R^2}) \\ L_{21} &= L_{12},\ L_{22} = \frac{EIn^2}{R^4} + \frac{EAn^2}{R^2} + k_c - \rho A {\omega_n}^2. \end{aligned} \tag{2.5}$$

For a nontrivial solution, the determinant of the coefficient matrix must be set to zero. Thus, the frequency equation is [19]:

$${\omega_n}^4 - K_1 {\omega_n}^2 + K_2 = 0 \tag{2.6}$$

where

$$\begin{aligned} K_1 &= \frac{n^2+1}{\rho A R^2}\Big(\frac{n^2 EI}{R^2} + EA\Big) + \frac{k_r + k_c}{\rho A}, \\ K_2 &= \frac{n^2(n^2-1)^2}{\rho^2 A^2 R^6} EAEI + \frac{k_r k_c + k_r (n^2 E/R^2)(I/R^2 + A) + k_c E/R^2 (n^4 I/R^2 + A)}{\rho^2 A^2}. \end{aligned} \tag{2.7}$$

The two sets of natural frequencies are obtained as

$$\omega_{n1}^2 = \frac{K_1}{2}\Big(1 - \sqrt{1 - 4\frac{K_2}{{K_1}^2}}\Big),\ \omega_{n2}^2 = \frac{K_1}{2}\Big(1 + \sqrt{1 - 4\frac{K_2}{{K_1}^2}}\Big) \tag{2.8}$$

Generally, the lower natural frequency set ω_{n1} corresponds the bending-dominated modes whereas the higher natural frequency set ω_{n2} is associated with predominantly tangential (extentional) motions[19]. Substituting the obtained natural frequencies back to Eq. (2.4), the mode shapes can be expressed as ($j = 1, 2$)

$$\begin{aligned} \frac{C_{wnj}}{C_{unj}} &= \frac{(n/R^2)(EIn^2/R^2 + EA)}{\rho A \omega_{nj}^2 - k_r - (1/R^2)(EIn^4/R^2 + EA)} \\ &= \frac{\rho A \omega_{nj}^2 - k_c - (n^2/R^2)(EI/R^2 + EA)}{(n/R^2)(EIn^2/R^2 + EA)} \end{aligned} \tag{2.9}$$

For modes $n \geq 1$, the ring vibrates in a flexural-extensional manner. The radial and circumferential motions are coupled due to curvature. The mode shapes are shown in Figs. 2.2-2.3 up to mode number $n = 4$.

Special attention needs to be paid to the $n = 0$ modes. When $n = 0$, the natural frequencies become:

$$\omega_{01} = \sqrt{k_c/(\rho A)},\ \omega_{02} = \sqrt{EA/(\rho A R^2) + k_r/(\rho A)}. \tag{2.10}$$

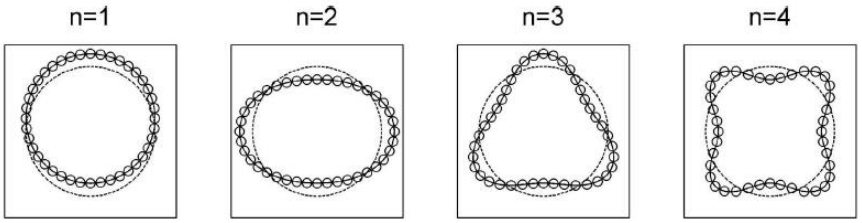

Figure 2.2: Bending-dominated mode shapes of a ring on elastic foundation * [67].

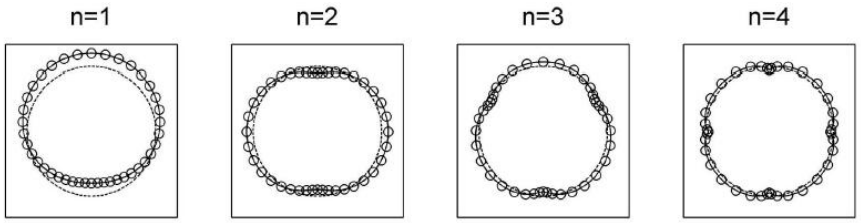

Figure 2.3: Extention-dominated mode shapes of a ring on elastic foundation [67].

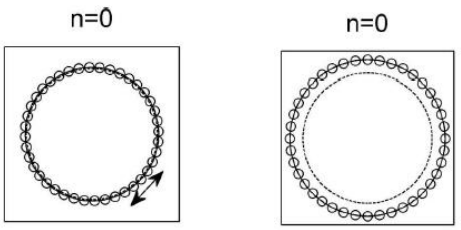

Figure 2.4: $n = 0$ modes of a ring on elastic foundation [67].

The radial and circumferential motions of $n = 0$ modes are decoupled. At ω_{01}, the ring shows only circumferential motions. This vibration mode is called rotational mode in [20]. For ω_{02}, the ring expands and contracts radially. If one considers a free-floating ring without an elastic foundation, the $n = 0$ mode with zero frequency corresponds to a rigid body rotation. The other $n = 0$ is the breathing mode in which the ring vibrates at the so-called "ring frequency" $\sqrt{EA/(\rho AR^2)}$ [68–70]. The ring frequency is also the cut-off frequency of the ring, above which the extensional modes are excited. At $n = 1$ for a free-floating ring, one of the frequencies (ω_{11}) is zero once $k_r = k_c = 0$ and the ring translates as a rigid body. The non-zero ω_{12} corresponds to a mode in which one compression and one tension regions exist around the ring.

*Note that for the mode $n = 1$ shown in Fig. 2.2 the ring translates as an almost perfectly rigid structure with a slight elastic deformation.

2.1.2. WAVE DISPERSIONS IN STATIONARY THIN RINGS

This subsection discusses the wave dispersion in stationary thin rings. The influences of foundation on wave dispersions are thoroughly discussed.

For convenience, the following dimensionless parameters are introduced [71]

$$\begin{aligned} &k=\sqrt{EI/EA},\ \tau=c_0 t/k,\ \bar{\omega}=\omega k/c_0,\ \bar{\theta}=\theta/\bar{k},\ W=w/R,\ U=u/R,\\ &\bar{k}=k/R,\ \bar{\gamma}=k\gamma,\ \bar{c}=c/c_0,\ (\bar{k}_r,\bar{k}_c)=(k_r,k_c)k^2/(EA) \end{aligned} \tag{2.11}$$

where $c_0=\sqrt{E/\rho}$ is the compressional wave speed in a thin straight bar made of the same material. The mode number n is expressed by

$$n=R\gamma=\bar{\gamma}/\bar{k} \tag{2.12}$$

where γ is the wavenumber.

Substitution of Eq. (2.11) into Eq. (2.2) yields:

$$\begin{aligned} &W_{\tau\tau}+W_{\bar{\theta}\bar{\theta}\bar{\theta}\bar{\theta}}-\bar{k}U_{\bar{\theta}\bar{\theta}\bar{\theta}}+\bar{k}^2W+\bar{k}U_{\bar{\theta}}+\bar{k}_rW=0,\\ &U_{\tau\tau}+\bar{k}W_{\bar{\theta}\bar{\theta}\bar{\theta}}-\bar{k}^2U_{\bar{\theta}\bar{\theta}}-\bar{k}W_{\bar{\theta}}-U_{\bar{\theta}\bar{\theta}}+\bar{k}_cU=0. \end{aligned} \tag{2.13}$$

The corresponding frequency equation in terms of dimensionless parameters reads:

$$(\bar{\omega}^2-\bar{k}^2-\bar{\gamma}^4-\bar{k}_r)(\bar{\omega}^2-\bar{\gamma}^2-\bar{k}^2\bar{\gamma}^2-\bar{k}_c)-\bar{k}^2\bar{\gamma}^2(\bar{\gamma}^2+1)^2=0 \tag{2.14}$$

Substitution of $\bar{\omega}=\bar{\gamma}\bar{c}$ into the above equation yields the dispersion relation:

$$(\bar{\gamma}^2\bar{c}^2-\bar{k}^2-\bar{\gamma}^4-\bar{k}_r)(\bar{\gamma}^2\bar{c}^2-\bar{\gamma}^2-\bar{k}^2\bar{\gamma}^2-\bar{k}_c)-\bar{k}^2\bar{\gamma}^2(\bar{\gamma}^2+1)^2=0. \tag{2.15}$$

Its corresponding straight case is obtained by setting $\bar{k}=0$ and $R\to+\infty$

$$\underbrace{(\bar{\omega}^2-\bar{\gamma}^4-\bar{k}_r)}_{\text{beam}}\underbrace{(\bar{\omega}^2-\bar{\gamma}^2-\bar{k}_c)}_{\text{rod}}=0. \tag{2.16}$$

The curvature coupling disappears and the dispersion relation stands for decoupled longitudinal vibration of a rod and bending vibration of an Euler-Bernoulli beam.

WAVE DISPERSION OF THIN RINGS WITHOUT ELASTIC FOUNDATION

In Fig. 2.5, the dispersion curves and phase speeds of the stationary ring without foundation are plotted. The solid lines are the dispersion curves for the ring (Eq. 2.15) and the dashed lines are those for the corresponding straight extensible beam (Eq. 2.16). Figs. 2.5(a)(b) correspond to the case $\bar{k}^2=0.05$ in [71]. (This value suggests a thick ring; it is chosen to demonstrate wave characteristics in lower wavenumber regions.) Figs. 2.5(c)(d) correspond to $\bar{k}^2=0.00083$ ($h/R=0.1$). Zero phase speed occurs at $\bar{\gamma}=\bar{k}$, which corresponds to a wavelength equal to the length of the circumference [71]. In terms of modes, $\bar{\gamma}=\bar{k}$ means that $n=1$, which corresponds to translational rigid body mode. The thinner the ring, the closer the dispersion curve of the ring to the dispersion curve of the corresponding straight extensible beam.

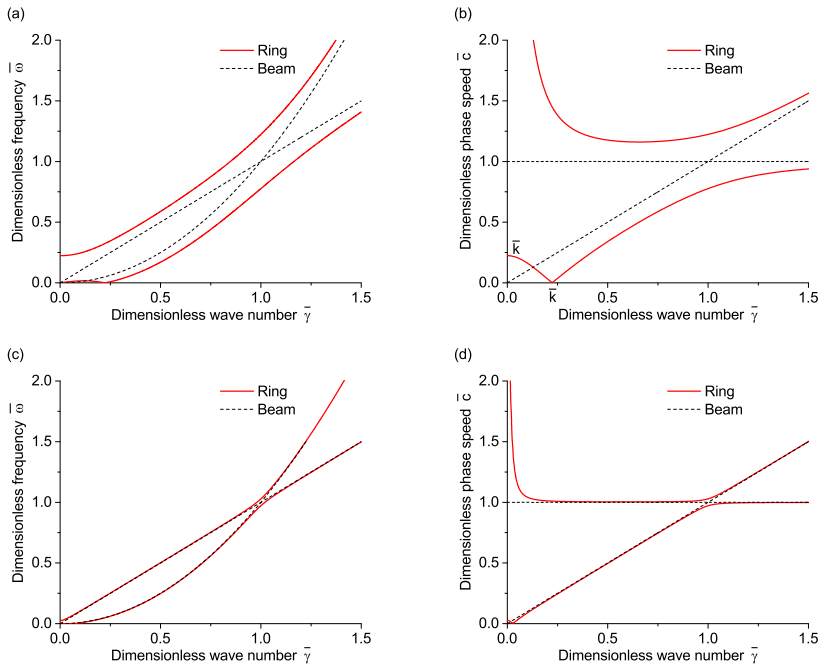

Figure 2.5: Dispersion curves of rings and corresponding extensible beams without foundation ($\bar{k}_r = \bar{k}_c = 0$): (a)(b) are reproductions of [71] with $\bar{k}^2 = 0.05$; (c)(d) correspond to $h/R = 0.1$.

There is a transition $\bar{\gamma} \approx 1$ at which the bending modes and the extensional modes interchange their eigenfunctions with increasing wavenumber as shown in Fig. 2.5. It is very much like the frequency veering; however, the varying parameter here is the wavenumber. The phenomena of veering, locking and strong coupling effects are comprehensively discussed in [72]. Frequency veering of two frequencies happens for a weakly coupled system when the stiffnesses corresponding to each frequency are almost equal [72, 73]. For a stationary ring without foundation ($\bar{k}_r = \bar{k}_c = 0$), the bending stiffness is $EIn^4/(R^4)$, whereas the extensional stiffness is $EAn^2/(R^2)$. It is clear that for small n, the bending stiffness is lower than the extensional one. With increasing n, $EIn^4/(R^4)$ exceeds $EAn^2/(R^2)$ and frequency veers when

$$\frac{EIn^4}{R^4} \approx \frac{EAn^2}{R^2}, \tag{2.17}$$

namely

$$n = R\gamma = R\sqrt{\frac{EA}{EI}}, \tag{2.18}$$

which corresponds to $\bar{\gamma} = 1$ in the wavenumber-frequency domain. The frequency at $\bar{\gamma} = 1$ is about $\bar{\omega} = 1$; it is called the cross-over frequency in the literature [74]. Note that this frequency is quite high. One is referred to [68, 69, 74] for more details on dispersion relations of a ring/curved beam.

Attention needs to be paid to the low-frequency limit, namely to the case of $\bar{\gamma} \to 0$. At this limit, the phase velocity of the lower branch in Fig 2.5(b)(d) is not infinite but tends to a finite value. Factoring $\bar{\gamma}^2$ in Eq. (2.15), results in

$$\left(\left(-\bar{c}^2+1\right)\bar{\gamma}^4+\left(\bar{c}^2\left(-\bar{k}^2+\bar{c}^2-1\right)-2\,\bar{k}^2\right)\bar{\gamma}^2+\left(-\bar{k}^2\left(-\bar{k}^2+\bar{c}^2-1\right)-\bar{k}^2\right)\right)\bar{\gamma}^2=0. \tag{2.19}$$

For small values of $\bar{\gamma}$ the above equation reduces to

$$\left(-\bar{k}^2\left(-\bar{k}^2+\bar{c}^2-1\right)-\bar{k}^2\right)=0, \tag{2.20}$$

solving the above equation for $\bar{c}$, one obtains

$$\bar{c}=\bar{k}, \tag{2.21}$$

which is the phase velocity of the lower branch when $\bar{\gamma}\approx 0$ as shown in Fig 2.5(b)(d).

WAVE DISPERSION OF THIN RINGS WITH ELASTIC FOUNDATION

In the presence of an elastic foundation, both the lower and higher cut-off frequencies are not zero. Fig. 2.6 shows the change of phase velocities with increasing stiffness of radial springs of the foundation. There are two branches for each combination of foundation stiffnesses, representing the bending dominant and extension dominant motions. Fig. 2.6(a) shows that when the stiffness of tangential springs is zero, one phase speed of the two waves is bounded at $\bar{\gamma}=0$ whereas the other is infinite. However, if $k_c \neq 0$, the wave speeds of both waves are infinite when $\bar{\gamma}=0$ as shown in Fig. 2.6(b). The minimum phase speed increases with increasing stiffness of the radial springs. For lower stiffness values of the radial springs, the phase speeds of the extension-dominated motion are larger than the ones of the bending-dominated motions. After a certain value of stiffness of the radial springs, the phase speeds change qualitatively. The bending-dominated motions can have higher wave speeds. The existence of elastic foundation and the magnitude of its stiffness can significantly change the wave dispersion characteristics both qualitatively and quantitatively.

To provide an insight into the influence of the stiffnesses of the foundation on the wave dispersion of the system, the curvature coupling is neglected temporarily. In this case, the total stiffness in the radial direction will be

$$K_r = k_r + \frac{EIn^4}{R^4} \tag{2.22}$$

whereas in the circumferential direction it will be

$$K_c = k_c + \frac{EAn^2}{R^2} \tag{2.23}$$

according to Eq. (2.5). Let us introduce the relative stiffness difference K_d between the radial and circumferential directions:

$$K_d(n) = K_r - K_c = k_r + \frac{EIn^4}{R^4} - k_c - \frac{EAn^2}{R^2} \tag{2.24}$$

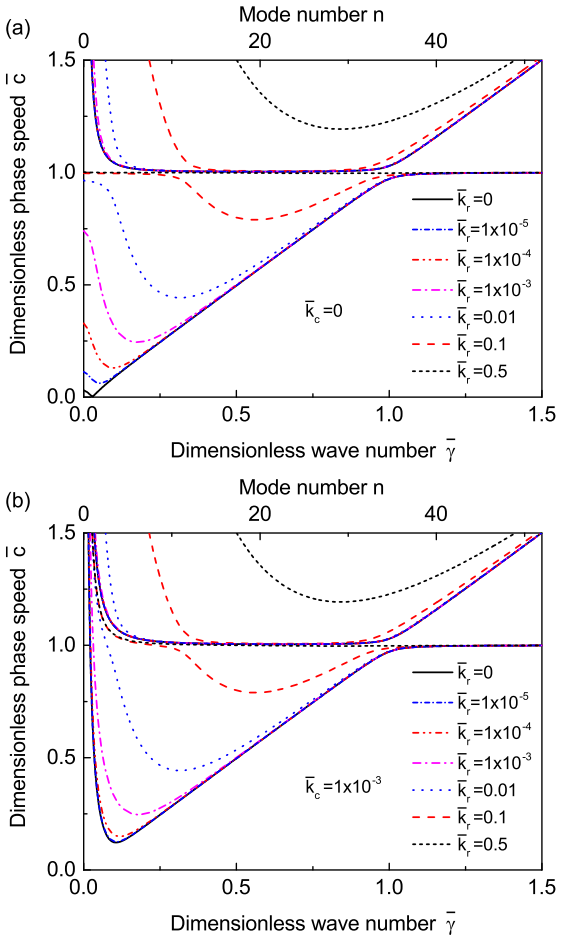

Figure 2.6: Phase speeds change for different foundation stiffness, $h/R = 0.1$, classical thin ring theory: (a) $\bar{k}_c = 0$; (b) $\bar{k}_c = 1 \times 10^{-3}$. In each figure, the branches with local minima represent the bending-dominated motions whereas the branches converging to $\bar{c} = 1$ are related to the extension-dominated motions.

From Eq. (2.24), one can conclude that if the stiffnesses of the springs are large enough, the contribution of n is small, namely the terms EIn^4 and EAn^2 are relatively small in comparison with k_r and k_c. Thus the natural frequencies (or wave characteristics) are dominated by the properties of the elastic foundation and not by the elastic properties of the ring. Considering K_d as a function of n, the minimum of K_d can be found at

$$n = R\sqrt{\frac{EA}{2EI}}. \tag{2.25}$$

For convenience, the dimensionless form of Eq. (2.24) is used, which is

$$\bar{K}_d(\bar{\gamma}) = \bar{k}_r + \bar{\gamma}^4 - \bar{k}_c - \bar{\gamma}^2. \tag{2.26}$$

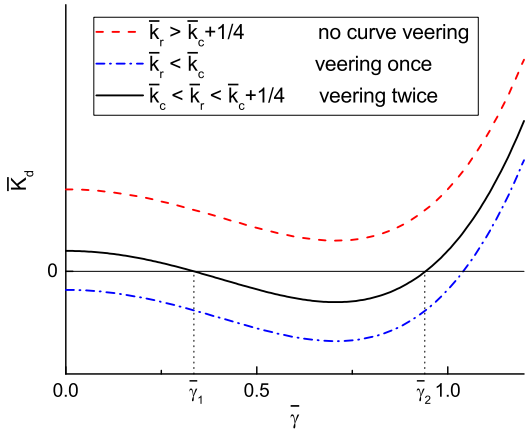

Figure 2.7: Difference between stiffnesses in the radial and circumferential directions versus the wavenumber.

It can be derived from Eq. (2.26) that the minima of $\bar{K}_d$ occurs when $\bar{\gamma} = \sqrt{2}/2$, namely

$$\bar{K}_{d_{\min}} = \bar{K}_d(\sqrt{2}/2). \tag{2.27}$$

There are three cases to be distinguished based on the relative values of the foundation stiffnesses and the elastic properties of the ring.

- Case 1: $\bar{k}_r > \bar{k}_c + \frac{1}{4} \Longleftrightarrow k_r > k_c + \frac{(EA)^2}{4EI}$

  Suppose $\bar{K}_d$ is larger than zero for all wavenumbers, in this case, it is expected that the natural frequencies of the bending-dominated motions are higher than those of the extensional motions. This corresponds to the red dashed line in Fig. 2.7. The phase speeds and wave spectra shown in Fig. 2.8(a)(b) belong to this category. The letters “B" and “E" represent bending-dominated waves and extension-dominated waves, respectively. The frequencies of bending-dominated motions are higher than those of the extensional motions (Fig. 2.8(a)). Meanwhile, the phase speeds of extension-dominated waves are lower than those of bending-dominated waves (Fig. 2.8(b)). The minimum phase speed approaches $\sqrt{E/\rho}$ at high wavenumbers.

- Case 2: $\bar{k}_c < \bar{k}_r < \bar{k}_c + \frac{1}{4} \Longleftrightarrow k_c < k_r < k_c + \frac{(EA)^2}{4EI}$

  This case corresponds to the black solid line in Fig. 2.7. For this combination of parameters, the total radial stiffness for small wavenumbers is larger than the total circumferential stiffness, meaning that the natural frequencies of bending-dominated motions are larger than the extension-dominated motions. There is an interval $\bar{\gamma} \in \{\bar{\gamma}_1, \bar{\gamma}_2\}$ of wavenumbers(or mode numbers) that the natural frequencies of the extensional motions are larger. With increasing wavenumber, the frequencies of bending-dominated motions become larger again. One can conclude

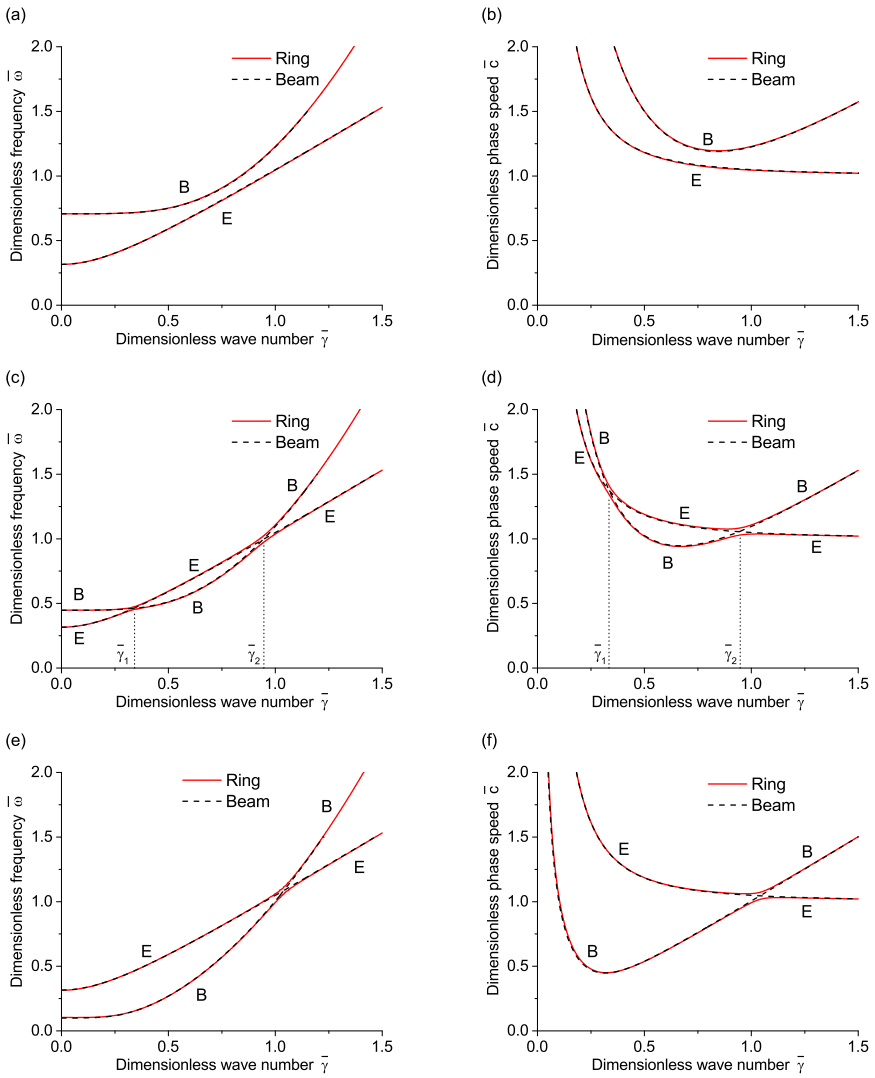

Figure 2.8: Dispersion curves of rings and corresponding extensible beams with foundation $\bar{k}_c = 0.1$, $h/R = 0.1$ for the ring: (a)(b) $\bar{k}_r = 0.5$; (c)(d) $\bar{k}_r = 0.2$; (e)(f) $\bar{k}_r = 0.01$.

that the bending and extension-dominated motions change their eigenfunctions twice with increasing mode number. The wavenumbers at which the frequencies veer can be obtained by solving $\bar{K}_d(\bar{\gamma}) = 0$ for $\bar{\gamma}$, which gives

$$\bar{\gamma}_1 = \sqrt{1/2 - 1/2\sqrt{1 + 4\bar{k}_c - 4\bar{k}_r}},\ \bar{\gamma}_2 = \sqrt{1/2 + 1/2\sqrt{1 + 4\bar{k}_c - 4\bar{k}_r}}. \tag{2.28}$$

The phase speeds and wave spectra plotted in Fig. 2.8(c)(d) fall into this group. In

the range $\bar{\gamma}_1 < \bar{\gamma} < \bar{\gamma}_2$, the frequencies and phase speeds of extensional waves are larger than those of bending waves. However, outside of this range, the frequencies and phase speeds of bending waves are higher. In addition, it can be checked that the minimum phase speed $\bar{c}_{\min}$ of a rotating ring whose parameters fall into this group is almost equal to the minimum phase speed $\sqrt[4]{4k_r EI/(\rho A)^2}$ [60, 75] of the corresponding straight extensible beam. In other words,

$$\bar{c}_{\min} = \sqrt[4]{4k_r EI/(\rho A)^2}/c_0 = \sqrt[4]{4\bar{k}_r}. \tag{2.29}$$

- Case 3: $0 < \bar{k}_r < \bar{k}_c \Longleftrightarrow 0 < k_r < k_c$

  When $\bar{k}_r < \bar{k}_c$, the natural frequencies veer once at about $\bar{\gamma} \approx 1$. The lower branch changes from bending-dominated motion to extension-dominated motion and the higher branch from extensional to bending-dominated motion as shown in Fig. 2.8(e). Fig. 2.8(f) shows the phase speeds versus wavenumbers in this case. Most of the engineering applications fall into this category. Moreover, the minimum phase speed of the ring can be approximated by Eq. (2.29) the same to case 2.

For special case in which

$$\bar{k}_r = \bar{k}_c + \frac{1}{4}, \tag{2.30}$$

the minimum phase speed of the bending-dominated motion is equal to the longitudinal wave speed $\sqrt{E/\rho}$. When $\bar{k}_r = \bar{k}_c$, it means that $n = 1$ translational mode is a perfectly rigid body translation even when the foundation is included. When $\bar{k}_r = \bar{k}_c$, the mode number (wavenumber) corresponding to eigenfunction interchange is the same as in the case of rings without foundation and is expressed by Eq. (2.18).

Once again, from Fig. 2.8 it can be concluded that the coupling through curvature is weak since the wave spectra and phase speeds of rings are close to their associated straight beam cases (the dotted lines in Fig. 2.8 as also suggested in Fig. 2.5 previously.).

2.2. REVIEWS OF ROTATING THIN RING MODELS

In this section, derivations of governing equations for rotating thin rings are first examined. Various resulting models are discussed with emphasis on differences of simplifications, assumptions and consequences of these differences. Subsequently, wave dispersion and modes of vibration of rotating rings are reviewed using the classical thin ring model adopted from [9]. This model is believed to be the most appropriate as it is developed with the help of a rigorous mathematical treatment as will be shown later.

2.2.1. GOVERNING EQUATIONS OF ROTATING THIN RINGS

Numerous rotating thin ring models can be found in the literature. In general, their governing equations are obtained using the Hamilton's principle:

$$\delta \int_{t_1}^{t_2} (S + V - T)\,\mathrm{d}t = \int_{t_1}^{t_2} (\delta S + \delta V - \delta T)\,\mathrm{d}t = 0 \tag{2.31}$$

in which S is the strain energy, V is the potential energy stored by the foundation and T is the kinetic energy.

To obtain the governing equations, the kinetic energy of the ring and potential energy stored in the elastic foundation are first formulated since these two energies are the same in all the rotating ring models. The kinetic energy can be expressed in either a rotating reference system or a space-fixed coordinate system, resulting in governing equations in the corresponding reference systems. The velocity of an infinitesimal element of the ring in the rotating reference system is given as [20]

$$\dot{\mathbf{r}} = (\dot{w} - u\Omega)\mathbf{e}_r + [\dot{u} + (R + w)\Omega]\mathbf{e}_\theta, \tag{2.32}$$

whereas that in the space-fixed reference system reads [25]

$$\dot{\mathbf{r}} = \big(\dot{w} + (w' - u)\Omega\big)\mathbf{e}_r + \big(\dot{u} + (r + w + u')\Omega\big)\mathbf{e}_\theta \tag{2.33}$$

The vectors $\mathbf{e}_r$ and $\mathbf{e}_\theta$ are unit vectors in the radial and circumferential directions in the chosen coordinate system, respectively. The overdot represents partial derivative with respect to time and the prime designates partial derivative with respect to θ.

The kinetic energy of the ring is expressed as [20]

$$T = \frac{1}{2}\rho AR\int_0^{2\pi}(\dot{\mathbf{r}}\cdot\dot{\mathbf{r}})\mathrm{d}\theta. \tag{2.34}$$

If the governing equations are formulated in the rotating coordinate system, then $\dot{\mathbf{r}}$ is chosen from Eq. (2.32); Eq. (2.33) should be used if one would like to obtain governing equations in the nonrotating coordinate system

The potential energy stored by the springs reads

$$V = \frac{R}{2}\int_0^{2\pi}(k_r w^2 + k_c u^2)\mathrm{d}\theta. \tag{2.35}$$

Let us now express the strain energy of the ring. Note that to capture the effect of the rotation-induced hoop stress, a nonlinear strain-displacement relation needs to be employed. Based on different expressions for the strain energy, there appear two categories of strain energy formulations in the literature. One will lead to linear governing equations directly by pre-defining the static equilibrium (and thus the initial hoop stress) caused by rotation. The other will result in nonlinear equations of motion from which the static equilibrium is solved for and linearised governing equations are obtained about the static equilibrium. The latter is more rigorous mathematically. However, both considerations are discussed herein since both of them are employed in the literature.

- Category 1:
  The expression for strain energy based on a pre-defined static equilibrium is given as [15, 20, 76]

$$S = Rb\int_{-h/2}^{h/2}\int_0^{2\pi}\left(\frac{1}{2}\sigma_\theta\varepsilon_\theta^L + {\sigma_\theta}^0\bar{\varepsilon}_\theta\right)\mathrm{d}\theta\mathrm{d}z = Rb\int_{-h/2}^{h/2}\int_0^{2\pi}\left(\frac{1}{2}E\left(\varepsilon_\theta^L\right)^2 + {\sigma_\theta}^0\bar{\varepsilon}_\theta\right)\mathrm{d}\theta\mathrm{d}z \tag{2.36}$$

where z is the location relative to the middle surface of the ring. The strain ε_θ^L in the first term is the linear strain component of the circumferential normal strain at a point on the centroidal line, which is given as

$$\varepsilon_\theta^L = \varepsilon_\theta^0 + zK_\theta \tag{2.37}$$

in which [19]

$$K_\theta = \frac{1}{R}\frac{\partial\beta}{\partial\theta} = \frac{1}{R^2}\left(u' - w''\right), \quad \varepsilon_\theta^0 = \frac{1}{R}\left(w + u'\right) \tag{2.38}$$

The rotation angle of the cross-section in Eq. (2.38) is expressed as [19]

$$\beta = \frac{1}{R}\left(u - w'\right). \tag{2.39}$$

In the second term in Eq. (2.36), $\bar{\varepsilon}_\theta$ contains both linear and nonlinear components of the strain in middle surface which is expressed as

$$\bar{\varepsilon}_\theta = \varepsilon_\theta^0 + \varepsilon_\theta^{Non}. \tag{2.40}$$

The nonlinear part of strain may take different forms according to Table 2.1. The initial hoop stress in Eq. (2.36) can be written as ${\sigma_\theta}^0 = N/A$ in which N is the initial rotation-induced hoop tension assumed a priori and is usually approximated by $N = \rho A R^2\Omega^2$ [15, 20, 29]. By assuming the pretension a priori, the static radial expansion is already determined. Thus, the equations of motion obtained govern the vibration about the assumed static equilibrium. The resulting equations obtained by applying the Hamilton's principle are linear.

The resulting linear equations of motion in the literature in the space-fixed reference frame have the following form:

$$\begin{aligned}
&\rho A\ddot{w} + 2\rho A\Omega(\dot{w}' - \dot{u}) + \rho A\Omega^2(w'' - 2u' - w) + \frac{N}{R^2}\Phi \\
&\qquad + \frac{EI}{R^4}(w'''' - u''') + \frac{EA}{R^3}(w + u') + k_r w = 0, \\
&\rho A\ddot{u} + 2\rho A\Omega(\dot{u}' + \dot{w}) + \rho A\Omega^2(u'' + 2w' - u) + \frac{N}{R^2}\Psi \\
&\qquad + \frac{EI}{R^4}(w''' - u'') - \frac{EA}{R^3}(w' + u'') + k_c u = 0.
\end{aligned} \tag{2.41}$$

The main difference between existing models arises from the different nonlinear strain expressions used for strain energy formulation to take into account the rotation effect. When different nonlinear strains are used, the resulting multipliers Φ and Ψ of initial hoop tension N in Eq. (2.41) have different forms. A summary of the resulting linear models is listed in Table 2.1 [†].

Model A is the most commonly employed rotating thin ring model in the literature. It is proposed by Endo et al. in [13] and almost at the same time presented by

[†] A further discussion on Green-Lagrange strain and Engineering strain can be found in Appendix A.

Table 2.1: Different nonlinear strains and the resulting linear models.

Models	Nonlinear component of strain	Resulting Φ and Ψ	Refs
Model A	Green-Lagrange strain: $\varepsilon_\theta^{Non} = ((\varepsilon_\theta^0)^2 + \beta^2)/2$	$\Phi = w + 2u' - w''$ $\Psi = u - 2w' - u''$	[13, 14]
Model B	Engineering strain: $\varepsilon_\theta^{Non} = \beta^2/2$	$\Phi = u' - w''$ $\Psi = u - w'$	[20]
Model C	Adoption from Donnell's nonlinear shell theory [77]: $\varepsilon_\theta^{Non} = (w')^2/2$	$\Phi = -w''$ $\Psi = 0$	[21, 22]

Huang and Soedel in [14]. This model is termed as the Endo-Huang-Soedel model for convenience of reference.

Besides the difference of the multipliers Φ and Ψ, the pretension N can take several forms as well. In most papers, the initial hoop tension is approximated by [20]

$$N = N_1 = \rho A R^2 \Omega^2. \tag{2.42}$$

However, if one considers a ring element and analyses the force balance, another possible expression is [7, 20, 78]

$$N = N_2 = \frac{EA}{R} \frac{\rho A R^2 \Omega^2}{EA/R + k_r R}. \tag{2.43}$$

It is further noted that in some references, e.g. [19], only the linear strain component is considered in Eq. (2.36), namely ${\sigma_\theta}^0 \bar{\varepsilon}_\theta$ in Eq. (2.36) is neglected. Consequently, the terms related to N disappear in Eq. (2.41). This assumption is only valid when the rotation-induced radial expansion is at most of the same order as the amplitude of in-plane oscillations [79]. In this manner, the stiffening due to the pretension is not considered.

- Category 2:
  The second category of the ring models can be found in [9, 23, 58] in which the strain energy is expressed as:

$$S = Rb \int_{-h/2}^{h/2} \int_0^{2\pi} \left(\frac{1}{2} \sigma_\theta \varepsilon_\theta \right) \mathrm{d}\theta \mathrm{d}z = Rb \int_{-h/2}^{h/2} \int_0^{2\pi} \left(\frac{1}{2} E {\varepsilon_\theta}^2 \right) \mathrm{d}\theta \mathrm{d}z \tag{2.44}$$

  where z is the location relative to the middle surface. ε_θ is a nonlinear strain-displacement relationship representing the normal strain of an arbitrary point on the ring which is given as [19]

$$\varepsilon_\theta = \varepsilon_\theta^L + \varepsilon_\theta^{Non} \tag{2.45}$$

in which the linear part ε_θ^L is given by Eq. (2.37) and nonlinear part ε_θ^{Non} may take different forms as shown in table 2.1.

Applying the Hamilton's principle, nonlinear governing equations are obtained. After finding the static equilibrium from the nonlinear equations, the linearised equations which govern small vibrations about the equilibrium position can be derived. This was first accomplished by Zadoks and Krousgrill [23] who used the nonlinear strain-displacement relation given by Stein [24]. Later, Kim and Chung [25] considered the effect of different strain-displacement relations on the free, small-amplitude vibration of the ring about the static equilibrium. Recently, Cooley and Parker [9] derived new governing equations applicable to the rings rotating at high speeds. The method of derivation was similar to that of Kim and Chung [25]. However, the static equilibrium and the linearised equations of motion were different because of the different nonlinear strain-displacement relations employed in their different papers.

In the early study [23] and in most of the recent studies [9, 26], the static equilibrium was derived from the nonlinear equations of motion as

$$w_e = \frac{\rho A R^2 \Omega^2}{EA/R + k_r R - \rho A R \Omega^2}. \tag{2.46}$$

and correspondingly the hoop tension is given by

$$N_3 = \frac{EA}{R} \frac{\rho A R^2 \Omega^2}{EA/R + k_r R - \rho A R \Omega^2} \tag{2.47}$$

The resulting linear equations of motion in the rotating coordinate system are written as [9, 26]

$$\begin{aligned}
&\rho A(\ddot{w} - 2\Omega\dot{u} - \Omega^2 w) + \frac{EI}{R^4}(w'''' - u''') + \frac{EA}{R^2}(w + u') + \frac{N_3}{R^2}(u' - w'') + k_r w = 0,\\
&\rho A(\ddot{u} + 2\Omega\dot{w} - \Omega^2 u) + \frac{EI}{R^4}(w''' - u'') - \frac{EA}{R^2}(w' + u'') + \frac{N_3}{R^2}(u - w') + k_c u = 0,
\end{aligned} \tag{2.48}$$

and in the nonrotating, space-fixed coordinate system as

$$\begin{aligned}
&\rho A\ddot{w} + 2\rho A\Omega(\dot{w}' - \dot{u}) - \rho A\Omega^2(w + 2u' - w'') + \frac{EI}{R^4}(w'''' - u''') +\\
&\frac{EA}{R^2}(w + u') + \frac{N_3}{R^2}(u' - w'') + k_r w = 0,\\
&\rho A\ddot{u} + 2\rho A\Omega(\dot{u}' + \dot{w}) - \rho A\Omega^2(u - 2w' - u'') + \frac{EI}{R^4}(w''' - u'') -\\
&\frac{EA}{R^2}(w' + u'') + \frac{N_3}{R^2}(u - w') + k_c u = 0.
\end{aligned} \tag{2.49}$$

In Eq. (2.48) and Eq. (2.49), overdots represent time derivatives, whereas the prime stands for spatial derivatives with respect to their corresponding polar coordinate.

The above governing equations can be grouped into Model B in table 2.1 but with $N = N_3$ now.

However, if the Green-Lagrange strain [25] is used for derivation, the following linearised governing equations in the nonrotating coordinate are obtained:

$$\begin{aligned}
&\rho A\ddot{w} + 2\rho A\Omega(\dot{w}' - \dot{u}) + \rho A\Omega^2(w'' - 2u' - w) + \frac{EI}{R^4}(w'''' - u''') + k_r w \\
&+\frac{EA}{2R^4}[(2R^2 + 6Rw_e + 3w_e^2)(w + u') - w_e(2R + w_e)(w'' - u')] = 0 \\
&\rho A\ddot{u} + 2\rho A\Omega(\dot{u}' + \dot{w}) + \rho A\Omega^2(u'' + 2w' - u) + \frac{EI}{R^4}(w''' - u'') + k_c u \\
&-\frac{EA}{2R^4}[(2R^2 + 6Rw_e + 3w_e^2)(w' + u'') + w_e(2R + w_e)(w' - u)] = 0
\end{aligned} \tag{2.50}$$

with the static expansion w_e defined by

$$(\frac{EA}{R} + k_r R - \rho AR\Omega^2)w_e + \frac{EA\left(3Rw_e{}^2 + w_e{}^3\right)}{2R^3} = \rho AR^2\Omega^2 \tag{2.51}$$

which is obtained directly from the nonlinear governing equations. Quadratic and cubic terms of w_e are present besides the linear term. The differences between Eq. (2.50-2.51) and the model developed by Cooley and Parker [9, 26] are obvious both in terms of the governing equations and the static equilibrium. It is expected that at high rotational speeds, the dynamic behaviour predicted by the different models will be significant.

2.2.2. CONCLUDING REMARK ON DERIVATION PROCEDURES

To summarise, depending on the choice of nonlinear strain-displacement relations and different formulations of the strain energy, the majority of the linear low-order rotating ring models can be expressed in terms of Eq. (2.41) with different forms of rotation-induced hoop tension given by Eqs. (2.42,2.43,2.47) and distinct multipliers of the rotation-induced hoop tension summarised in Table 2.1. Exception is a combination of employment of Green-Lagrange strain and nonlinear formulation of the strain energy (Eq. (2.44)), which leads to the governing equations given by Eq. (2.50).

Although various rotating thin ring models exist, it is argued that the model proposed by Cooley and Parker [9, 26] is the mathematically correct one. The static equilibrium should not be pre-defined as has been done in many references [15, 20]. The equilibrium should be obtained from the geometrical nonlinear governing equations. Furthermore, the choice of Engineering strain in [9, 26] is in line with the way of obtaining the elastic properties, e.g. the Young's modulus of the material. Therefore, in the following analysis of modes and wave dispersion of rotating rings, the model adopted from [9, 26], namely Eq. (2.48) and Eq. (2.49) will be used.

2.2.3. MODES OF ROTATING RINGS

For a rotating ring, the natural frequencies can be computed in either a rotating coordinate or a space-fixed coordinate system. By substituting a wave-like solution $w(\theta, t) =$

$C_{wn}e^{(i\omega t+in\theta)}$, $u(\theta,t)=C_{un}e^{(i\omega t+in\theta)}$ in the equations of motion and then letting the determinant of the coefficient matrix of $[C_{wn},C_{un}]^T$ be zero, the resulting matrix form of Eq. (2.49) or Eq. (2.48) takes the following form:

$$\begin{bmatrix} L_{11}(\Omega) & L_{12}(\Omega) \\ L_{21}(\Omega) & L_{22}(\Omega) \end{bmatrix} \begin{bmatrix} C_{wn} \\ C_{un} \end{bmatrix} = \mathbf{0} \tag{2.52}$$

in which the operators $L_{11}(\Omega), L_{12}(\Omega), L_{21}(\Omega), L_{22}(\Omega)$ are functions of the rotational speed. Subsequently, the resulting characteristic equation in the rotating coordinate is of the form

$$a_4{\omega_{rn}}^4 + a_3{\omega_{rn}}^3 + a_2{\omega_{rn}}^2 + a_1\omega_{rn} + a_0 = 0. \tag{2.53}$$

The characteristic equation in a space-fixed coordinate can be written as

$$b_4{\omega_n}^4 + b_3{\omega_n}^3 + b_2{\omega_n}^2 + b_1\omega_n + b_0 = 0. \tag{2.54}$$

In Eqs. (2.53) and (2.54) the non-zero $a_0 - a_4$ and $b_0 - b_4$ are coefficients of the corresponding characteristic equation and they are functions of the ring properties and the rotational speed. ω_n and ω_{rn} are the natural frequencies in space-fixed coordinate and rotating coordinate, respectively. The natural frequencies obtained by solving Eq. (2.53) and Eq. (2.54)in the two coordinates are related by

$$\omega_n = \omega_{rn} - n\Omega \tag{2.55}$$

From wave point of view, a positive natural frequency represents a backward-travelling wave and a negative natural frequency represents a forward-travelling wave in each coordinate system according to the assumed wave-like solution for a positive n. Note that $\omega_n = 0$, or equivalently $b_0 = 0$ in Eq. (2.54), is the condition to determine the "stationary modes" or resonance conditions [19].

Unlike the characteristic equation (2.6) in which the coefficients of the odd-order power in the frequency are all zero, indicating in total two natural frequencies for a specific mode when $n \geq 1$, the characteristic equations (2.53 and 2.54) of a rotating ring are fourth order polynomials in which all coefficients are non-zero and real-valued. This yields four distinct frequencies for every mode $n \geq 1$. This phenomenon is called frequency bifurcation [14]. Two of the natural frequencies correspond to backward travelling waves (with positive natural frequencies) whereas the other two correspond to forward travelling waves (with negative natural frequencies). The relations of natural frequencies of mode n in rotating and space-fixed coordinate systems are illustrated in Fig. 2.9 in accordance with [80]. The kinematic shift $n\Omega$ (Eq. (2.55)) of natural frequencies in different reference systems is shown. Resonance would happen when the backward-travelling wave (line D) intersects the zero-frequency line or when the excitation line (the exciting frequency is considered as a per-revolution source the same as in [80]) has intersections with either the forward or backward-travelling wave lines. When line D crosses the horizontal axis, resonance would occur due to a stationary point load of constant magnitude. At this rotational velocity, observers in a space-fixed coordinate system note a stationary deformation pattern with respect to the space-fixed coordinate. Point P_3 and P_4 stand for different resonances. At point P_3, resonance would happen because of

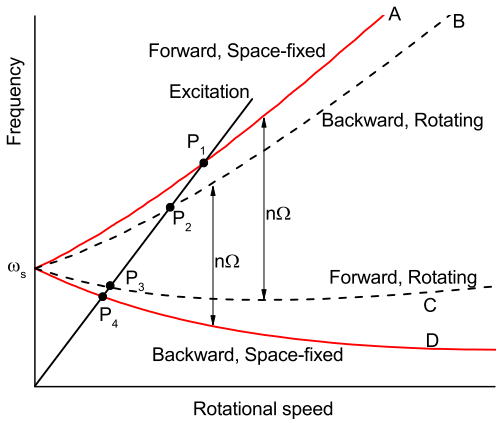

Figure 2.9: Campbell diagram for the n-th mode of a rotating ring.

a harmonic co-rotating load. The frequency of this load equals the natural frequency of the ring measured in the rotating coordinate. For point P_4, this resonance corresponds to a stationary harmonic load whose frequency is equal to the natural frequency measured in the space-fixed coordinate system.

2.2.4. WAVE DISPERSIONS IN ROTATING RINGS

To stude the effect of the rotational speed, a new dimensionless rotational speed is introduced as

$$\bar{v} = v/c_0 = R\Omega/c_0 = R\Omega/(\sqrt{E/\rho}). \tag{2.56}$$

Other dimensionless parameters are the same as defined in Eq. (2.11). The dispersion relation in the rotating coordinate system according to Eq. (2.48) is

$$\begin{aligned}&(\bar{\omega}^2 - \bar{k}^2 - \bar{\gamma}^4 - \bar{k}_r + \bar{v}^2\bar{k}^2 - \bar{N}\bar{\gamma}^2)(\bar{\omega}^2 - \bar{\gamma}^2 - \bar{k}^2\bar{\gamma}^2 - \bar{k}_c + \bar{v}^2\bar{k}^2 - \bar{N}\bar{k}^2)\\ &-(\bar{k}\bar{\gamma}^3 + \bar{k}\bar{\gamma} + \bar{k}\bar{\gamma}\bar{N} - 2\bar{v}\bar{k}\bar{\omega})^2 = 0.\end{aligned} \tag{2.57}$$

The hoop tension expressed in terms of $\bar{v}$ is

$$\bar{N} = \frac{N_3}{EA} = \frac{\bar{v}^2\bar{k}^2}{\bar{k}^2 + \bar{k}_r - \bar{v}^2\bar{k}^2}. \tag{2.58}$$

When $\bar{k} = 0$, the dispersion relation Eq. (2.57) degenerates to Eq. (2.16) which is the dispersion relation of a stationary extensible beam with decoupled transverse and extensional motions.

The dispersion relation in the space-fixed coordinate system according to Eq. (2.49)

is

$$
\begin{aligned}
&(\bar{\omega}^2 - \bar{k}^2 - \bar{\gamma}^4 - \bar{k}_r + \bar{v}^2\bar{k}^2 - \bar{N}\bar{\gamma}^2 + \bar{v}^2\bar{\gamma}^2 + 2\bar{v}\bar{\omega}\bar{\gamma})\times \\
&(\bar{\omega}^2 - \bar{\gamma}^2 - \bar{k}^2\bar{\gamma}^2 - \bar{k}_c + \bar{v}^2\bar{k}^2 - \bar{N}\bar{k}^2 + \bar{v}^2\bar{\gamma}^2 + 2\bar{v}\bar{\omega}\bar{\gamma}) \\
&-(\bar{k}\bar{\gamma}^3 + \bar{k}\bar{\gamma} + \bar{k}\bar{\gamma}\bar{N} - 2\bar{v}\bar{k}\bar{\omega} - 2\bar{v}^2\bar{\gamma}\bar{k})^2 = 0.
\end{aligned}
\tag{2.59}
$$

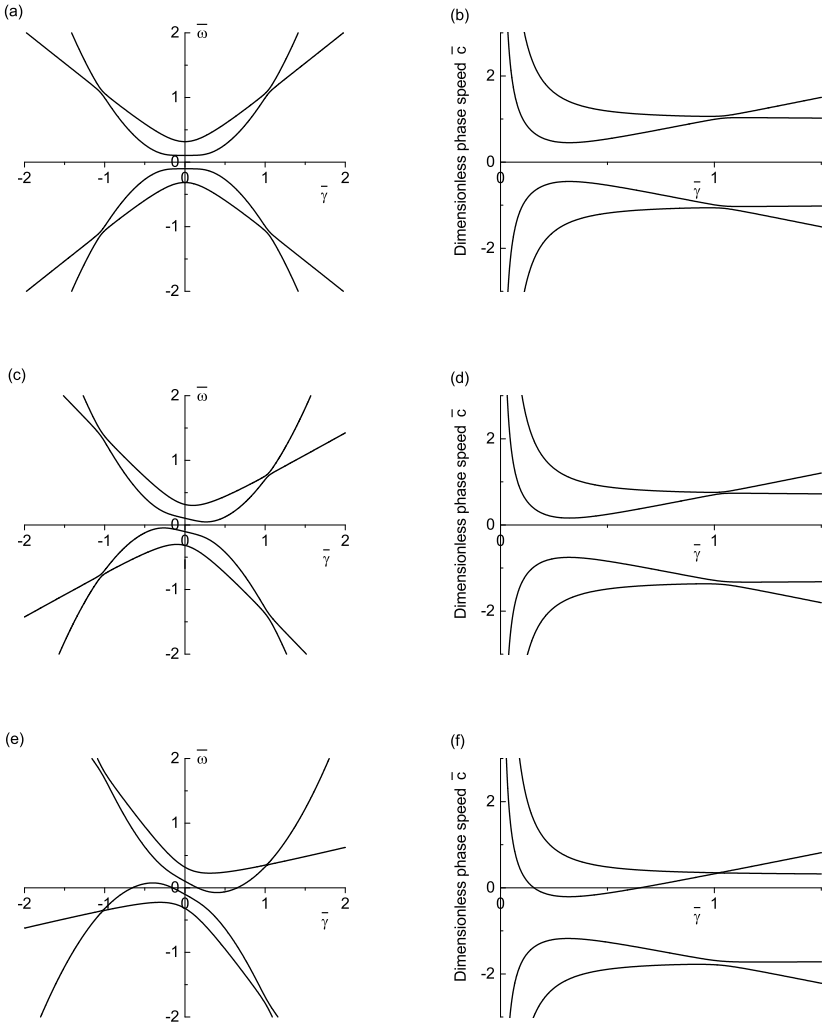

Figure 2.10: Dispersion curves and phase speeds of a rotating ring for $h/R = 0.1, \bar{k}_c = 0.1, \bar{k}_r = 0.01$: (a)(b) rotational speed $\bar{v} = 0$; (c)(d) rotational speed $\bar{v} = 0.3$; (e)(f) rotational speed $\bar{v} = 0.7$.

Eq. (2.59) degenerates to

$$(\bar{\omega}^2 - \bar{\gamma}^4 - \bar{k}_r + \bar{v}^2\bar{\gamma}^2 + 2\bar{v}\bar{\omega}\bar{\gamma})(\bar{\omega}^2 - \bar{\gamma}^2 - \bar{k}_c + \bar{v}^2\bar{\gamma}^2 + 2\bar{v}\bar{\omega}\bar{\gamma}) = 0 \tag{2.60}$$

when $\bar{k} = 0$. The above frequency equation is the one given in [81, 82] for a moving beam with both transverse and extensional motions when only linear terms are retained.

Fig. 2.10 shows the dispersion curves and phase speeds of waves of a ring rotating at different velocities. The classical rotating thin theory [9] is employed, and a space-fixed coordinate system is considered. In each of Fig. 2.10(a)(c)(e) the vertical axis represents the dimensionless frequencies whereas in Fig. 2.10(b)(d)(f) the vertical axes are the dimensionless phase speeds. The horizontal axes are the dimensionless wavenumber in Fig. 2.10. As shown in Fig. 2.10, the dispersion relation becomes an odd function with respect to the wavenumber. The rotational symmetry is caused by the Coriolis force. The backward-travelling waves branches (branches in the first quadrant in Fig. 2.10(b)(d)(f)) have a trend to move towards the horizontal axis with increasing rotational speeds. The dispersion curves become tangent to the horizontal axis at a certain velocity and cross the axis downwards if the velocity increases further. Correspondingly, the phase speed of the back-travelling waves decreases and becomes zero at the rotational speeds when the dispersion curve touches the wavenumber axis. At this velocity, the phase speed of the back-travelling wave is zero, and thus "standing waves" are initiated if a constant stationary excitation is present. One can consult Ref. [32] for wave propagation in a rotating ring without an elastic foundation.

2.2.5. REMARKS ON EXISTING ROTATING THIN RING MODELS

This section provides a thorough discussion on the differences between the existing rotating thin ring models in the literature with the aim to spot the deficiencies of current models which will be tackled further in Chapters 3-5.

CONSIDERATION OF THE STIFFENING EFFECTS

The effect of rotation is twofold. On the one hand, the gyroscopic nature (reflected by the Coriolis and centrifugal force terms) of the system has the tendency to soften the ring. On the other hand, the hoop tension caused by the rotation has a stiffening role which tends to stabilise the ring. For various rotating ring models, the ultimate differences, which result from various approximations and differences in the derivation procedure, are in the resulting terms in the equations of motion related to these softening and stiffening effects. In terms of existing models based on Love's thin shell theory, the inclusion of gyroscopic effects are identical, whereas the considerations of the stiffening effect due to rotation are still in disagreement. In some of the early studies [28, 83, 84] and in Soedel's book [19], the influence of the initial stress is overlooked and thus the stiffening effect. Consequently, the terms $N\Psi/R^2$ and $N\Phi/R^2$ in governing equations (2.41) disappear altogether.

The omission of the stiffening effect causes erroneous predictions of the natural frequencies of rotating rings as stated in [13], in which experimental results are compared with the predictions by various analytical models. The same holds for the conclusions drawn on resonance speeds and instability of free vibration.

CHOICE OF NONLINEAR STRAIN-DISPLACEMENT RELATIONS

i) As already shown previously, nonlinear strain-displacement relations are needed to capture rotation-induced prestress. The proper choice of the nonlinear strain-displacement relation is crucial for the consideration of the stiffening effect. Basically, there are three options as listed in Table 2.1. However, if one uses the nonlinear strain component adopted from the Donnell's thin shell theory, the natural frequencies predicted deviate from the experimental data as shown in Fig. 2.11. Therefore, it is concluded that Model C in Table 2.1 is not suitable to study rotating ring dynamics.

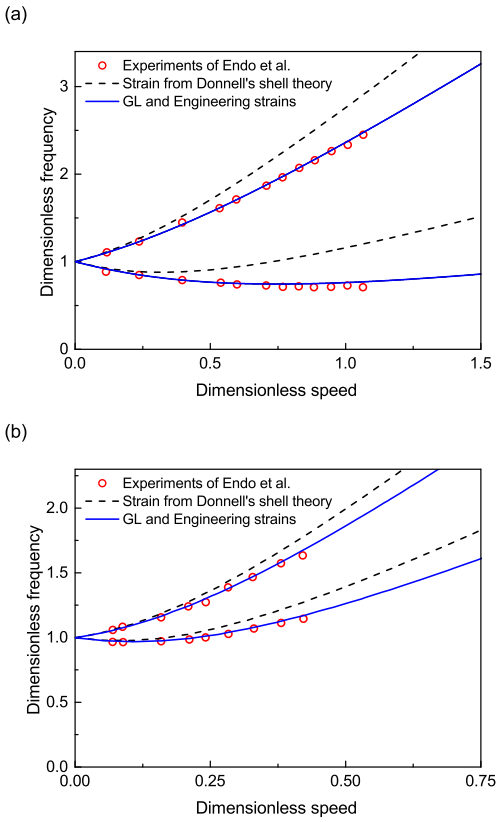

Figure 2.11: Comparisons of the experimental results in [13] with those of the models listed in Table 2.1 for: (a) $n = 2$; (b) $n = 3$.

ii) Another conclusion that can directly be drawn from Fig. 2.11 is that the predictions from models using engineering strain and Green-Lagrange strain, no matter whether Category 1 or Category 2 in subsection 2.2.1 are employed, show good agreement with the experimental results. The reason is that the ring investigated in [13] is composed of steel. Because of this, the radial expansion is marginal, and the hoop stress predicted by different models is similar. Thus, the stiffening effect

predicted by various models is practically the same.

iii) The different nonlinear strain-displacement relations do influence the predictions of dynamic behaviour of a rotating ring, especially at high rotating speeds. To illustrate this, Figs. 2.12 and 2.13 compare the predictions of natural frequencies using the model (Eq. (2.49)) in [9, 26] by Cooley and Parker and the model given by Eqs. (2.50). Although both of them are obtained employing the Category 2 procedure in subsection 2.2.1), the former uses Engineering strain while the latter employes the Green-Lagrange strain. The parameters are chosen from a spinning ring based on a compliant gear [26]. The nondimensional rotational speed $\bar{\Omega}$ is defined as

$$\bar{\Omega} = \Omega \sqrt{\frac{\rho A R^4}{EI}} \tag{2.61}$$

to be consistent with the one used in [26]. In Figs. 2.12 and 2.13, the numbers in brackets represent the mode numbers. The horizontal axis is the nondimensional rotational speeds of the ring and the vertical one represents the nondimensional natural frequencies. The red dotted lines represent frequencies of $n = 1$ in Fig. 2.12 whereas the blue dashed lines stand for $n = 0$ modes in both Fig. 2.12 and 2.13. Figs. 2.12 and 2.13 show that the natural frequencies become different at high speeds of rotation due to differences in the nonlinear strain-displacement relations assumed. This discrepancy is expected because the static radial expansion of the model used for Fig. 2.12(a) and 2.13(a) differs from the one used for Fig. 2.12(b) and 2.13(b). The former is based on Eq. (2.46) and the latter is calculated by Eq. (2.51).

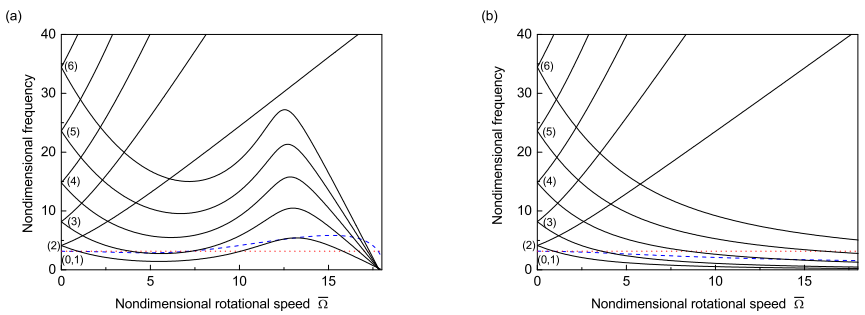

Figure 2.12: Comparison of the natural frequencies of bending dominant modes of a spinning ring on a compliant gear: (a) Engineering strain, (Eq. (2.49), reproduction of Cooley and Parker [26]); (b) Green-Lagrange strain, (Eq. (2.50)).

It is not the aim to explain the results in Figs. 2.12 and 2.13 nor to judge which model is better, but rather to show how different the predicted natural frequencies can be by employing different nonlinear strain-displacement relations. The proper choice of the nonlinear strain-displacement relations will be discussed in detail in Chapter 3. The ultimate judgement of choice of nonlinear strain-displacement relation requires experimental validations.

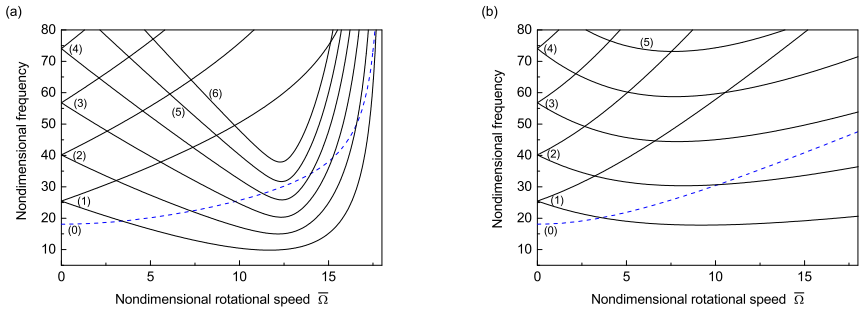

Figure 2.13: Comparison of the natural frequencies of extension dominant modes of a spinning ring on a compliant gear: (a) Engineering strain, (Eq. (2.49), reproduction of Cooley and Parker [26]); (b) Green-Lagrange strain, (Eq. (2.50)).

PREDICTION OF CRITICAL SPEEDS USING CLASSICAL ROTATING THIN RING THEORIES

Resonance of a ring occurs when a constant load moves uniformly along the ring at speeds equal to a natural frequency divided by the corresponding mode number [60, 61, 65, 85, 86]. However, different opinions exist as to the critical speeds of a rotating ring subjected to a stationary constant load. Theoretically speaking, the resonance condition for a rotating ring under a stationary load is [19, 58]

$$\omega(\Omega) = 0 \tag{2.62}$$

In Eq. (2.62) ω (implicit function of the rotational speed Ω) is the natural frequency in a space-fixed reference system. Various rotating thin ring models have been developed and, among those, the models based on the Love's thin shell theory in Ref. [14, 20, 21] are most commonly used. Critical speed clearly exists for a constant load moving around an elastic ring [60] but the existence of the critical speed for a rotating ring subjected to a stationary constant load is still being debated.

Significant wave-like deformation was observed when a pneumatic tire rolls on the ground with a speed higher than a certain critical value which suggests that a rotating ring may have a critical rotation speed [87]. However, the theoretical predictions for the critical speed are not convincing and, sometimes, confusing when use is made of the existing rotating ring models. Some references show a prediction of the critical speed associated with resonance but the pretension due to rotation was not properly included in those works [12, 35]. Many other references do not mention the critical speed at all [20, 21]. Huang and Hsu [65] concluded that no critical rotational speeds exist for the forced response to a stationary constant point load subjected to a rotating thin shell using the Endo-Huang-Soedel model. After substituting the resonance condition Eq. (2.62) into the dispersion relation obtained from the Endo-Huang-Soedel model, one obtains

$$\frac{EIEA}{R^6}n^6 + (\frac{EIk_c}{R^4} - \frac{2EAEI}{R^6})n^4 + (\frac{EAEI}{R^6} + \frac{k_rEI}{R^4} + \frac{k_rEA}{R^2})n^2 + \frac{EAk_c}{R^2} + k_rk_c = 0, \tag{2.63}$$

which is not related to the rotational speed. Thus, no critical speed is predicted. However, it is concluded in [88] that critical speeds do exist for rings supported by relatively

stiff foundation and the critical speeds can be predicted by the classical rotating thin ring models if $N = N_2$ (Eq. (2.43)) or $N = N_3$ (Eq. (2.47)) is used.

PROBLEMS OF CATEGORY 1 MODELS

Despite the choice of nonlinear strain-displacement relations, the 'linear derivation' procedure described as Category 1 in subsection 2.2.1 and applied in Refs. [13, 14, 17, 20] is problematic for several reasons. The initial hoop tension is predefined as either Eq. (2.42) or Eq. (2.43). As a consequence, the static equilibrium due to steady rotation is predefined. It must be realised that the expressions for the rotation-associated pretension used in the aforementioned papers are approximate and do not account for the centrifugal force associated with the radial expansion of the ring due to rotation. The latter force is indeed negligible at relatively low rotation speeds. However, this force cannot be neglected when the dynamics of the rings rotating at high speeds is focused upon. More importantly, the most commonly used Endo-Huang-Soedel model, which is the use of combination of 'linear derivation' procedure and the Green-Lagrange strain [13, 14], gives an erroneous prediction when the steady-state response of the ring subject to a stationary constant load is considered. Only when one employs the 'nonlinear derivation' stated as Category 2 [9, 23, 25, 26, 58] the static equilibrium and initial hoop tension can be determined correctly.

INEXTENSIONAL ASSUMPTION

The inextensional assumption

$$w = -\frac{\partial u}{\partial \theta}. \tag{2.64}$$

is widely used in the literature to simplify the analysis. Note that the resulting governing equations of inextensible rotating rings obtained from Ref. [14] (Model A in Table 2.1) and [20] (Model B in Table 2.1) are the same after employing the inextensibility assumption. It has been pointed out recently by Cooley and Parker [26] that the in-extensional assumption "works poorly at high speeds". The frequency equation obtained based on the inextensional assumption is not valid for the $n = 0$ modes since the elasticity in circumferential direction was removed [19]. With the inextensional assumption, the instability of a rotating ring is also not captured because the unstable motion occurs for the $n = 0$ rotational mode but the inextensibility assumption eliminates the circumferential motion.

2.3. APPLICABILITY AND LIMITATION OF CLASSICAL ROTATING THIN RING MODELS

For classical thin ring models, it is assumed that the shear deformation and rotatory inertia can be neglected. In Soedel's monograph [19], it is stated that for the thin ring assumption to hold, the thickness h needs to be small compared to the length between nodes of the highest modes of interest, which means $h << \lambda$ (λ is the shortest wavelength of mode of interest). For ring cases, the wavelength of a specific wavenumber n can be expressed by

$$\lambda = \frac{2\pi R}{n} \tag{2.65}$$

Thus, only if

$$h << \frac{2\pi R}{n} \tag{2.66}$$

one can safely ignore shear and rotatory inertia. This means

$$\frac{h}{R} << \frac{2\pi}{n} \Longrightarrow n << 2\pi\frac{R}{h} \tag{2.67}$$

or equivalently

$$\bar{\gamma} = k\gamma = k\frac{n}{R} << \frac{2\pi k}{h} = \frac{2\pi}{h}\sqrt{\frac{EI}{EA}}. \tag{2.68}$$

If the ring has a rectangular cross-section, then the above inequality becomes

$$\bar{\gamma} << \frac{\sqrt{3}\pi}{3} \approx 1.81. \tag{2.69}$$

In fact, the upper limit determined by expression (2.69) is still too high. The phase speed of waves in a structure with at least one traction-free surface converges to the Rayleigh wave speed [71]. Taking a thin ring without foundation in Fig. (2.5d) as an example, the phase speed of the first wave branch starts to converge to the longitudinal wave speed $\sqrt{E/\rho}$ at $\bar{\gamma} \approx 1$. This result obtained using the classical thin ring model violates the fact that the phase speeds should converge to the Rayleigh wave speed. Therefore, the upper limit of the applicable wavenumber range essentially reads at least $\bar{\gamma} < 1$. This is also true for rings on relatively soft foundation as shown in Fig. (2.8e-f). However, for more stiffer foundation cases as shown e.g. in Fig. (2.8a-b), the thin ring model is completely inapplicable since the phase speeds are all larger than the longitudinal wave speed $\sqrt{E/\rho}$ of the ring for case 1 listed subsection 2.1.2 for all wavenumbers. In general, classical low order theories are not suitable for rings supported by stiff foundation.

In addition, rings should rotate at much lower speeds compared with the wave speeds (Rayleigh wave speed or shear wave speed) of the ring for classical thin rotating ring models to be accurate. For relatively low rotational speeds, all models yield similar results since the effect of rotation is limited.

The study in this chapter has shown that the most commonly used Endo-Huang-Soedel model [13, 14] cannot be used for rings rotating at high speeds for two reasons. First, the centrifugal force associated with the radial expansion is not accounted for (the same drawback holds for the model in Ref. [20]). Second, the model does not predict critical speeds because of the use of 'linear derivation' procedure and the Green-Lagrange strain as discussed in section 2.2.5.

The model proposed by Cooley and Parker [9] can be applied to rings on elastic foundation which rotate at high speeds. However, the stresses at the ring's inner surface, which is directly connected to the foundation are not zero. These stresses are high when the ring is supported by stiff foundation or rotating at high speeds. Therefore, the variations of transverse stresses trough the ring thickness should be accounted for. To consider stress variations along the thickness, higher order terms in the through-thickness displacement fields are needed as discussed in the sequel.

2.4. CONCLUSIONS

In this chapter, modes of, and wave dispersions in stationary and rotating rings are reviewed based on the classical thin ring theories. Following conclusions can be drawn:

i) The curvature coupling in most cases is weak for thin rings, especially for thin rings supported by relatively stiff elastic foundation. Depending on relative values of the radial and tangential stiffnesses of the foundation, as well as the elastic properties of the ring itself, three dissimilar wave characteristics are found for stationary rings. The minimum phase speed can either be equal to $\sqrt{E/\rho}$ or close to the minimum phase speed $\sqrt[4]{4k_r EI/(\rho A)^2}$ of the corresponding straight extensible beam case. Curve veering is found, meaning interchange of eigenfunctions with increasing wavenumbers.

ii) Various existing rotating thin ring models are discussed focused upon the derivation procedure and assumptions employed. It is shown that to properly capture the stiffening effect due to rotation, nonlinear strain-displacement relation needs to be used. Different choices of nonlinear strain-displacement relations result in different predictions of natural frequencies; sometimes even erroneous results are obtained. It is concluded that the nonlinear strain-displacement relation obtained by using the Donnell's nonlinear shell theory should not be applied in the studies of dynamics of rotating rings. The inextensibility assumption is not suitable for rings that rotate at high speeds. The 'linear derivation' procedure is not recommended since the centrifugal force associated with the dynamic radial motion is not included.

iii) In the literature, resonance speeds are not found using the classical rotating thin ring models. The reason is twofold. From the modelling point of view, the most commonly used Endo-Huang-Soedel model can not predict critical speeds due to its intrinsic flaw. On the other hand, most studies are focusing on stiff rings, such as rings made of steel. The operational speeds of these rings are way smaller than resonance speeds. Furthermore, resonance speeds do not always exist for rotating rings; their existence depends on the ring properties.

iv) The classical thin ring models are not applicable for rings resting on stiff foundation. All the classical rotating thin ring models are not accurate when it comes to the study of rings rotating at high speeds due to the fact that the through-thickness variation of transverse stresses is not considered. The effect of through-thickness variation of radial stress will be addressed in Chapter 3. The inapplicability of classical low order ring models will be further discussed by comparing the results using classical low-order theories and results obtained from the high-order model in Chapters 4 and 5.

3

STABILITY OF IN-PLANE FREE VIBRATION OF A ROTATING THIN RING REVISITED

In the previous chapter, various existing models used for the prediction of the in-plane free vibrations of rotating rings are reviewed. The models discussed were based on the classical theories without consideration of high-order effects. It has been argued that the presence of an elastic foundation can significantly change the dynamic behaviour of a rotating ring. The inner surface of the ring is connected to a hub through the elastic foundation, therefore, the radial expansion due to rotation causes elongation of the radial springs. It is natural to assume that when the foundation is stiff or when the radial (static) expansion is significant, the radial (normal to the surface) traction imposed on the inner surface of the ring is no longer negligible. Thus, the classical models are inapplicable because their derivation is based on the assumption that the boundaries are traction-free.

The in-plane free vibration of a ring rotating at high speed is revisited in this chapter. Only thin rings are considered, meaning that the transverse shear deformation and rotatory inertia are neglected. It will be shown in Chapter 5 that these higher order effects have marginal influence on the critical speed that corresponds to the onset of instability. A new thin ring model which accounts for the elastic foundation and the through-thickness variation of the radial stress is proposed. The emphasis is placed on a proper consideration of the geometrical nonlinearity, which is essential for the consistent consideration of the rotation effects. A rotating ring, which is a typical gyroscopic system, is non-conservative since torques which maintain rotation can supply energy to the system continuously. Thus, the system can become unstable. The in-plane stability of a thin rotating ring is analysed thoroughly. In the previous chapter it is argued that the

This chapter has been published as a journal paper in *Journal of Sound and Vibration* **402**, 203(2017) [58]. Minor changes are made.

incapability of certain models to predict instability is related to assumptions employed in the derivation. In this chapter a new model is developed and it is shown that the ring can become unstable should the rotational speed exceed a critical value.

This chapter is structured as follows. In section 3.1, the nonlinear equations of motion are derived for a rotating thin ring which is mounted on an immovable axis through an elastic foundation. A quadratic displacement field in the radial direction is assumed to account for the through-thickness variation of the radial stress. Then, the linearised equations in the vicinity of the static equilibrium are obtained and compared to the classical model based on Love's thin shell theory [9]. The linearised equations are used to investigate stability of the static equilibrium of the rotating ring in section 3.2. Modes, which are stationary when observed in a space-fixed reference system, are also investigated. In section 3.3, the effects of parameters of the ring on the stability are studied. A remark on the governing equations obtained by applying different geometrical nonlinearities is included in section 3.4. Finally, section 3.5 summarises all the important conclusions of this chapter.

The main original contributions of this chapter are: i) the through-thickness variation of the radial stress is considered which turns out to be important for rings supported by a relatively stiff foundation; ii) the instability of high-speed rotating thin rings is predicted using a rigorous model. The latter result is fundamentally new as in most known to the author previous studies the stability problem is either not considered or it is stated that the in-plane vibration of a rotating ring is stable [13, 14].

3.1. GOVERNING EQUATIONS FOR A ROTATING THIN RING

In this section, the governing equations for a thin rotating ring are first derived taking into account through-thickness variation of the radial stress. The transverse shear deformation and rotatory inertia are not incorporated in the formulation of the governing equations.

3.1.1. DERIVATION OF THE NONLINEAR GOVERNING EQUATIONS

The configuration of the rotating ring is shown in Fig. 3.1. It consists of a flexible rotating ring and radial and circumferential springs that connect the inner surface of the ring to an immovable axis. To describe the motion of a differential element on the ring, one can use either a coordinate system (r,φ) that rotates at the same speed as the ring or a space-fixed, non-rotating coordinate system (r,θ). The origins of both coordinate systems can be chosen to coincide with the immovable axis of the ring. The transformation from the rotating reference system to the space-fixed one can be accomplished by applying the following formula,

$$\theta = \varphi + \Omega t, \tag{3.1}$$

where Ω is the rotational speed of the ring. In this chapter, the governing equations are formulated in the space-fixed reference system.

It is assumed that the mean radius of the ring is R. In order to simplify mathematical expressions, an auxiliary coordinate z is introduced as $z = r - R$, where r is the radial coordinate. The ring occupies the region $-h/2 \le z \le h/2$ with h being the thickness of the ring. The radial and circumferential displacements of the ring with respect to the

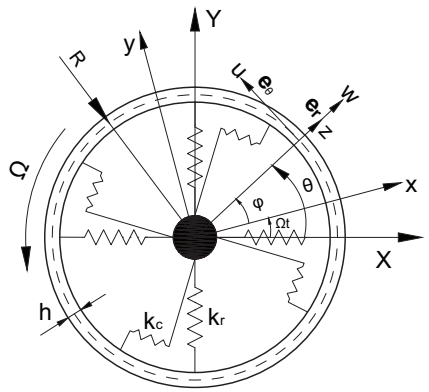

Figure 3.1: A rotating thin ring on an elastic foundation

undeformed configuration are designated by $w(z,\theta,t)$ and $u(z,\theta,t)$, respectively. The stiffnesses of the radial and circumferential springs per unit length are designated as k_r and k_c, respectively. Furthermore, ρ is the mass density of the ring, E is the Young's modulus, A is the cross-sectional area and I is the cross-sectional moment of inertia and b is the width of the ring.

Assume that the radial displacement $w(z,\theta,t)$ and the circumferential displacement $u(z,\theta,t)$ of an arbitrary element on the ring are defined by *

$$\begin{aligned} w(z,\theta,t) &= w_0(\theta,t) + z w_1(\theta,t) + z^2 w_2(\theta,t), \\ u(z,\theta,t) &= u_0(\theta,t) + z\beta(\theta,t), \end{aligned} \tag{3.2}$$

where w_0 and u_0 are the radial and circumferential displacements of the middle surface, respectively; w_1 and w_2 are the higher order corrections of the radial displacement. These corrections enable us to take the through-thickness variation of the radial stress into account. The radial traction at the inner surface of the ring is non-zero because of the presence of the radial springs. By introducing a quadratic term in the radial displacement field, a linear distribution of the through-thickness variation of the radial stress can be treated. β is the rotation angle of the cross-section [19]:

$$\beta = \frac{u_0}{r} - \frac{w'}{r}. \tag{3.3}$$

Hereafter the prime stands for the partial derivative with respect to θ.

The transverse shear stress is neglected because the ring is assumed to be thin. According to [24], the nonlinear term in the strain-displacement relation is related solely to

*The model presented is an improved version of the classical thin ring model. Only high-order corrections of displacement in radial direction is considered. Consequently, only the radial stress variation along the thickness is accounted for. The reason for this consideration is that in the majority of engineering applications, the support stiffness in radial direction is larger than that in the circumferential direction.

the rotation angle of the cross-section; therefore the circumferential strain at the middle surface of the ring is

$$\bar{\varepsilon}_\theta = \varepsilon_0 + \frac{1}{2}(\beta)^2, \tag{3.4}$$

where ε_0 is the linear part of the circumferential strain [14]:

$$\varepsilon_0 = \frac{u_0'}{r} + \frac{w}{r} \tag{3.5}$$

Close attention needs to be paid here to the circumferential displacement. In the space-fixed coordinate system, the total displacement in the circumferential direction is actually the elastic part plus $R\Omega t$. However the latter does not cause any strain, so it is not included in the strain-displacement relation.

Since the ring is assumed thin, the plane cross-section can be assumed to remain plane after deformation, like in the case of the Euler-Bernoulli beam. The circumferential normal strain of an arbitrary element of the ring can be represented as

$$\varepsilon_\theta = \bar{\varepsilon}_\theta + zK_\theta, \tag{3.6}$$

where K_θ is the change-in-curvature due to bending, which is given by [14, 19]

$$K_\theta = \frac{\beta'}{r} = \frac{u_0{}' - w''}{r^2}. \tag{3.7}$$

The through-thickness radial strain ε_r of an arbitrary element of the ring is given by

$$\varepsilon_r = w_{,r} = \frac{\partial w}{\partial z} = w_1 + 2zw_2. \tag{3.8}$$

The velocity vector in the space-fixed frame reads (neglecting the rotatory inertia):

$$\begin{aligned} \dot{\mathbf{r}} &= \big(\dot{w} + (w' - u_0)\Omega\big)\mathbf{e}_r + \big(\dot{u}_0 + (r + w + u_0')\Omega\big)\mathbf{e}_\theta \\ &= v_1\mathbf{e}_r + v_2\mathbf{e}_\theta. \end{aligned} \tag{3.9}$$

The vectors $\mathbf{e}_r$ and $\mathbf{e}_\theta$ are unit vectors in the radial and circumferential directions, respectively. The overdot represents partial derivative with respect to time.

The inner surface of the ring is connected by means of distributed radial and circumferential springs to an immovable axis. The boundary conditions for the inner and outer surfaces of the ring must be satisfied at all times. The material of the ring is considered to be linearly elastic. For the outer surface of the ring, the radial stress should be zero, which implies that [†]

$$\sigma_r|_{h/2} = E\varepsilon_r|_{h/2} = E(w_1 + hw_2) = 0. \tag{3.10}$$

[†]The Poisson's ratio effect is not considered for simplicity. By neglecting the Poisson's ratio, the boundary conditions at both surfaces can be exactly satisfied by relating the higher order displacement components to the lower order terms in a linear manner as shown in Eq. (3.12). However, the message of the existence of instability is successfully conveyed with this model. Meanwhile, the proposed model is an improved version of the classical lower order model in which no Poisson's ratio is included either.

The inner surface is connected to the springs, thus

$$\begin{aligned} b\sigma_r|_{-h/2} &= Eb\varepsilon_r|_{-h/2} = Eb(w_1 - hw_2) = k_r w|_{-h/2} \\ &= k_r(w_0 - w_1 h/2 + w_2 h^2/4). \end{aligned} \tag{3.11}$$

Combining Eqs. (3.10) and (3.11), w_1 and w_2 can be solved for to give

$$w_1 = c_1 w_0,\ w_2 = c_2 w_0, \tag{3.12}$$

where

$$c_1 = \frac{4k_r h}{8EA + 3k_r h^2},\ c_2 = \frac{-4k_r}{8EA + 3k_r h^2}. \tag{3.13}$$

The unit of c_1 is 1/m whereas the unit of c_2 is $1/\mathrm{m}^2$.

The variation of the strain energy is given by

$$\delta S = \delta S_1 + \delta S_2, \tag{3.14}$$

in which δS_1 is the variation of the strain energy associated with circumferential strain and δS_2 is the addition to that due to a non-zero through-thickness radial strain.

Integrating δS_1 between two time instants, t_1 and t_2 yields

$$\begin{aligned} \int_{t_1}^{t_2} \delta S_1 \mathrm{d}t &= b\int_{t_1}^{t_2}\int_{-h/2}^{h/2}\int_0^{2\pi} (\sigma_\theta \delta\varepsilon_\theta) r \mathrm{d}\theta \mathrm{d}z \mathrm{d}t \\ &= b\int_{t_1}^{t_2}\int_{-h/2}^{h/2}\int_0^{2\pi} \sigma_\theta \delta\big(\varepsilon_0 + \frac{1}{2}(\beta)^2 + z\frac{\beta'}{r}\big) r \mathrm{d}\theta \mathrm{d}z \mathrm{d}t \\ &= b\int_{t_1}^{t_2}\int_{-h/2}^{h/2}\int_0^{2\pi} \sigma_\theta (\delta\varepsilon_0 + \beta\delta\beta + z\frac{\delta\beta'}{r}) r \mathrm{d}\theta \mathrm{d}z \mathrm{d}t \\ &= b\int_{t_1}^{t_2}\int_{-h/2}^{h/2}\int_0^{2\pi} \big((\sigma_\theta + (\sigma_\theta\beta)' - \frac{z(\sigma_\theta)''}{r})\delta w \\ &\quad - ((\sigma_\theta)' - \sigma_\theta\beta + \frac{z(\sigma_\theta)'}{r})\delta u_0\big) \mathrm{d}\theta \mathrm{d}z \mathrm{d}t. \end{aligned} \tag{3.15}$$

In correspondence with Eq. (3.2),

$$\begin{aligned} \delta w &= \delta w_0 + z\delta w_1 + z^2 \delta w_2 \\ &= \delta w_0 + z\delta(c_1 w_0) + z^2\delta(c_2 w_0) \\ &= C_1 \delta w_0, \end{aligned} \tag{3.16}$$

with

$$C_1 = 1 + c_1 z + c_2 z^2. \tag{3.17}$$

Re-writting Eq. (3.15), taking into account Eq. (3.16), yields:

$$\begin{aligned} \int_{t_1}^{t_2} \delta S_1 \mathrm{d}t = b\int_{t_1}^{t_2}\int_{-h/2}^{h/2}\int_0^{2\pi} &\big((\sigma_\theta + (\sigma_\theta\beta)' - \frac{z(\sigma_\theta)''}{r})C_1\delta w_0 \\ &- ((\sigma_\theta)' - \sigma_\theta\beta + \frac{z(\sigma_\theta)'}{r})\delta u_0\big) \mathrm{d}\theta \mathrm{d}z \mathrm{d}t. \end{aligned} \tag{3.18}$$

Integration of δS_2 from t_1 to t_2 gives

$$\begin{aligned}\int_{t_1}^{t_2}\delta S_2\mathrm{d}t &= b\int_{t_1}^{t_2}\int_{-h/2}^{h/2}\int_0^{2\pi}(\sigma_r\delta\varepsilon_r)r\mathrm{d}\theta\mathrm{d}z\mathrm{d}t\\ &= b\int_{t_1}^{t_2}\int_{-h/2}^{h/2}\int_0^{2\pi}\sigma_r\delta(w_{,r})r\mathrm{d}\theta\mathrm{d}z\mathrm{d}t\\ &= b\int_{t_1}^{t_2}\int_{-h/2}^{h/2}\int_0^{2\pi}\sigma_r(\delta w_1+2z\delta w_2)r\mathrm{d}\theta\mathrm{d}z\mathrm{d}t\\ &= b\int_{t_1}^{t_2}\int_{-h/2}^{h/2}\int_0^{2\pi}\sigma_r C_2\delta w_0 r\mathrm{d}\theta\mathrm{d}z\mathrm{d}t,\end{aligned}\tag{3.19}$$

with:

$$C_2 = c_1 + 2zc_2.\tag{3.20}$$

Integration over time of the kinetic energy variation yields

$$\begin{aligned}\int_{t_1}^{t_2}\delta T\mathrm{d}t &= \frac{\rho b}{2}\int_{t_1}^{t_2}\int_{-h/2}^{h/2}\int_0^{2\pi}\delta(\dot{\mathbf{r}}\cdot\dot{\mathbf{r}})r\mathrm{d}\theta\mathrm{d}z\mathrm{d}t\\ &= \frac{\rho b}{2}\int_{t_1}^{t_2}\int_{-h/2}^{h/2}\int_0^{2\pi}\delta({v_1}^2+{v_2}^2)r\mathrm{d}\theta\mathrm{d}z\mathrm{d}t\\ &= \frac{\rho b}{2}\int_{t_1}^{t_2}\int_{-h/2}^{h/2}\int_0^{2\pi}(2v_1\delta v_1+2v_2\delta v_2)r\mathrm{d}\theta\mathrm{d}z\mathrm{d}t\\ &= \rho b\int_{t_1}^{t_2}\int_{-h/2}^{h/2}\int_0^{2\pi}\big((-\dot{v}_1-\Omega {v_1}'+v_2\Omega)\delta w\\ &\quad-(\dot{v}_2+\Omega {v_2}'+v_1\Omega)\delta u_0\big)r\mathrm{d}\theta\mathrm{d}z\mathrm{d}t\\ &= \rho b\int_{t_1}^{t_2}\int_{-h/2}^{h/2}\int_0^{2\pi}\big((-\dot{v}_1-\Omega {v_1}'+v_2\Omega)C_1\delta w_0\\ &\quad-(\dot{v}_2+\Omega {v_2}'+v_1\Omega)\delta u_0\big)r\mathrm{d}\theta\mathrm{d}z\mathrm{d}t.\end{aligned}\tag{3.21}$$

The variation of the potential energy of the elastic foundation includes two parts, namely

$$\delta V = \delta V_1 + \delta V_2,\tag{3.22}$$

in which δV_1 and δV_2 are related to the potential energies caused by the radial and circumferential springs which connect the inner surface of the ring to its axis. The integral over time of δV_1 can be evaluated as

$$\begin{aligned}\int_{t_1}^{t_2}\delta V_1\mathrm{d}t &= \int_{t_1}^{t_2}\int_0^{2\pi}k_r w|_{-h/2}\,(R-h/2)\delta w|_{-h/2}\,\mathrm{d}\theta\mathrm{d}t\\ &= \int_{t_1}^{t_2}\int_0^{2\pi}\big(k_r(w_0-w_1h/2+w_2h^2/4)(R-h/2)\delta w_0\\ &\quad-k_rh/2(w_0-w_1h/2+w_2h^2/4)(R-h/2)\delta w_1\\ &\quad+k_rh^2/4(w_0-w_1h/2+w_2h^2/4)(R-h/2)\delta w_2\big)\mathrm{d}\theta\mathrm{d}t\\ &= \int_{t_1}^{t_2}\int_0^{2\pi}k_r w_0(c_3)^2(R-h/2)\delta w_0\mathrm{d}\theta\mathrm{d}t,\end{aligned}\tag{3.23}$$

with

$$c_3 = 1 - \frac{h}{2}c_1 + \frac{h^2}{4}c_2 = 1 - \frac{3k_r h^2}{8EA + 3k_r h^2} < 1. \tag{3.24}$$

Assuming the circumferential springs act on the middle surface of the ring, the integral of δV_2 can be evaluated as

$$\int_{t_1}^{t_2} \delta V_2 \mathrm{d}t = \int_{t_1}^{t_2} \int_0^{2\pi} k_c u_0 R \delta u_0 \mathrm{d}\theta \mathrm{d}t. \tag{3.25}$$

Using the Hamilton's principle,

$$\delta \int_{t_1}^{t_2} (S + V - T)\mathrm{d}t = \int_{t_1}^{t_2} (\delta S + \delta V - \delta T)\mathrm{d}t = 0 \tag{3.26}$$

and by making use of Eq. (3.15) to Eq. (3.25), the nonlinear governing equations can be written in the following integral form:

$$\begin{aligned} & b\int_{\frac{-h}{2}}^{\frac{h}{2}} \Big\{(\sigma_\theta + (\sigma_\theta\beta)' - z(\sigma_\theta)''/r)C_1 + \sigma_r C_2 r\Big\}\mathrm{d}z \\ & + \rho b \int_{\frac{-h}{2}}^{\frac{h}{2}} (\dot{v}_1 + \Omega {v_1}' - \Omega v_2) C_1 r \mathrm{d}z \\ & + k_r w_0 (c_3)^2 (R - h/2) = 0, \end{aligned} \tag{3.27}$$

$$\begin{aligned} & b\int_{\frac{-h}{2}}^{\frac{h}{2}} \Big\{-(\sigma_\theta)' + \sigma_\theta\beta - z(\sigma_\theta)'/r\Big\}\mathrm{d}z \\ & + \rho b \int_{\frac{-h}{2}}^{\frac{h}{2}} (\dot{v}_2 + \Omega {v_2}' + \Omega v_1) r \mathrm{d}z + k_c u_0 R = 0. \end{aligned} \tag{3.28}$$

Eqs. (3.27) and (3.28) govern vibrations of the ring in the radial and circumferential directions. The material the ring is made of is considered to be homogeneous, isotropic and linearly elastic, thus the stress-strain relations are given by

$$\sigma_\theta = E\varepsilon_\theta,\ \sigma_r = E\varepsilon_r. \tag{3.29}$$

3.1.2. STATIC EQUILIBRIUM AND LINEARISED EQUATIONS OF MOTION

The next step is to find the static equilibrium of the rotating ring and then linearise the nonlinear equations in the vicinity thereof. The static equilibrium can be found by solving the nonlinear governing equations. By means of numerical analysis of Eqs. (3.27) and (3.28) under the condition of $\partial/\partial t = 0$, it can be shown that the circumferential displacement vanishes, whereas the radial displacement becomes angle-independent. A qualitatively similar result (no circumferential displacement and a constant radial displacement) was obtained in [9]. Thus, in order to derive the static equilibrium, one may substitute $w_0(\theta, t) = w_{0e}$ and $u_0(\theta, t) = 0$ into Eqs. (3.27) and (3.28) to obtain

$$\begin{aligned} & Eb\int_{\frac{-h}{2}}^{\frac{h}{2}} \Big\{\frac{{C_1}^2 w_{0e}}{r} + r{C_2}^2 w_{0e}\Big\}\mathrm{d}z + k_r w_{0e} {c_3}^2 (R - \frac{h}{2}) \\ & - \rho b \int_{\frac{-h}{2}}^{\frac{h}{2}} \Big\{\Omega^2 r C_1 (r + C_1 w_{0e})\Big\}\mathrm{d}z = 0 \end{aligned} \tag{3.30}$$

where w_{0e} is the static expansion of the middle surface of the ring. One needs to always keep in mind that the static equilibrium co-rotates with the ring at constant angular speed Ω.

Eqs. (3.27) and (3.28) can now be linearised in the vicinity of the static equilibrium by substituting $w_0(\theta,t) = w_{0e} + w_d(\theta,t)$, $u_0(\theta,t) = u_d(\theta,t)$ into Eqs. (3.27) and (3.28), and then neglecting the nonlinear terms with respect to $w_d(\theta,t)$ and $u_d(\theta,t)$. The so-obtained linearised governing equations read

$$\begin{aligned}
&\rho b\int_{\frac{-h}{2}}^{\frac{h}{2}}\Big\{\ddot{w}C_1+2\Omega(\dot{w}'C_1-\dot{u})+\Omega^2(w''C_1-2u'-wC_1)\Big\}C_1 r\,\mathrm{d}z\\
&+Eb\int_{\frac{-h}{2}}^{\frac{h}{2}}\Big\{[(\frac{z}{r^2}+\frac{C_1w_{0e}}{r^2})(u'-C_1w'')+\frac{1}{r}(C_1w+u')-\frac{z}{r^2}(u'''+C_1w'')\\
&+\frac{z^2}{r^3}(C_1w''''-u''')]C_1+rC_2{}^2w\Big\}\mathrm{d}z+k_rwc_3{}^2(R-\frac{h}{2})=0,
\end{aligned}\tag{3.31}$$

$$\begin{aligned}
&\rho b\int_{\frac{-h}{2}}^{\frac{h}{2}}\Big\{\ddot{u}+2\Omega(\dot{u}'+\dot{w}C_1)+\Omega^2(u''+2w'C_1-u)\Big\}r\,\mathrm{d}z\\
&+Eb\int_{\frac{-h}{2}}^{\frac{h}{2}}\Big\{(\frac{z}{r^2}+\frac{z^2}{r^3})(C_1w'''-u'')-(\frac{1}{r}+\frac{z}{r^2})(C_1w'+u'')\\
&-\frac{C_1w_{0e}}{r^2}(C_1w'-u)\Big\}\mathrm{d}z+k_cuR=0,
\end{aligned}\tag{3.32}$$

in which the subscript d in w_d and u_d is omitted for brevity. Eqs. (3.31-3.32) describe small vibrations of the rotating ring about its equilibrium in a space-fixed reference system. These equations can be further simplified by adopting the following truncations:

$$\frac{1}{r}\approx\frac{1}{R}\big(1-\frac{z}{R}+\frac{z^2}{R^2}\big),\ \frac{1}{r^2}\approx\frac{1}{R^2}\big(1-\frac{2z}{R}+\frac{3z^2}{R^2}\big),\ \frac{1}{r^3}\approx\frac{1}{R^3}\big(1-\frac{3z}{R}+\frac{6z^2}{R^2}\big).\tag{3.33}$$

In order to compare the current model with the classical model in [9], it is convenient to introduce the same dimensionless parameters and variables as follows

$$\begin{aligned}
&t_0^2=\frac{\rho AR^4}{EI},\ \tau=\frac{t}{t_0},\ \bar{\Omega}=\Omega t_0,\ \omega=\omega_{\mathrm{dim}}t_0,\ \chi=\frac{AR^2}{I},\ \bar{K}_c=\frac{k_cR^4}{EI},\\
&\bar{K}_r=\frac{k_rR^4}{EI},\ \bar{K}=\frac{k_c}{k_r},\ w=RW,\ u=RU,\ w_{0e}=RW_{0e}
\end{aligned}\tag{3.34}$$

where ω_{dim} is the natural frequency in rad/s. Note that if the cross-section of the ring is rectangular, then $\chi = AR^2/I = 12*(R/h)^2$, where h is the thickness of the cross-section of the ring. Here only rings of rectangular cross-section are considered without loss of generality. It is worth mentioning that the relations between dimensionless parameters used here and the ones introduced in Eq. (2.11) are as follows:

$$(\bar{k}_r,\bar{k}_c)=(\bar{K}_r,\bar{K}_c)/(\chi^2),\ \bar{k}^2=1/\chi,\ \bar{\omega}=\omega/\chi,\ \bar{\gamma}=\bar{k}n,\ \bar{v}=\bar{\Omega}/\sqrt{\chi}.\tag{3.35}$$

By neglecting higher than cubic order terms of h/R, the dimensionless form of the linear governing equations can be written as:

$$(\mathbf{L}+\mathbf{L_{mod}}+\mathbf{K_{mod}})\mathbf{U}=\mathbf{0}. \tag{3.36}$$

The displacement vector $\mathbf{U}$ is $[W,\ U]^T$. Matrix operators $\mathbf{L}$ and $\mathbf{L_{mod}}$ are given by

$$\mathbf{L}=\begin{bmatrix} L_{11} & L_{12} \\ L_{21} & L_{22} \end{bmatrix},\ \mathbf{L_{mod}}=\begin{bmatrix} L_{mod11} & L_{mod12} \\ L_{mod21} & L_{mod22} \end{bmatrix}, \tag{3.37}$$

in which:

$$\begin{aligned}
L_{11} &= \frac{\partial^2}{\partial\tau^2}+2\bar{\Omega}\frac{\partial^2}{\partial\tau\partial\theta}+\left(\bar{\Omega}^2-\bar{N}_0\right)\frac{\partial^2}{\partial\theta^2}+\frac{\partial^4}{\partial\theta^4}-\bar{\Omega}^2+\chi,\\
L_{12} &= -2\bar{\Omega}\frac{\partial}{\partial\tau}-\left(2\bar{\Omega}^2-\chi-\bar{N}_0\right)\frac{\partial}{\partial\theta}-\frac{\partial^3}{\partial\theta^3},\\
L_{21} &= -L_{12},\\
L_{22} &= \frac{\partial^2}{\partial\tau^2}+2\bar{\Omega}\frac{\partial^2}{\partial\tau\partial\theta}+\left(\bar{\Omega}^2-1-\chi\right)\frac{\partial^2}{\partial\theta^2}-\bar{\Omega}^2+\bar{N}_0,
\end{aligned} \tag{3.38}$$

$$\begin{aligned}
L_{mod11} =& \Big(\frac{\alpha\bar{N}_0}{4}-\frac{\alpha^2\bar{N}_0}{4}-\frac{2\alpha\sqrt{3\chi}}{3}-\frac{\alpha\bar{\Omega}^2}{6}+\frac{\alpha^2\bar{\Omega}^2}{12}+\frac{\alpha\bar{\Omega}^2}{3}\sqrt{\frac{3}{\chi}}+\alpha W_{0e}\sqrt{3\chi}-3W_{0e}\\
&+4\Big)\frac{\partial^2}{\partial\theta^2}+\Big(\frac{\alpha^2\bar{\Omega}}{6}-\frac{\alpha\bar{\Omega}}{3}+\frac{2\alpha\bar{\Omega}}{3}\sqrt{\frac{3}{\chi}}\Big)\frac{\partial^2}{\partial\tau\partial\theta}+\Big(\frac{\alpha^2}{12}-\frac{\alpha}{6}+\frac{\alpha}{3}\sqrt{\frac{3}{\chi}}\Big)\frac{\partial^2}{\partial\tau^2}\\
&+\Big(\frac{\alpha^2\chi^2}{9}-\frac{\alpha\chi}{6}+\frac{\alpha^2\chi}{12}+\frac{\alpha\bar{\Omega}^2}{6}-\frac{\alpha^2\bar{\Omega}^2}{12}-\frac{\alpha\sqrt{3\chi}}{3}-\frac{\alpha^2\chi\sqrt{3\chi}}{18}-\frac{\alpha\bar{\Omega}^2}{3}\sqrt{\frac{3}{\chi}}+1\Big),\\
L_{mod12} =& \Big(-\frac{\alpha\bar{N}_0}{6}+\frac{\alpha^2\bar{N}_0}{12}-\frac{\alpha\chi}{12}+\frac{\alpha\bar{\Omega}^2}{6}-1+3W_{0e}-\frac{2\alpha W_{0e}\sqrt{3\chi}}{3}-\frac{\alpha\bar{\Omega}^2}{3}\sqrt{\frac{3}{\chi}}\Big)\frac{\partial}{\partial\theta}\\
&-\Big(\frac{\alpha\sqrt{3\chi}}{6}-2\Big)\frac{\partial^3}{\partial\theta^3}+\Big(\frac{\alpha\bar{\Omega}}{6}-\frac{\alpha\bar{\Omega}}{3}\sqrt{\frac{3}{\chi}}\Big)\frac{\partial}{\partial\tau},\\
L_{mod21} =& -L_{mod12},\\
L_{mod22} =& 3\frac{\partial^2}{\partial\theta^2}-\frac{\alpha\bar{N}_0}{12}-\frac{\alpha W_{0e}\sqrt{3\chi}}{3}+3W_{0e}.
\end{aligned} \tag{3.39}$$

The dimensionless pretension is expressed as

$$\bar{N}_0=\chi W_{0e}. \tag{3.40}$$

W_{0e} is given by the dimensionless form of Eq. (3.30) as follows:

$$W_{0e}=\frac{\bar{\Omega}^2\beta_3}{\beta_1-\beta_2\bar{\Omega}^2}, \tag{3.41}$$

with

$$\begin{aligned}
\beta_1 =& \frac{99\alpha^2}{560} - \frac{3\alpha}{10} + \frac{\alpha^2\sqrt{3\chi}}{20} + \frac{23\alpha^2\chi}{240} + 1 + \bar{K}_m + \chi + \frac{\alpha^2\chi^2}{9} \\
& - \frac{\alpha\chi}{6} - \frac{\alpha\sqrt{3\chi}}{3} - \frac{\sqrt{3}}{18}\alpha^2\chi^{3/2}, \\
\beta_2 =& \frac{\alpha^2}{80} - \frac{\alpha^2}{20}\sqrt{\frac{3}{\chi}} + 1 - \frac{\alpha}{6} + \frac{\alpha^2}{12} + \frac{\alpha}{3}\sqrt{\frac{3}{\chi}}, \\
\beta_3 =& 1 - \frac{\alpha}{12} - \frac{3\alpha}{20\chi} + \frac{1}{\chi} + \frac{\alpha}{3}\sqrt{\frac{3}{\chi}}.
\end{aligned} \tag{3.42}$$

The dimensionless parameter α is defined as

$$\alpha = \frac{4k_r h^2}{8EA + 3k_r h^2} = \frac{48\bar{K}_r}{8\chi^2 + 36\bar{K}_r}. \tag{3.43}$$

The matrix operator $\mathbf{K_{mod}}$ denotes the contribution of the foundation

$$\mathbf{K_{mod}} = \begin{bmatrix} \bar{K}_m & 0 \\ 0 & \bar{K}_c \end{bmatrix}, \tag{3.44}$$

with

$$\bar{K}_m = \bar{K}_r {c_3}^2 \left(1 - \sqrt{\frac{3}{\chi}}\right). \tag{3.45}$$

Recall the expression of c_3 in Eq. (3.24), the dimensionless form of it in terms of α is

$$c_3 = 1 - \frac{3\alpha}{4}. \tag{3.46}$$

If one assumes that $r = R$ and the radial displacement does not vary across the thickness, namely that $w_1 = w_2 = 0$, the governing equations reduce to the ones obtained by Cooley and Parker [9] based on Love's thin shell theory. In this case, the dimensionless form of the governing equations in [9] after rewriting those in a matrix form takes the form:

$$(\mathbf{L} + \mathbf{K})\mathbf{U} = \mathbf{0}. \tag{3.47}$$

Matrix $\mathbf{K}$ represents the contribution of the foundation, which is given by

$$\mathbf{K} = \begin{bmatrix} \bar{K}_r & 0 \\ 0 & \bar{K}_c \end{bmatrix} \tag{3.48}$$

and $\mathbf{L}$ is given by Eq. (3.38). The static expansion of the middle surface W_{0e} is defined by the following dimensionless equality

$$(\chi + \bar{K}_r - \bar{\Omega}^2) W_{0e} = \bar{\Omega}^2. \tag{3.49}$$

Comparing the matrices in Eq. (3.44) and Eq. (3.48) which represent the foundation stiffness, one notes that in the proposed model, the influence of radial springs $\bar{K}_m$ is reduced from $\bar{K}_r$ by the factor

$$c_3{}^2\left(1-\sqrt{\frac{3}{\chi}}\right)<1. \tag{3.50}$$

By observing the entries of the $\mathbf{L_{mod}}$ and $\mathbf{K_{mod}}$, one may notice that the dimensionless parameter α is of importance. It appears in every entry of $\mathbf{L_{mod}}$. Meanwhile, since $\bar{K}_r$ in $\mathbf{K}$ is replaced by $\bar{K}_m$, the contribution of the radial springs is reduced and the magnitude of the reduction is related to α. Thus, the theory introduced in this chapter can be expected to predict a different behaviour of the ring as compared to that predicted by the theory introduced in [9]. This dissimilarity of the predictions will be addressed in the sequel.

Note that in Eq. (3.41), a velocity exists at which the multiplier of W_{0e} becomes zero. This means that at this velocity, the radial expansion and thus the hoop tension become infinitely large. This velocity is termed as $\bar{\Omega}_{cr}$;, a critical rotational speed which is given as

$$\bar{\Omega}_{cr}=\sqrt{\beta_1/\beta_2} \tag{3.51}$$

according to Eq. (3.41). The following analysis is restricted to velocities smaller than $\bar{\Omega}_{cr}$. In [9], this velocity is different and governed by Eq. (3.49) according to which $\bar{\Omega}_{cr}$ equals $\sqrt{\chi+\bar{K}_r}$ in its dimensionless form.

3.2. STABILITY ANALYSIS

In order to maintain the rotation speed constant, power has to be supplied by applying a torque to the ring. Thus, the ring may experience instability at high rotational speeds. In most of the papers devoted to the dynamics of rotating rings, the existence of instability is described in a confusing manner and no solid conclusions are drawn as to its occurrence. In most papers known to the author, the in-plane vibrations of a thin ring are either reported to be stable or the stability matter is not mentioned [9, 13]. In the few papers in which instability is addressed, its occurrence is associated with the velocity at which one of the natural frequencies (considered in the rotating reference system) of the first mode becomes zero. This is a misconception as this situation will not lead to the exponential increase of the ring displacements when a set of initial conditions are applied. This speed is, actually, the speed at which the ring experiences resonance (a linear growth of the displacement in time) when subjected to a co-rotating radial load. Thus, further investigation is needed in order to clarify the presence of instability. In this section, the eigenvalue problem for a rotating thin ring is solved to prove the existence of instability in a theoretical framework.

3.2.1. NATURAL FREQUENCIES OF A ROTATING THIN RING

The natural frequencies of the ring can be obtained by substituting

$$W=W_n\mathrm{e}^{\mathrm{i}n\theta+\mathrm{i}\omega\tau},U=U_n\mathrm{e}^{\mathrm{i}n\theta+\mathrm{i}\omega\tau} \tag{3.52}$$

into Eq. (3.36) and, subsequently, setting the determinant of the coefficient matrix equal to zero. In Eq. (3.52), n is the circumferential wave number and ω is the dimensionless natural frequency.

Since the radial expansion of the ring increases with increasing rotational speed, there should be an upper limit of the rotational speed above which the prestresses due to rotation may exceed the strength of the materials. The prestresses and static expansion need to be examined before one proceeds further. There are two kinds of prestresses which should be examined beforehand [58]; the maximum hoop stress which occurs at the outer surface of the ring [58]

$$\sigma_\theta{}^0|_{h/2} = EW_{0e}(1+\frac{\alpha}{4}) \tag{3.53}$$

and the maximum radial prestress which appears at the inner surface of the ring [58]

$$\sigma_r{}^0|_{-h/2} = E\varepsilon_r|_{-h/2} = EW_{0e}\alpha\sqrt{3\chi}/3. \tag{3.54}$$

At a certain value of the rotational speed, the stress level might exceed the yield stress of the ring and thus the assumption of linear material behaviour would become invalid. Thus, one may use the stress levels of the rotating ring as a criterion for the applicability of a physically linear model. However, in order to avoid a discussion of the physical behaviour of different materials, the maximum prestress $\sigma^0_{max} \leq 0.2E$ is chosen to define the regime in which the ring material is assumed to behave linearly. The rotational speed corresponds to

$$\sigma_\theta{}^0|_{h/2} = 0.2E \tag{3.55}$$

is termed as $\bar{\Omega}_{\theta 02}$, whereas $\bar{\Omega}_{r02}$ is given by

$$\sigma_r{}^0|_{-h/2} = 0.2E. \tag{3.56}$$

The allowable speed for the model to be valid is determined by

$$\bar{\Omega}_a = \min\{\bar{\Omega}_{\theta 02}, \bar{\Omega}_{r02}\}. \tag{3.57}$$

In order to illustrate that instability can occur prior to material failure, the following dimensionless parameters are chosen:

$$\chi = 1200,\ \bar{K}_r = 4\times 10^5,\ \bar{K} = 0.001. \tag{3.58}$$

$\chi = 1200$ corresponds to $h/R = 0.1$ for a ring with rectangular cross-section. These parameters correspond to a ring with small bending stiffness and stiff foundation.

Fig. 3.2 illustrates the relationship between the rotational speeds and the natural frequencies of the first six modes in the space-fixed reference system. Only the real-valued frequencies are drawn and the absolute values are used for convenience. The vertical dotted line corresponds to the speed $\bar{\Omega}_a$ as determined by Eq. (3.57). For the chosen parameters, $\bar{\Omega}_{r02} < \bar{\Omega}_{\theta 02}$ and, therefore, $\bar{\Omega}_a$ is equal to $\bar{\Omega}_{r02}$. For mode number greater than zero, both the lower and higher natural frequencies split into two branches which result in four distinct natural frequencies per mode. However, for the $n = 0$ mode, the natural frequencies do not bifurcate.

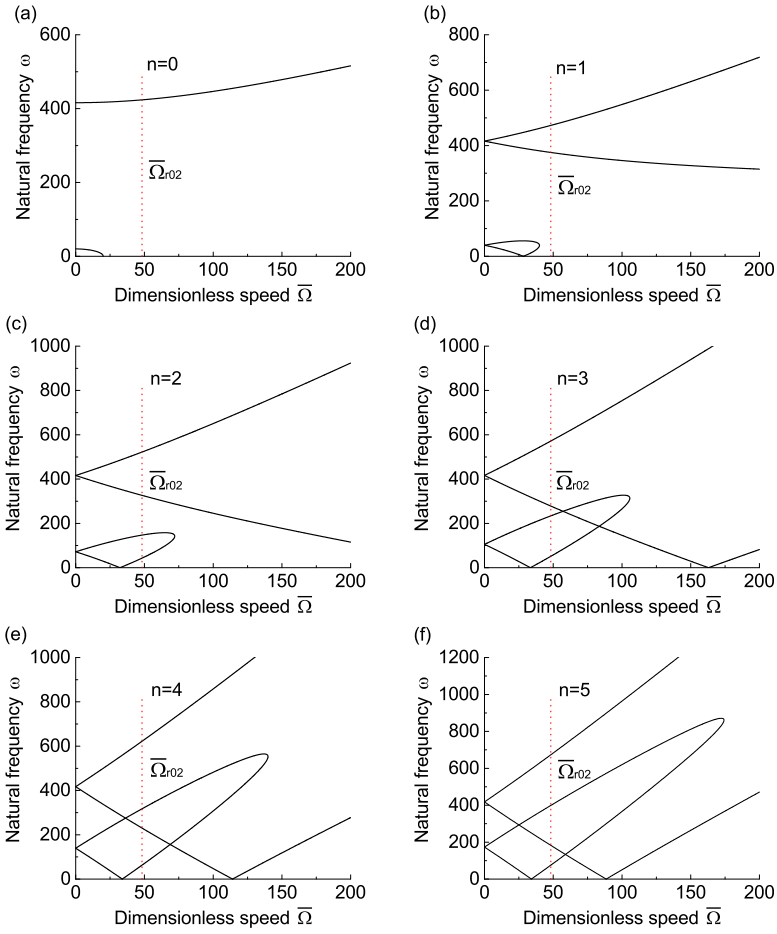

Figure 3.2: Dimensionless natural frequencies versus rotational speeds : $\bar{K}_r = 4 \times 10^5$ and $\bar{K} = 0.001$.

The upper branch of the $n = 0$ mode increases monotonically as the speed of rotation grows. The lower branch first descends and then crosses the horizontal axis at a certain rotational speed. It can be shown that above this speed, the natural frequency becomes purely imaginary which indicates the onset of instability of the divergence type, i.e. the ring becomes unstable without oscillations and its circumferential displacement increases exponentially in time. It is the $n = 0$ rotational mode which becomes unstable. Recently, similar instability was found for magnetically levitated rotating rings by Arena and Lacarbonara [59].

For modes $n \geq 1$, one can see that the lower set of natural frequencies first branches into two curves at $\bar{\Omega} > 0$, then the two curves collide with each other and disappear from the real plane (become complex-valued) after a certain speed. Since the characteristic polynomial has real-valued coefficients, the complex roots appear in conjugate pairs and one may say that flutter occurs after the collision speed, i.e. the ring becomes unstable

while vibrating. If natural frequencies are computed in the rotating coordinate system, the same conclusion regarding instability is reached because the natural frequencies in the rotating and space-fixed reference systems are related by a real-valued kinematic shift [21]. This shift only changes the real part of the natural frequencies which has no effect on the stability. In contrast to ref. [15], the lower natural frequency of $n = 1$ in space-fixed reference system may also bifurcate.

From Fig. 3.2 one can also observe that the lowest speed at which instability occurs is for the mode $n = 0$. Thus in this case, flutter instability is unrealistic as the divergence instability always occurs first [89].

3.2.2. STATIONARY MODES

Another observation from Fig. 3.2 is that at some rotational speeds, the natural frequencies of the backward travelling waves become zero. These speeds correspond to stationary modes observed in the space-fixed reference [19]. According to [19], in the case of a rotating ring, when the natural modes in space-fixed reference system are considered, the motion becomes stationary if

$$\Omega = \frac{\omega_{rn}}{n}, (n\text{=}1,2,3...) \tag{3.59}$$

where ω_{rn} (implicit function of Ω) is the nth natural frequency in the rotating reference system. The mode appears as a stationary displacement pattern of the ring to an observer in a space-fixed reference system. This condition is also the resonance condition for a rotating ring subjected to a stationary constant load. When Eq. (3.59) is satisfied, the ring length is divisible by the wavelength of one of the waves excited by the load.

Since the natural frequency ω_n in the space-fixed reference system is related to the corresponding one in the rotating reference system via a constant kinematic shift [21], i.e. $\omega_n = \omega_{rn} - n\Omega$, the condition for stationary modes given by Eq. (3.59) reduces to

$$\omega_n = \omega = 0. \tag{3.60}$$

The theoretical prediction of resonances of a rotating ring subjected to a stationary load is still a disputed matter. The most commonly used Endo-Huang-Soedel model [13, 14] predicts no resonances for any speeds. However, Lin and Soedel argued that the inability of the classical theory to predict resonances is due to the use of incomplete strain-displacement relation and resonance speeds are shown in [18]. In this study, resonances are found. The lowest resonance speed is the critical speed at which the “standing wave" of a rolling tyre is initiated. However, proper equivalent parameters need to be determined [88].

For the chosen parameters, resonance occurs at rotational speeds higher than the speed at which divergence instability of $n = 0$ mode is initiated. However, with increasing circumferential stiffness of the foundation, the instability of $n = 0$ mode may take place at a speed higher than the minimum resonance speed.

3.2.3. COMPARISON WITH THE CLASSICAL THEORIES

As stated before, it is a high stiffness of the elastic foundation that can make the through-thickness variation of the radial stress significant. To illustrate the influence of this varia-

tion, the static radial expansion w_{0e} of the middle surface of the ring is considered. This expansion is usually obtained as [9]

$$W_{0e} = \frac{\bar{\Omega}^2}{\bar{K}_r + \chi - \bar{\Omega}^2} \tag{3.61}$$

or approximated by [13, 14]

$$W_{0e} = \bar{\Omega}^2/\chi. \tag{3.62}$$

Fig. 3.3(a) shows W_{0e} predicted by the current model, i.e. Eq. (3.41) and Eqs. (3.61-3.62). Fig. 3.3(b) shows the stiffness of the radial springs versus the speed of rotation at which $W_{0e} = 0.2$ (and thus the initial hoop stress of the middle surface is $0.2E$) for the current model and Eq. (3.61). For Eq. (3.62), the velocity corresponding to $W_{0e} = 0.2$ is constant and independent of $\bar{K}_r$. As expected, the comparison shows that for a ring on stiff foundation, the model in [13, 14] overestimates the radial expansion whereas the model in [9] underestimates it. The larger the stiffness of the radial springs, the stronger the effect of the through-thickness variation of the radial stress.

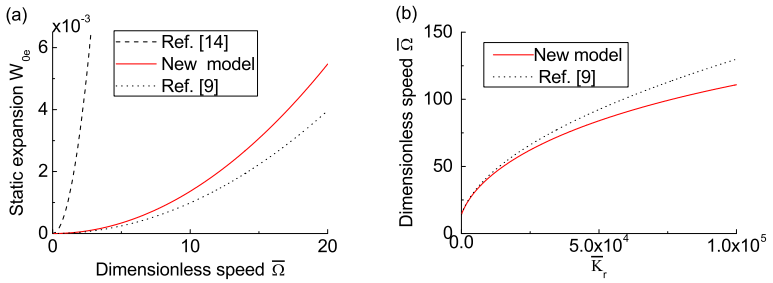

Figure 3.3: Radial expansion comparisons for $\chi = 1200$ and $\bar{K}_r = 1\times10^5$: (a) W_{0e} versus $\bar{\Omega}$; (b) Rotational speeds correspond to $W_{0e} = 0.2$.

3.3. PARAMETRIC STUDY

The influence of the ring parameters on the system stability is investigated in this section. The focus is placed on the effect of the dimensionless extensional stiffness χ and the stiffness of the elastic foundation. Our analysis is restricted to speeds lower than $\bar{\Omega}_{cr}$ predicted by Eq. (3.51).

3.3.1. INFLUENCE OF EXTENSIONAL STIFFNESS

In this subsection, the influence of extensional stiffness χ is discussed. For a ring of a rectangular cross-section, χ is related to the h/R ratio. The discussion will be limited to $\chi > 300$.

Fig. 3.4 shows the influence of the extensional stiffness on stability for different values of the foundation stiffness. In real applications, the stiffness of circumferential springs is usually smaller than that of the radial springs. In each subplot of Fig. 3.4, there are three dotted lines representing the speeds $\bar{\Omega}_{\theta 02}$, $\bar{\Omega}_{r02}$ and $\bar{\Omega}_{cr}$ predicted by Eqs.

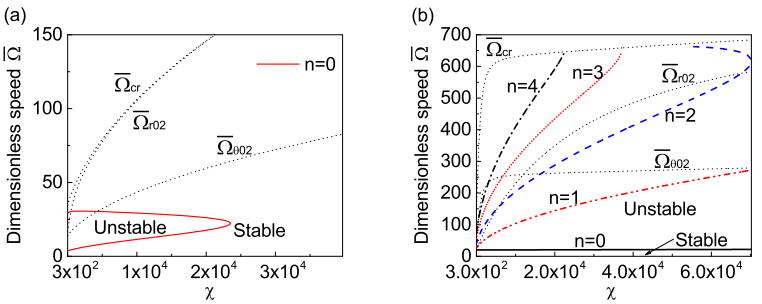

Figure 3.4: Influence of extensional stiffness on stability regions: (a) $\bar{K}_c = 10$ and $\bar{K}_r = 1000$; (b) $\bar{K}_c = 4 \times 10^2$ and $\bar{K}_r = 4 \times 10^5$.

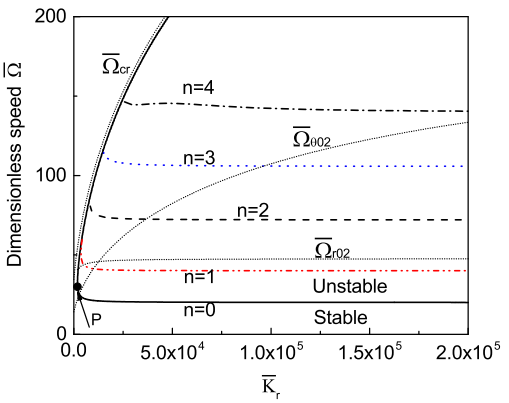

Figure 3.5: Influence of radial springs on stability regions: $\chi = 1200$ and $\bar{K}_c = 4 \times 10^2$.

(3.55-3.56) and Eq. (3.51), respectively. The model is assumed to be valid when the rotational speeds are smaller than the allowable speed $\bar{\Omega}_a$ given by Eq. (3.57). The other curves represent the stability boundary for a specific mode as indicated in the figures. There exist two situations in which the influence of the extensional stiffness is qualitatively different. The area in the enclosed region of Fig. 3.4(a) and the area which is located at the upper side of the $n = 0$ curve of Fig. 3.4(b) are the unstable regions. Fig. 3.4(a) is drawn assuming a relatively soft foundation. For the chosen parameters of the foundation, only divergence instability of mode 0 exists. The figure implies that when χ increases, the unstable region shrinks and finally instability disappears. In contrast, in Fig. 3.4(b), in which a relatively stiff foundation is assumed, the speed that corresponds to the onset of instability at $n = 0$ is almost constant regardless of the value of χ. In both cases, the onset of instability is associated with the divergence of the mode $n = 0$. Fig. 3.4(b) also shows flutter at higher modes. However divergence develops always at lower rotational speed.

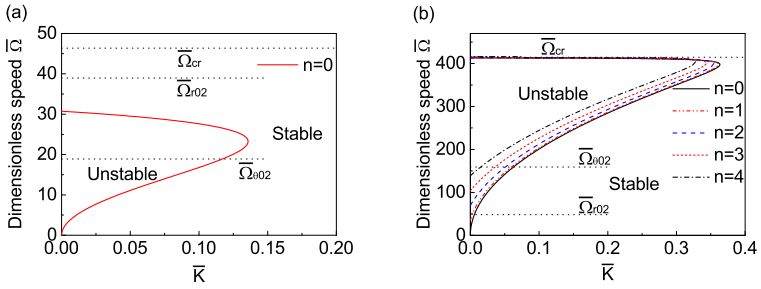

Figure 3.6: Influence of circumferential springs on stability regions: (a) $\chi = 1200$ and $\bar{K}_r = 1000$; (b) $\chi = 1200$ and $\bar{K}_r = 4 \times 10^5$.

3.3.2. INFLUENCE OF THE ELASTIC FOUNDATION

In this subsection, the influence of the radial and circumferential springs on the instability is investigated. Fig. 3.5 shows the evolution of the stability regions with increasing stiffness of the radial springs. The extensional stiffness χ is 1200 and $\bar{K}_c = 4 \times 10^2$ in this plot. The speeds $\bar{\Omega}_{\theta 02}$, $\bar{\Omega}_{r02}$ and $\bar{\Omega}_{cr}$ are plotted together with the stability boundaries for modes 0 to 4. The divergence of $n = 0$ mode occurs at lower speed than flutter and thus is the boundary of stability and instability. The results show that with increasing $\bar{K}_r$, the speeds associated with the occurrence of instability converge to a constant value for all the modes for the chosen parameters. When the value of $\bar{K}_c$ is changed, the plot is qualitatively the same. It is interesting to note that there exists a certain value of $\bar{K}_r$, namely the value of $\bar{K}_r$ at point P, below which the rotating ring is always stable.

Suppose $\bar{K}_c = 0$, namely the circumferential springs are omitted. Solving Eq. (3.41) for $\bar{\Omega}$ and then substituting the obtained $\bar{\Omega}$ together with $n = 0$ and $\omega = 0$ to the characteristic polynomial, one will obtain

$$FW_{0e} = 0, \tag{3.63}$$

where coefficient F is a function of the rotational speed and the parameters of the ring. One solution for the above equation is $W_{0e} = 0$, and consequently $\bar{\Omega} = 0$. This means that actually for $\bar{K} = 0$, an infinitesimal rotating speed would yield divergence. This conclusion is only of mathematical interest since in reality, no such rings exist.

There are two qualitatively different situations regarding the influence of circumferential springs. This is similar to the influence of the extensional stiffness on instability. Fig. 3.6 illustrates the stable and unstable regions of a rotating ring with $\chi = 1200$ for both of the subplots. Fig. 3.6(a) is plotted for relatively soft radial springs and Fig. 3.6(b) for relatively stiff ones. The area in the enclosed region in Fig. 3.6(a) and the area which is located on the left side of the $n = 0$ curve of Fig. 3.6 (b) are the unstable regions. The horizontal dotted lines stand for the velocities determined by Eqs. (3.55-3.56) and Eq. (3.51). For soft radial springs, only $n = 0$ divergence will occur and for stiff ones, high order flutter instability is predicted mathematically. The plot shows that the circumferential foundation is a stabilising factor.

One can also conclude from Fig. 3.6 that for a fixed value of $\bar{K}_r$, there exists a certain value of $\bar{K}$, after which the ring is stable at all speeds of rotation. Fig. 3.7(a) maps the

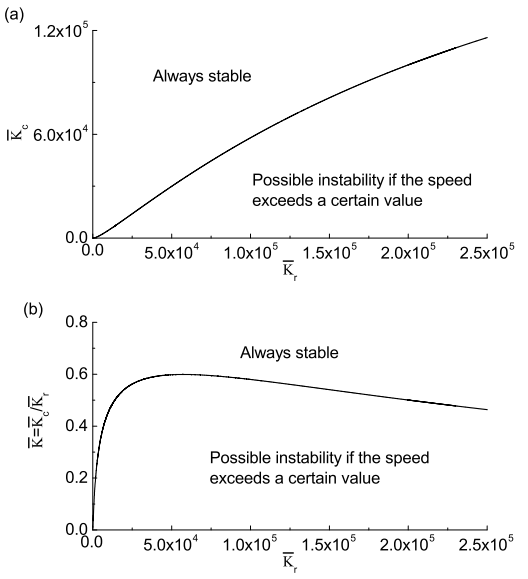

Figure 3.7: Stable and possibly unstable regions with $\chi = 1200$: (a) $\bar{K}_r$ and $\bar{K}_c$ plane; (b) $\bar{K}_r$ and $\bar{K}$ plane.

relation between this certain value of $\bar{K}_r$ and the corresponding $\bar{K}_c$. The curve separates the stable and possible unstable regions for every combination of $\bar{K}_r$ and $\bar{K}_c$. For the parameters in the upper region, the ring is stable at any speed of rotation. In contrast, in the lower region, the ring can be unstable if the rotational speed exceeds a critical value. This speed depends on the physical parameters of the ring and the foundation. Fig. 3.7(b) maps the stable and possible unstable regions in the $\bar{K}_r$ and $\bar{K}$ plane. It can be seen that for small $\bar{K}_c/\bar{K}_r$ ratio, the ring is destabilised by increasing $\bar{K}_r$. The effect of $\bar{K}_r$ is more complicated for larger $\bar{K}$. If $\bar{K}$ is fixed, when $\bar{K}_r$ increases from zero, the ring will be destabilised at a certain value and then stabilised again.

3.4. TRUNCATION OF THE GEOMETRICALLY-EXACT STRAIN

One can also employ the geometrically exact strain-displacement relations to derive the governing equations. The exact strain-displacement relation in the middle surface of the ring given by Stein [24] is of the form

$$\bar{\varepsilon}_\theta = \sqrt{(1+\varepsilon_0)^2 + \beta^2} - 1 = e \tag{3.64}$$

where β and ε_0 are given by Eqs. (3.3) and (3.5). When the exact strain-displacement relation is used, the variation of δS_1 is given by

$$\begin{aligned}
\int_{t_1}^{t_2} \delta S_1 \mathrm{d}t &= b\int_{t_1}^{t_2}\int_{-h/2}^{h/2}\int_0^{2\pi} (\sigma_\theta \delta\varepsilon_\theta) r \mathrm{d}\theta \mathrm{d}z \mathrm{d}t \\
&= b\int_{t_1}^{t_2}\int_{-h/2}^{h/2}\int_0^{2\pi} \sigma_\theta \delta\Big(\sqrt{(1+\varepsilon_0)^2+\beta^2} - 1 + z\frac{\beta'}{r}\Big) r \mathrm{d}\theta \mathrm{d}z \mathrm{d}t \\
&= b\int_{t_1}^{t_2}\int_{-h/2}^{h/2}\int_0^{2\pi} \Big(\frac{\sigma_\theta}{e+1}\delta((1+\varepsilon_0)^2+\beta^2) + z\sigma_\theta\frac{\delta\beta'}{r}\Big) r \mathrm{d}\theta \mathrm{d}z \mathrm{d}t \\
&= b\int_{t_1}^{t_2}\int_{-h/2}^{h/2}\int_0^{2\pi} \Big\{\frac{\sigma_\theta}{e+1}\big(2(1+\varepsilon_0)\delta\varepsilon_0 + 2\beta\delta\beta\big) \\
&+ z\sigma_\theta\frac{\delta u' - \delta w''}{r^2}\Big\} r \mathrm{d}\theta \mathrm{d}z \mathrm{d}t \\
&= b\int_{t_1}^{t_2}\int_{-h/2}^{h/2}\int_0^{2\pi} \Big\{\big(\sigma_{\theta\,mod} + (\sigma_{\theta\,mod}\beta)' + \sigma_{\theta\,mod}\varepsilon_0 - \frac{z(\sigma_\theta)''}{r}\big)\delta w \\
&- \big((\sigma_{\theta\,mod})' - \sigma_{\theta\,mod}\beta + (\sigma_{\theta\,mod}\varepsilon_0)' + \frac{z(\sigma_\theta)'}{r}\big)\delta u\Big\} \mathrm{d}\theta \mathrm{d}z \mathrm{d}t
\end{aligned} \tag{3.65}$$

with

$$\sigma_{\theta\,mod} = \frac{\sigma_\theta}{e+1} = \frac{E(e+zK_\theta)}{1+e} \tag{3.66}$$

where K_θ is given in Eq. (3.7). It can be verified that the axisymmetric static equilibria are the same regardless of whether the geometrically exact strain-displacement relation or its quadratic truncation (the engineering strain) is applied. However, the linearised governing equations do change.

In order to linearise the governing equations, the Taylor expansion of $\sigma_{\theta\,mod}$ to the third order is applied (it is not possible to keep the square root in the derivation), which is given by (neglecting high order terms related to z/r^2 since the ring is assumed to be thin)

$$\sigma_{\theta\,mod} \approx E(\varepsilon_0 + zK_\theta - {\varepsilon_0}^2 + \frac{\beta^2}{2} + {\varepsilon_0}^3 - \frac{3\varepsilon_0\beta^2}{2}). \tag{3.67}$$

The Taylor expansion of σ_θ to the second order is given by

$$\sigma_\theta \approx E(\varepsilon_0 + zK_\theta + \frac{\beta^2}{2}). \tag{3.68}$$

If σ_θ is expanded to the third order in order to be consistent with Eq. (3.67), one obtains

$$\sigma_\theta \approx E(\varepsilon_0 + zK_\theta + \frac{\beta^2}{2} - \frac{\varepsilon_0\beta^2}{2}). \tag{3.69}$$

The choice of Eq. (3.68) or Eq. (3.69) does not influence the linearised governing equations if we work out the derivation. Therefore, for brevity Eq. (3.68) is used in the follow-

ing. Thus the integrands of Eq. (3.65) become

$$
\begin{aligned}
&\Big(\sigma_{\theta mod} + (\sigma_{\theta mod}\beta)' + \sigma_{\theta mod}\varepsilon_0 - \frac{z(\sigma_\theta)''}{r}\Big)\delta w \\
=&\Big(E(\varepsilon_0 + zK_\theta - {\varepsilon_0}^2 + \frac{\beta^2}{2} + {\varepsilon_0}^3 - \frac{3\varepsilon_0\beta^2}{2}) + (E(\varepsilon_0 + zK_\theta - {\varepsilon_0}^2 + \frac{\beta^2}{2})\beta)' + \\
&E(\varepsilon_0 + zK_\theta - {\varepsilon_0}^2 + \frac{\beta^2}{2})\varepsilon_0 - \frac{z(E(\varepsilon_0 + zK_\theta + \frac{\beta^2}{2}))''}{r}\Big)\delta w \\
=&\Big(E(\varepsilon_0 + zK_\theta + \frac{\beta^2}{2}) + \boxed{(E(\varepsilon_0 + zK_\theta + \frac{\beta^2}{2})\beta)'} - \frac{zE(\varepsilon_0 + zK_\theta + \frac{\beta^2}{2})''}{r} \\
&\underbrace{-(E{\varepsilon_0}^2\beta)' - E\varepsilon_0\beta^2}\Big)\delta w
\end{aligned}
\tag{3.70}
$$

and

$$
\begin{aligned}
&-\Big((\sigma_{\theta mod})' - \sigma_{\theta mod}\beta + (\sigma_{\theta mod}\varepsilon_0)' + \frac{z(\sigma_\theta)'}{r}\Big)\delta u \\
=&\Big(-E(\varepsilon_0 + zK_\theta - {\varepsilon_0}^2 + \frac{\beta^2}{2} + {\varepsilon_0}^3 - \frac{3\varepsilon_0\beta^2}{2})' + E(\varepsilon_0 + zK_\theta - {\varepsilon_0}^2 + \frac{\beta^2}{2})\beta - \\
&(E(\varepsilon_0 + zK_\theta - {\varepsilon_0}^2 + \frac{\beta^2}{2})\varepsilon_0)' - \frac{zE(\varepsilon_0 + zK_\theta + \frac{\beta^2}{2})'}{r}\Big)\delta u \\
=&\Big(-E(\varepsilon_0 + zK_\theta + \frac{\beta^2}{2})' + \boxed{E(\varepsilon_0 + zK_\theta + \frac{\beta^2}{2})\beta} - \frac{zE(\varepsilon_0 + zK_\theta + \frac{\beta^2}{2})'}{r} \\
&\underbrace{-(E{\varepsilon_0}^2\beta) + (E\varepsilon_0\beta^2)'}\Big)\delta u
\end{aligned}
\tag{3.71}
$$

to the cubic truncation. Two extra terms in each equation of motion are present as indicated by the wavy lines underlying these terms. The two terms may be important for the nonlinear behaviour of the ring, however, their contributions to the linear governing equations are one order smaller than the corresponding terms in the boxes in Eqs. (3.70) and (3.71). Specifically, the linear contribution of the boxed term in Eq. (3.70) is

$$
\boxed{(E(\varepsilon_0 + zK_\theta + \frac{\beta^2}{2})\beta)'} \to E\frac{w_{0e}}{r}\beta' \tag{3.72}
$$

whereas the contribution from the extra terms is

$$
\underbrace{-(E{\varepsilon_0}^2\beta)' - E\varepsilon_0\beta^2} \to E(\frac{w_{0e}}{r})^2\beta'. \tag{3.73}
$$

Similarly, for Eq. (3.71)

$$
\boxed{E(\varepsilon_0 + zK_\theta + \frac{\beta^2}{2})\beta} \to E\frac{w_{0e}}{r}\beta \tag{3.74}
$$

whereas

$$
\underbrace{-(E{\varepsilon_0}^2\beta) + (E\varepsilon_0\beta^2)'} \to E(\frac{w_{0e}}{r})^2\beta. \tag{3.75}
$$

Thus it is concluded that the extra terms are not important for predicting the onset and type of instability of the equilibrium of the rotating ring.

3.5. CONCLUSIONS

In this chapter, an improved rotating thin ring model which accounts for the through-thickness variation of the radial stress has been developed to investigate stability of the in-plane free vibration of the ring. The choice of the nonlinear strain-displacement relation is essential for the consideration of the stiffening effect. The nonlinear strain expression is based on the quadratic truncation of the exact strain-displacement relation. The proposed model takes into account the distribution of through-thickness variation of the radial stress. This is of importance especially for rings that are supported by relatively stiff foundation and rotate at high speeds. In this case, the radial stress is zero at the outer surface of the ring but can be large at the inner surface. By considering the through-thickness variation of the radial stress, additional inertial and stiffness terms are included in the governing equations.

Instability, which is usually overlooked in the literature, has been predicted. Divergence instability of the 0th mode always occurs before flutter instability of higher modes, i.e. $n \geq 1$. The influences of ring parameters on the stability of rotating rings have been investigated. It is shown that the stiffness of circumferential springs influences strongly the critical speed at which instability occurs. If the circumferential stiffness is absent, then for an infinitesimal rotating speed divergence will occur. However, the stiffness of radial springs is a destabilising factor since it constrains the radial expansion of the ring and thus the stiffening effect due to hoop tension decreases. More interestingly, if the stiffness of radial springs is smaller than a certain value for a fixed value of the stiffness of circumferential springs, instability never occurs. This observation may be useful in engineering design. An experiment for a soft ring is needed to close the debate on the existence of instability of in-plane vibrations of a rotating ring.

Stationary modes, which may take place at speeds lower or higher than the one related to instability have been briefly discussed as well. These modes correspond to resonances of a rotating ring subjected to a stationary load.

Although the model proposed in this chapter introduces through-thickness variation of radial stress which allows the satisfaction of the boundary conditions at $z = -h/2$ and $z = h/2$, the model is classified as an improved classical low-order model since the resulting equations of motion are associated with displacements of middle surface only. In addition, the Poisson's ratio effect is neglected. By neglecting the Poisson's ratio, the boundary conditions at both surfaces can be exactly satisfied by relating the higher order displacement components to the lower order terms in a linear manner. In the next Chapter, a generic high-order model is developed including the Poisson's ratio effect to further improve the predictions of dynamics of rotating rings.

4

A HIGH-ORDER THEORY FOR ROTATING RINGS ON ELASTIC FOUNDATION

An elastic foundation can considerably change the coupling of the flexural and extensional motions of a rotating ring as shown in Chapters 2 and 3. Based on thin ring model, the non-zero radial stress at the inner surface of the ring and its through-thickness variation are accounted for in Chapter 3 by introducing higher order terms in the radial displacement component. Thus, the model can deal with rotating thin rings with stiff radial supports whereas the circumferential supports are relatively soft. In fact the shear stress at the inner surface is non-zero because of the presence of circumferential springs. The stress boundary effect regarding shear stress requires higher order corrections in circumferential direction to be taken into account. In addition, for rings resting on stiff foundation, the wave dispersion characteristics are not correctly predicted by the classical low-order theories and improved model based on them, as shown in chapters 2-3. This fact calls for theories which can account for higher order effects, e.g. transverse shear deformation and beyond.

A high-order model for in-plane vibrations of rotating rings is developed in this chapter. The developed model enables the dynamic analysis of the rings on stiff elastic foundation that rotate with a high speed. The traction force at the inner surface of such rings is so high that it influences significantly the through-thickness stress distribution. This effect cannot be captured by the classical low order theories while the model proposed in this chapter can account for this effect. The displacement fields are assumed to be polynomials of the through-thickness coordinate in both the radial and circumferential directions. The derivation is generic and can yield ring theories of different order, i.e. of the Timoshenko-type and beyond, with proper consideration of both the internal state

This chapter has been published as a journal paper in *Journal of Sound and Vibration* **455**, 118(2019) [90]. Minor changes are made.

of the body and the stress boundary effects at the surfaces.

The main contribution of this chapter is the introduction of a relatively versatile and generic rotating ring model. The model developed in this chapter extends the model introduced in Chapter 3, in which only the variation of through-thickness radial stress is accounted for. The proposed model can be implemented to deal with vibrations of moderately thick rings, rings supported by stiff foundation, vibrations of rotating rings at high frequencies and high rotational speeds. The superiority of the present high-order theory over existing models is examined by comparing the frequency spectrum obtained from various models and the linear elasticity theory for the corresponding stationary ring case.

4.1. DERIVATION OF THE NONLINEAR GOVERNING EQUATIONS

In this section, the governing equations for a rotating ring of rectangular cross-section are derived taking into account the through-thickness variation of displacements and stresses.

The model under consideration is the same as shown in Fig. 3.1. The definitions of the properties of the ring and the coordinate system are the same as the ones defined in Chapter 3. The ring rotates at an angular speed Ω. During this derivation, a space-fixed coordinate (r,θ) is used. The radial and circumferential displacements of the ring with respect to the undeformed configuration are designated by $w(z,\theta,t)$ and $u(z,\theta,t)$, respectively. Note that the stiffnesses of the radial and circumferential springs *per unit area* are defined as k_r and k_c (N/m^3), respectively.

The nonlinear strain-displacement relation for the circumferential strain ε_θ, the radial strain ε_r and the shear strain $\gamma_{\theta r}$ of a differential element in the ring are given by [24]

$$\begin{aligned}
\varepsilon_\theta &= \varepsilon_0 + \frac{1}{2}(\beta)^2,\\
\varepsilon_r &= w_{,r} + \frac{1}{2}(u_{,r})^2,\\
\gamma_{\theta r} &= (1-w_{,r})u_{,r} - \beta\eta,
\end{aligned} \tag{4.1}$$

with:

$$\begin{aligned}
&\varepsilon_0 = \frac{u'}{r} + \frac{w}{r},\ \beta = \frac{u}{r} - \frac{w'}{r},\ \eta = 1-\varepsilon_0,\\
&u_{,r} = \frac{\partial u}{\partial r} = \frac{\partial u}{\partial z},\ w_{,r} = \frac{\partial w}{\partial r} = \frac{\partial w}{\partial z}.
\end{aligned} \tag{4.2}$$

Hereafter, the prime stands for the partial derivative with respect to θ whereas the subscript $(,r)$ stands for the partial derivative with respect to r. Since $r = R+z$ the derivative with respect to r equals that with respect to z. All strain components are functions of (z,θ,t), e.g. $\varepsilon_\theta \rightarrow \varepsilon_\theta(z,\theta,t)$.

The in-plane motions of the ring can either be considered within the plane strain or plane stress formulations, depending on the ring geometry. Without loss of generality,

the isotropic linear elastic stress-strain relations can be written as [91]:

$$\begin{Bmatrix} \sigma_r \\ \sigma_\theta \\ \tau_{r\theta} \end{Bmatrix} = \begin{bmatrix} 2\mu+\bar{\lambda} & \bar{\lambda} & 0 \\ \bar{\lambda} & 2\mu+\bar{\lambda} & 0 \\ 0 & 0 & \mu \end{bmatrix} \begin{Bmatrix} \varepsilon_r \\ \varepsilon_\theta \\ \gamma_{r\theta} \end{Bmatrix} \tag{4.3}$$

in which the coefficient $\bar{\lambda}$ is defined as

$$\bar{\lambda} = \lambda \qquad \text{(plane strain)}, \tag{4.4a}$$

$$\bar{\lambda} = \frac{2\mu\lambda}{2\mu+\lambda} = \frac{E\nu}{1-\nu^2} \qquad \text{(plane stress)} \tag{4.4b}$$

where λ and μ are the Lamé constants of the material which can be expressed by

$$\lambda = \frac{E\nu}{(1+\nu)(1-2\nu)}, \quad \mu = G = \frac{E}{2(1+\nu)} \tag{4.5}$$

in terms of Poisson's ratio ν and Young's modulus E; G is the shear modulus.

The velocity vector of a differential element of the ring in the space-fixed frame reads

$$\begin{aligned} \dot{\mathbf{r}} &= \big(\dot{w} + (w' - u)\Omega\big)\mathbf{e}_r + \big(\dot{u} + (r + w + u')\Omega\big)\mathbf{e}_\theta \\ &= v_1\,\mathbf{e}_r + v_2\,\mathbf{e}_\theta. \end{aligned} \tag{4.6}$$

The vectors $\mathbf{e}_r$ and $\mathbf{e}_\theta$ are unit vectors in the radial and circumferential directions, respectively. The overdot represents partial derivative with respect to time.

To derive the complete equations of motion, the Hamilton's principle is used, i.e.

$$\delta \int_{t_1}^{t_2} (S + V - T)\,\mathrm{d}t = \int_{t_1}^{t_2} (\delta S + \delta V - \delta T)\,\mathrm{d}t = 0 \tag{4.7}$$

where S is the strain energy, T is the kinetic energy and V is the potential energy stored in the elastic foundation.

The variation of strain energy is given by

$$\delta S = \delta S_1 + \delta S_2 + \delta S_3 \tag{4.8}$$

in which δS_1 is the variation of the strain energy associated with circumferential strain, δS_2 is the strain energy related to shear strain and δS_3 is the addition to that due to a non-zero radial strain.

Integrating δS_1 between two time instants, t_1 and t_2, yields

$$\begin{aligned}
\int_{t_1}^{t_2} \delta S_1 \,\mathrm{d}t &= b\int_{t_1}^{t_2}\int_{-h/2}^{h/2}\int_0^{2\pi} (\sigma_\theta\,\delta\varepsilon_\theta) r\,\mathrm{d}\theta\mathrm{d}z\mathrm{d}t \\
&= b\int_{t_1}^{t_2}\int_{-h/2}^{h/2}\int_0^{2\pi} \sigma_\theta\,\delta\big[\varepsilon_0+\frac{1}{2}(\beta)^2\big] r\,\mathrm{d}\theta\mathrm{d}z\mathrm{d}t \\
&= b\int_{t_1}^{t_2}\int_{-h/2}^{h/2}\int_0^{2\pi} \sigma_\theta(\delta\varepsilon_0+\beta\,\delta\beta) r\,\mathrm{d}\theta\mathrm{d}z\mathrm{d}t \\
&= b\int_{t_1}^{t_2}\int_{-h/2}^{h/2}\int_0^{2\pi} \big\{[\sigma_\theta+(\sigma_\theta\,\beta)']\delta w \\
&\quad -[(\sigma_\theta)'-\sigma_\theta\,\beta]\delta u\big\}\,\mathrm{d}\theta\mathrm{d}z\mathrm{d}t \\
&\quad + b\int_{t_1}^{t_2}\int_{-h/2}^{h/2}\Big[\,(\sigma_\theta\delta u)\,\big|_0^{2\pi} - \big(\sigma_\theta\beta\delta w\big)\,\big|_0^{2\pi}\,\Big]\,\mathrm{d}z\mathrm{d}t.
\end{aligned} \tag{4.9}$$

The last integral in Eq. (4.9) vanishes because the displacements at $\theta = 0$ and at $\theta = 2\pi$ are equal.

The integration of δS_2 from t_1 to t_2 reads

$$\begin{aligned}
\int_{t_1}^{t_2} \delta S_2 \,\mathrm{d}t &= b\int_{t_1}^{t_2}\int_{-h/2}^{h/2}\int_0^{2\pi} (\tau_{\theta r}\,\delta\gamma_{\theta r}) r\,\mathrm{d}\theta\mathrm{d}z\mathrm{d}t \\
&= b\int_{t_1}^{t_2}\int_{-h/2}^{h/2}\int_0^{2\pi} \tau_{\theta r}\,\delta[u_{,r}(1-w_{,r})-\beta\eta] r\,\mathrm{d}\theta\mathrm{d}z\mathrm{d}t \\
&= b\int_{t_1}^{t_2}\int_{-h/2}^{h/2}\int_0^{2\pi} \Big\{r\,\tau_{\theta r}(1-w_{,r})\delta u_{,r} - r\,\tau_{\theta r}\,u_{,r}\,\delta w_{,r} \\
&\quad + r\big[\frac{\tau_{\theta r}\,\beta}{r} - \frac{(\tau_{\theta r}\,\eta)'}{r}\big]\delta w - r\big[\frac{\tau_{\theta r}\,\eta}{r} + \frac{(\tau_{\theta r}\,\beta)'}{r}\big]\delta u\Big\}\,\mathrm{d}\theta\mathrm{d}z\mathrm{d}t \\
&= b\int_{t_1}^{t_2}\int_{-h/2}^{h/2}\int_0^{2\pi} \Big\{\big[\tau_{\theta r}\,\beta - (\tau_{\theta r}\,\eta)' + (r\,\tau_{\theta r}\,u_{,r})_{,r}\big]\delta w \\
&\quad -\big[\tau_{\theta r}\,\eta + (\tau_{\theta r}\,\beta)' + (r\,\tau_{\theta r}(1-w_{,r}))_{,r}\big]\delta u\Big\}\,\mathrm{d}\theta\mathrm{d}z\mathrm{d}t \\
&\quad + b\int_{t_1}^{t_2}\int_0^{2\pi}\Big\{\big(-\tau_{\theta r}\,u_{,r}\,\delta w\big)\,\Big|_{-h/2}^{h/2} + [r\,\tau_{\theta r}(1-w_{,r})\delta u]\,\Big|_{-h/2}^{h/2}\Big\}\,\mathrm{d}\theta\mathrm{d}t \\
&\quad + b\int_{t_1}^{t_2}\int_{-h/2}^{h/2}\big[\,\big(\tau_{\theta r}\beta\delta u\big)\,\big|_0^{2\pi} + \big(\tau_{\theta r}\eta\,\delta w\big)\,\big|_0^{2\pi}\,\big]\,\mathrm{d}z\mathrm{d}t.
\end{aligned} \tag{4.10}$$

The last integral in Eq. (4.11) over time and z vanishes due to the equivalence of the displacements and stresses at $\theta = 0$ and at $\theta = 2\pi$.

The integration of δS_3 from t_1 to t_2 gives

$$\begin{aligned}
\int_{t_1}^{t_2} \delta S_3 \,\mathrm{d}t &= b\int_{t_1}^{t_2}\int_{-h/2}^{h/2}\int_0^{2\pi} (\sigma_r\,\delta\varepsilon_r) r\,\mathrm{d}\theta\mathrm{d}z\mathrm{d}t \\
&= b\int_{t_1}^{t_2}\int_{-h/2}^{h/2}\int_0^{2\pi} \sigma_r\,\delta\big[w_{,r}+\frac{1}{2}(u_{,r})^2\big] r\,\mathrm{d}\theta\mathrm{d}z\mathrm{d}t \\
&= b\int_{t_1}^{t_2}\int_{-h/2}^{h/2}\int_0^{2\pi} (r\sigma_r\,\delta w_{,r} + r\sigma_r\,u_{,r}\,\delta u_{,r})\,\mathrm{d}\theta\mathrm{d}z\mathrm{d}t \\
&= -b\int_{t_1}^{t_2}\int_{-h/2}^{h/2}\int_0^{2\pi} \big[(r\sigma_r)_{,r}\,\delta w + (r\sigma_r\,u_{,r})_{,r}\,\delta u\big]\,\mathrm{d}\theta\mathrm{d}z\mathrm{d}t \\
&+ b\int_{t_1}^{t_2}\int_0^{2\pi} \Big[\,(r\,\sigma_r\delta w)\Big|_{-h/2}^{h/2} + \big(r\,\sigma_r\,u_{,r}\delta u\big)\Big|_{-h/2}^{h/2}\,\Big]\,\mathrm{d}\theta\mathrm{d}t.
\end{aligned} \tag{4.11}$$

Integration over time of the kinetic energy variation can be evaluated as

$$\begin{aligned}
\int_{t_1}^{t_2} \delta T \,\mathrm{d}t &= \frac{\rho b}{2}\int_{t_1}^{t_2}\int_{-h/2}^{h/2}\int_0^{2\pi} \delta(\dot{\mathbf{r}}\cdot\dot{\mathbf{r}}) r\,\mathrm{d}\theta\mathrm{d}z\mathrm{d}t \\
&= \frac{\rho b}{2}\int_{t_1}^{t_2}\int_{-h/2}^{h/2}\int_0^{2\pi} \delta({v_1}^2+{v_2}^2) r\,\mathrm{d}\theta\mathrm{d}z\mathrm{d}t \\
&= \frac{\rho b}{2}\int_{t_1}^{t_2}\int_{-h/2}^{h/2}\int_0^{2\pi} (2v_1\,\delta v_1 + 2v_2\,\delta v_2) r\,\mathrm{d}\theta\mathrm{d}z\mathrm{d}t \\
&= \rho b\int_{t_1}^{t_2}\int_{-h/2}^{h/2}\int_0^{2\pi} \big[(-\dot{v}_1 - \Omega\,v_1' + v_2\,\Omega)\delta w \\
&- (\dot{v}_2 + \Omega\,v_2' + v_1\,\Omega)\delta u\big] r\,\mathrm{d}\theta\mathrm{d}z\mathrm{d}t
\end{aligned} \tag{4.12}$$

where v_1 and v_2 are given in Eq. (4.6).

The variation of the potential energy stored in the elastic foundation includes two parts, namely

$$\delta V = \delta V_1 + \delta V_2 \tag{4.13}$$

in which δV_1 is related to the radial springs which connect the inner surface of the ring to its hub while δV_2 to that of the tangential springs. The integration over time of δV_1 and δV_2 yields

$$\int_{t_1}^{t_2} \delta V_1 \,\mathrm{d}t = b\int_{t_1}^{t_2}\int_0^{2\pi} [(k_r\,w\,r\,\delta w)|_{z=-h/2}]\,\mathrm{d}\theta\mathrm{d}t \tag{4.14}$$

and

$$\int_{t_1}^{t_2} \delta V_2 \,\mathrm{d}t = b\int_{t_1}^{t_2}\int_0^{2\pi} [(k_c\,u\,r\,\delta u)|_{z=-h/2}]\,\mathrm{d}\theta\mathrm{d}t. \tag{4.15}$$

Upon substitutions of Eqs. (4.9-4.15) to Eq. (4.7) and after consideration of variational calculus, the governing equations are obtained.

First, after substitutions of Eqs. (4.9-4.15) to Eq. (4.7), the double integrals which are

associated with the effects of the boundaries at $z = \pm h/2$ are collected, i.e.:

$$
\begin{aligned}
&b\int_{t_1}^{t_2}\int_0^{2\pi}\left\{\left[(r\,\sigma_r - r\,\tau_{\theta r}\,u_{,r})\delta w\right]|_{z=h/2}\right\}\mathrm{d}\theta\mathrm{d}t\\
&-b\int_{t_1}^{t_2}\int_0^{2\pi}\left\{\left[(r\,\sigma_r - r\,\tau_{\theta r}\,u_{,r} - k_r\,w\,r)\delta w\right]|_{z=-h/2}\right\}\mathrm{d}\theta\mathrm{d}t\\
&+b\int_{t_1}^{t_2}\int_0^{2\pi}\left\{\left[(r\,\sigma_r\,u_{,r} + r\,\tau_{\theta r}(1-w_{,r}))\delta u\right]|_{z=h/2}\right\}\mathrm{d}\theta\mathrm{d}t\\
&-b\int_{t_1}^{t_2}\int_0^{2\pi}\left\{\left[(r\,\sigma_r\,u_{,r} + r\,\tau_{\theta r}(1-w_{,r}) - k_c\,u\,r)\delta u\right]|_{z=-h/2}\right\}\mathrm{d}\theta\mathrm{d}t\\
&=b\int_{t_1}^{t_2}\int_0^{2\pi}\left(f_1\,\delta w|_{z=h/2} - f_2\,\delta w|_{z=-h/2} + f_3\,\delta u|_{z=h/2} - f_4\,\delta u|_{z=-h/2}\right)\mathrm{d}\theta\mathrm{d}t
\end{aligned}
\tag{4.16}
$$

in which

$$f_1 = \left\{r\left(\sigma_r - \tau_{\theta r}\,u_{,r}\right)\right\}|_{z=h/2}\,, \tag{4.17a}$$

$$f_2 = \left\{r\left(\sigma_r - \tau_{\theta r}\,u_{,r} - k_r\,w\right)\right\}|_{z=-h/2}\,, \tag{4.17b}$$

$$f_3 = \left\{r\left[\sigma_r\,u_{,r} + \tau_{\theta r}(1-w_{,r})\right]\right\}|_{z=h/2}\,, \tag{4.17c}$$

$$f_4 = \left\{r\left[\sigma_r\,u_{,r} + \tau_{\theta r}(1-w_{,r}) - k_c\,u\right]\right\}|_{z=-h/2}\,. \tag{4.17d}$$

Second, the displacement fields are expressed as polynomials in both radial and circumferential directions:

$$w(z,\theta,t) = \sum_{l=0}^{l=N_1} w_l(\theta,t)\,z^l,\; u(z,\theta,t) = \sum_{q=0}^{q=N_2} u_q(\theta,t)\,z^q \tag{4.18}$$

in which l, q are integers and $l \geq 0$, $q \geq 0$. This results in

$$\delta w = \sum_{l=0}^{l=N_1} \delta w_l\,z^l,\; \delta u = \sum_{q=0}^{q=N_2} \delta u_q\,z^q \tag{4.19}$$

and

$$\delta w|_{z=\pm h/2} = \sum_{l=0}^{l=N_1} \delta w_l\,(\pm h/2)^l,\; \delta u|_{z=\pm h/2} = \sum_{q=0}^{q=N_2} \delta u_q\,(\pm h/2)^q \tag{4.20}$$

Combining Eqs. (4.7-4.20) and collecting coefficients of δw_l and δu_q, the nonlinear governing equations can be obtained by setting the coefficients of δw_l and δu_q equal to zero. The equations of motion that govern the dynamic equilibrium in the radial direction read

$$
\begin{aligned}
&\int_{\frac{-h}{2}}^{\frac{h}{2}}(\mathrm{I}_1\,z^l)\,\mathrm{d}z + \rho\int_{\frac{-h}{2}}^{\frac{h}{2}}\left[r(\dot{v}_1 + \Omega\,v_1' - \Omega\,v_2)z^l\right]\mathrm{d}z + \left[f_1 - f_2(-1)^l\right]\left(\frac{h}{2}\right)^l = 0,\\
&(l = 0,1,2,3...N_1).
\end{aligned}
\tag{4.21}
$$

The equations of motion that govern the circumferential equilibrium are given as

$$
\begin{aligned}
&\int_{\frac{-h}{2}}^{\frac{h}{2}}(\mathrm{I}_2\,z^q)\,\mathrm{d}z + \rho\int_{\frac{-h}{2}}^{\frac{h}{2}}\left[r(\dot{v}_2 + \Omega\,v_2' + \Omega\,v_1)z^q\right]\mathrm{d}z + \left[f_3 - f_4(-1)^q\right]\left(\frac{h}{2}\right)^q = 0,\\
&(q = 0,1,2,3...N_2)
\end{aligned}
\tag{4.22}
$$

in which

$$\mathrm{I}_1 = \sigma_\theta + (\sigma_\theta \beta)' - (r\,\sigma_r)_{,r} - (\tau_{\theta r}\,\eta)' + \tau_{\theta r}\,\beta + (r\,u_{,r}\,\tau_{\theta r})_{,r}, \tag{4.23a}$$

$$\mathrm{I}_2 = -(\sigma_\theta)' + \sigma_\theta\,\beta - (r\,\sigma_r\,u_{,r})_{,r} - \tau_{\theta r}\,\eta - (\tau_{\theta r}\,\beta)' - \left[r\,\tau_{\theta r}(1-w_{,r})\right]_{,r}. \tag{4.23b}$$

The Eqs. (4.21-4.22) present the new mathematical description of the dynamics of a rotating ring on an elastic foundation that takes into account the effect of the tractions on the boundaries of the ring.

Up to now, the derivation is generic and one may truncate the number of terms in Eq. (4.18) as deemed appropriate. For instance, if one retains w_0, u_0 and u_1, the Timoshenko-type model is obtained and a shear correction needs to be introduced [27]. When one chooses a higher truncation limit, no shear correction coefficient needs to be introduced separately because a proper distribution of shear stress is considered implicitly by the model. This is the same as in the Carrera unified formulation [92–95].

4.2. STATIC EQUILIBRIUM

To derive the linear governing equations, the static equilibrium needs to be obtained first from the nonlinear equations. As shown in [9, 58] an angle-independent static equilibrium will be reached when the ring rotates at a constant angular velocity. The static expansion $w_e(z)$ of the ring can be found by substitution of

$$\begin{aligned} w(z,\theta,t) &= w_e(z) = \sum_{l=0}^{l=N_1} w_{el}\,z^l, \\ u(z,\theta,t) &= 0 \end{aligned} \tag{4.24}$$

into the governing equation, i.t. Eqs. (4.21-4.22). Upon substitution, the following N_1+1 equations can be used to determine w_{el}:

$$\int_{\frac{-h}{2}}^{\frac{h}{2}} (\mathrm{I}_1^0\,z^l)\,\mathrm{d}z - \rho \int_{\frac{-h}{2}}^{\frac{h}{2}} r\,\Omega^2 (r+w_e) z^l\,\mathrm{d}z + \left[f_1^0 - f_2^0(-1)^l\right]\left(\frac{h}{2}\right)^l = 0, \tag{4.25}$$

where

$$\begin{aligned} \mathrm{I}_1^0 &= 2\mu\left(\frac{w_e}{r} - \frac{\partial w_e}{\partial r}\right) - r\left[(2\mu+\bar{\lambda})\left(\frac{\partial^2 w_e}{\partial r^2}\right) + \frac{\bar{\lambda}}{r}\frac{\partial w_e}{\partial r}\right], \\ f_1^0 &= \left\{\left[(2\mu+\bar{\lambda})\frac{\partial w_e}{\partial r} + \bar{\lambda}\frac{w_e}{r}\right] r\right\}|_{z=h/2}, \\ f_2^0 &= \left\{\left[(2\mu+\bar{\lambda})\frac{\partial w_e}{\partial r} + \bar{\lambda}\frac{w_e}{r} - k_r\,w_e\right] r\right\}|_{z=-h/2}. \end{aligned} \tag{4.26}$$

Each w_{el} of the total N_1+1 terms is obtained separately as a function of the rotational speed Ω. Subsequently, $w_e(z)$ is obtained by applying Eq. (4.24).

4.3. LINEARISED EQUATIONS OF MOTION

Considering small vibrations around the static equilibrium, the displacements can be expressed as

$$\begin{aligned} w(z,\theta,t) &= w_d(z,\theta,t) + w_e(z) = \sum_{l=0}^{l=N_1} w_{dl}(\theta,t)\, z^l + \sum_{l=0}^{l=N_1} w_{el}\, z^l, \\ u(z,\theta,t) &= u_d(z,\theta,t) = \sum_{q=0}^{q=N_2} u_{dq}(\theta,t)\, z^q \end{aligned} \tag{4.27}$$

in which all time dependent terms are assumed small, i.e. $|w_{dl}(\theta,t)| \ll |w_{el}|$, $|u_{dq}| \ll 1$. The linearised governing equations are obtained by dropping all the nonlinear terms in Eqs. (4.21-4.22).

Linearising Eq. (4.21), the equations of motion that govern the small vibrations about the static equilibrium in the radial direction (the coefficient of δw_l, contains N_1+1) read

$$\int_{\frac{-h}{2}}^{\frac{h}{2}} (\mathrm{I}_1^{lin} z^l)\,\mathrm{d}z + \rho \int_{\frac{-h}{2}}^{\frac{h}{2}} \left[r(\dot{v}_1 + \Omega\, v_1' - \Omega\, v_2) z^l \right] \mathrm{d}z + \left[f_1^{lin} - f_2^{lin}(-1)^l \right] \left(\frac{h}{2}\right)^l = 0, \tag{4.28}$$

The linearised equations of motion in the circumferential direction (the coefficient of δu_q, contains N_2+1) are given as

$$\int_{\frac{-h}{2}}^{\frac{h}{2}} (\mathrm{I}_2^{lin} z^q)\,\mathrm{d}z + \rho \int_{\frac{-h}{2}}^{\frac{h}{2}} \left[r(\dot{v}_2 + \Omega\, v_2' + \Omega\, v_1) z^q \right] \mathrm{d}z + \left[f_3^{lin} - f_4^{lin}(-1)^q \right] \left(\frac{h}{2}\right)^q = 0. \tag{4.29}$$

after linearisation of Eq. (4.22). In Eqs. (4.28-4.29),

$$\mathrm{I}_1^{lin} = \sigma_\theta^{lin} + \sigma_\theta^0(\beta)' - (r\,\sigma_r^{lin})_{,r} - \left[(\tau_{\theta r}\,\eta)'\right]^{lin}, \tag{4.30a}$$

$$\mathrm{I}_2^{lin} = -(\sigma_\theta^{lin})' + \sigma_\theta^0\,\beta - \left[r(\sigma_r^0)\,u_{,r}\right]_{,r} - (\tau_{\theta r}\,\eta)^{lin} - \left\{\left[r\,\tau_{\theta r}(1-w_{,r})\right]_{,r}\right\}^{lin} \tag{4.30b}$$

$$f_1^{lin} = \left[r(2\mu+\bar{\lambda})\frac{\partial w}{\partial r} + \bar{\lambda}(u'+w) \right] |_{z=h/2}\,, \tag{4.30c}$$

$$f_2^{lin} = \left[r(2\mu+\bar{\lambda})\frac{\partial w}{\partial r} + \bar{\lambda}(u'+w) - k_r\, w\, r \right] |_{z=-h/2}\,, \tag{4.30d}$$

$$f_3^{lin} = \left\{ \frac{G(r-w_e)(1-w_{e,r})}{r}(w'-u) + \left[Gr(1+(w_{e,rr})^2) + \bar{\lambda}(r\,w_{e,r}+w_e)\right] u_{,r} \right\} |_{z=h/2}\,, \tag{4.30e}$$

$$f_4^{lin} = \left\{ \frac{G(r-w_e)(1-w_{e,r})}{r}(w'-u) + \left[Gr(1+(w_{e,rr})^2) + \bar{\lambda}(r\,w_{e,r}+w_e)\right] u_{,r} - k_c\, u\, r \right\} \Big|_{z=-\frac{h}{2}}\,. \tag{4.30f}$$

The expressions with superscript lin are the linearised versions of the earlier introduced nonlinear expressions. The stresses σ_r^0 and σ_θ^0 are prestresses caused by rotation in radial and circumferential directions, respectively. From the Hooke's law shown in Eq. (4.3), the prestress in radial direction is given by

$$\sigma_r{}^0 = 2\mu\,\varepsilon_r{}^0 + \bar{\lambda}\left(\varepsilon_r{}^0 + \varepsilon_\theta{}^0\right) \tag{4.31}$$

and in circumferential direction it reads

$$\sigma_\theta{}^0 = 2\mu\varepsilon_\theta{}^0 + \bar{\lambda}\left(\varepsilon_r{}^0 + \varepsilon_\theta{}^0\right) \tag{4.32}$$

where the strains caused by rotation are

$$\varepsilon_r{}^0 = \frac{\partial w_e}{\partial r},\ \varepsilon_\theta{}^0 = \frac{w_e}{r} \tag{4.33}$$

in which w_e is given by Eq. (4.24).

For brevity, in all the above expressions in Eq. (4.30), w and u stand for w_d and u_d, respectively. The velocities v_1 and v_2 are now only related to the vibrational velocities, namely

$$v_1 = \left(\dot{w}_d + (w_d' - u_d)\Omega\right),\ v_2 = \left(\dot{u}_d + (u_d' + w_d)\Omega\right). \tag{4.34}$$

To obtain the characteristic equation one needs to first substitute

$$w_{dl}(\theta,t) = W_{dl}\,\mathrm{e}^{\mathrm{i}n\theta+\mathrm{i}\omega t},\ u_{dq}(\theta,t) = U_{dq}\,\mathrm{e}^{\mathrm{i}n\theta+\mathrm{i}\omega t},\ (l = 0,1,2,3...N_1, q = 0,1,2,3...N_2), \tag{4.35}$$

into Eqs. (4.28-4.29). In Eq. (4.35) ω is the natural frequency in space-fixed reference system, n is the circumferential mode number and $\mathrm{i} = \sqrt{-1}$. This substitution yields the following matrix equation

$$\mathbf{Da} = \mathbf{0}, \tag{4.36}$$

in which $\mathbf{a} = \left[W_0, W_1, ..., W_{N_1}, U_0, U_1, ..., U_{N_2}\right]^T$ and $\mathbf{D}$ is the coefficient matrix of order $(N_1+N_2+2)\times(N_1+N_2+2)$. The characteristic equation can be obtained by setting the determinant equal to zero:

$$f(\omega, n, \Omega) = \det\langle\mathbf{D}\rangle = 0. \tag{4.37}$$

Here no approximations are introduced for the integrations along the thickness coordinate "z". Instead, the exact integral form of the governing equations is considered.

To derive the non-dimensional form of the governing equations, the following dimensionless parameters are introduced [71]:

$$\begin{aligned} &k = \sqrt{EI/(EA)},\ \bar{k} = k/R,\ \bar{\gamma} = n\,\bar{k},\ \bar{\omega} = \omega\,k/c_0,\ \bar{v} = R\,\Omega/c_0,\\ &(\bar{k}_r, \bar{k}_c) = (k_r, k_c)k^2/(Eh),\ W_{0e} = w_{0e}/R, \end{aligned} \tag{4.38}$$

where $c_0 = \sqrt{E/\rho}$ is the speed of the longitudinal wave in the rod, $I = bh^3/12$ is the cross section area moment of inertia and $\bar{k}$ is the non-dimensional radius of gyration.

Thus, the dimensionless form of the characteristic equation Eq. (4.37) reads*

$$f(\bar{\omega}, \bar{\gamma}, \bar{v}) = 0. \tag{4.39}$$

The model developed can deal with both plane strain and plane stress problems by choosing different expression of the parameter $\bar{\lambda}$ as shown in Eq. (4.4). Naturally, the model also works for stationary rings by letting $\Omega = 0$.

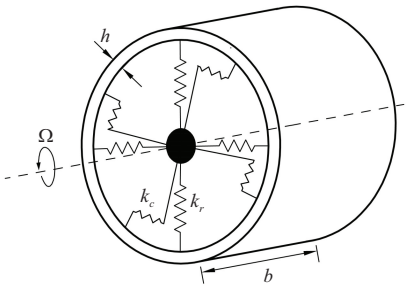

Figure 4.1: A rotating ring with $b >> h$.

4.4. COMPARISONS BETWEEN VARIOUS RING MODELS AND THE ELASTICITY THEORY FOR STATIONARY RINGS

To illustrate the significance of the stress boundary effects, the proposed model is compared with the Timoshenko-type model [27] and elasticity theory for stationary ring case ($\Omega = 0$). A comparison of the stationary ring case suffices for the following reason. Once it is shown that boundary effects are important for stationary rings, one may conclude that the latter will also be of importance for rotating rings since the tractions at the inner surface in the latter case are larger than those of the stationary ring case. Plane strain is assumed since a ring whose out-of-plane thickness b is much larger than the in-plane thickness h is considered as shown in Fig. 4.1 hereafter. For the Timoshenko-type theory, the shear coefficient is adopted from [96] to be

$$K = \frac{10(1+\nu)}{12+11\nu} \tag{4.40}$$

for rectangular cross-section.

The dispersion curves are plotted in Fig. 4.2 for the three sets of foundation stiffness discussed previously. A short recollection of the two-dimensional elasticity theory employed can be found in Appendix B. Throughout this Chapter and Chapter 5, the Poisson's ratio $\nu = 0.4$ is employed. In each plot of Fig. 4.2, results obtained from the Timoshenko-type theory [27] consist of three branches, representing bending-dominated motion, extension-dominated motion and shear-dominated motion, respectively. The first four branches of the dispersion curves calculated from the elasticity theory are drawn to compare with the results from the Timoshenko-type model and the high-order model proposed. The truncation orders in Eq. (4.18) are chosen to be $N_1 = N_2 = 5$.

Comparison of Fig. 2.8(a)(c)(e) in which the dispersion curves resulting from the classical thin ring model are present with the same parameters, and Fig. 4.2 shows the applicability range of the new model is much wider than the existing classical thin ring model [9] and the Timoshenko-type model [27]. The classical thin ring model cannot predict the dispersion curves when the foundation stiffness increases. This also holds

*Due to complexity, the dimensionless form of the characteristic equation is not explicitly given here.

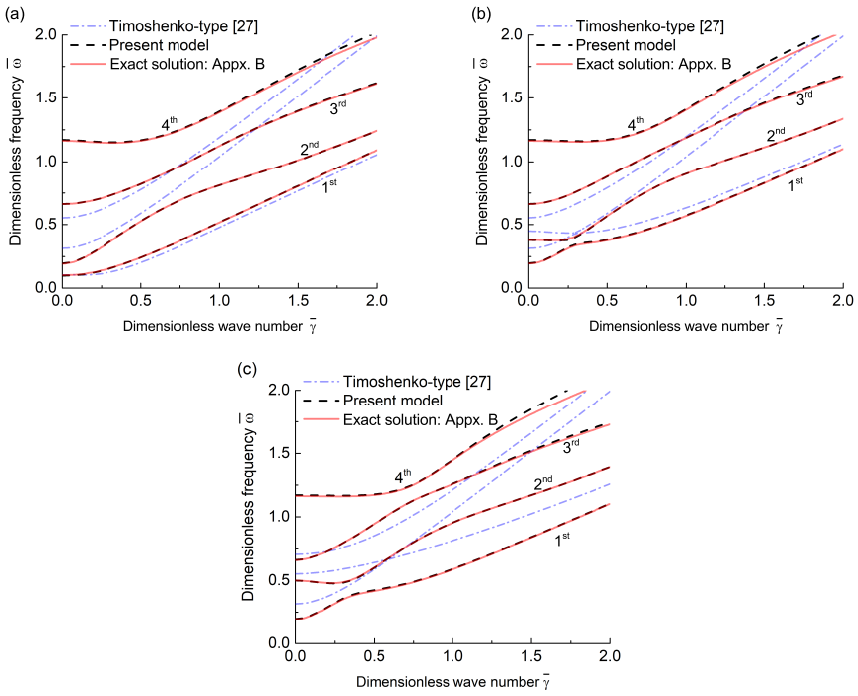

Figure 4.2: Dispersion curves (plane strain) for $h/R = 0.1$, $\bar{k}_c = 0.1$ and $\Omega = 0$: (a) $\bar{k}_r = 0.01$; (b) $\bar{k}_r = 0.2$; (c) $\bar{k}_r = 0.5$.

for the Timoshenko model the predictions of which deviate significantly from the exact solution for increased foundation stiffness. In contrast, the current model can accurately predict the first four branches of the dispersion curves in the whole range of wavenumbers also in the case of stiff foundation (and thus strong through-thickness variation of the stress components) with the choice of quintic polynomials ($N_1 = N_2 = 5$) for both the radial displacement and circumferential displacement fields. More dispersion curves can be accurately predicted by increasing the degrees of the polynomial displacements accordingly. To conclude, the high-order theory which considers the stress boundary effects at the surfaces and the through-thickness variations of stresses is shown to be superior to the existing ring models.

4.5. CONCLUSIONS

In this chapter, the in-plane vibration of steadily rotating rings on elastic foundation (distributed springs) is considered. Due to rotation-induced radial expansion, the inner surface which is connected by springs, experiences traction force because of stretching of springs at the static equilibrium. The traction force at the inner surface can be considerably high when the ring rotates at high speeds, resulting in non-negligible through-thickness variations of stresses from non-zero at the inner surface to zero at the outer

surface. The same situation also holds for the dynamic forces and stresses at the ring surfaces and in the rings. The classical lower order theories cannot account for either the stress boundary effects at surfaces or the variations of stresses along the thickness of the ring whereas the developed high-order theory is able to. The present model can precisely describe high order wave motions by increasing the degrees of displacement polynomials. The proposed model can be used in the following cases of high-speed rotating rings: high frequency vibrations, moderately thick rings, rings on stiff foundation. By comparing the frequency spectrum of the present model and those obtained from various existing models and the linear elasticity theory, it has been shown that the high-order theory which considers the stress boundary effects at the surfaces and the though-thickness variations of stresses is superior to all existing ring models. The proposed model in this chapter will be used throughout the following chapters.

5

CRITICAL SPEEDS OF A LOAD ON A RING: ROTATING RING VERSUS MOVING LOAD

It is well-known that resonances of a ring occur when the speed of a circumferentially moving load satisfies a certain condition, namely the ring length is divisible by the wavelength of a wave radiated by the load [60, 61]. In contrast, the existence of resonances of the reciprocal problem, namely a rotating ring subjected to a stationary load, is still debatable. The most commonly used Endo-Huang-Soedel model [13–15] does not predict resonances for a rotating ring subjected a constant stationary load as discussed in Chapter 2. This result is a consequence of the chosen strain-displacement relation and of the applied linearisation procedure, which led to a so-called cancellation of rotation effect. The latter implies that the Coriolis and centrifugal forces totally neutralise the pretension effect in this model. It becomes almost a commonsense that no critical speeds assoiciated with resonances exist for rotating thin rings in the literature with very few counterviews. A rigorous mathematical treatment of a similar problem, namely a rotating cylinder bonded to a rigid inner hub, is carried out in the monograph [97] by Rabier and Oden. In their study, critical speed related to resonances is found. For rotating rings, Lin and Soedel [17] developed new governing equations using a different nonlinear strain-displacement relation proposed by Stein [24]. Critical speeds (resonance speeds) are given in [18] using the model proposed in [17] and thus it is shown that the softening effect can dominate the stress stiffening effect. However, the linearisation procedure adopted in [17, 18] is discussable. Recent contributions on the existence of resonance speeds can be found in [62–64].

There are two kinds of critical speeds of a rotating ring one may be interested in. One corresponds to the onset of instability of free vibrations, whereas the other corre-

This chapter has been published as a journal paper in *Journal of Sound and Vibration* **455**, 118(2019) [90]. Minor changes are made.

sponds to resonances of a rotating ring subjected to a constant stationary load. It has been shown in Chapter 3 (as well as [58]) that instability and resonances may occur for some combinations of the ring parameters. In this chapter (section 5.1), the critical speeds of rotating rings are predicted employing the higher order model proposed in Chapter 4 and comparisons are made between the predictions using the high-order model and low-order ones in the literature. Importance of higher order corrections are addressed. Effects of stiffness of the elastic foundation on the applicability of various models are discussed. This is the main contribution of this chapter. Furthermore, the reciprocal problem, a circumferentially moving load on a stationary ring is studied as well in order to gain insight into the conditions under which the two problems are approximately equivalent to each other in section 5.2. In section 5.3, the effects of rotation on critical speeds of the rotating ring case are discussed. Section 5.4 summarises all the main results of this chapter.

5.1. CRITICAL SPEEDS OF A ROTATING RING

In this section, the critical speeds are calculated using different models to illustrate the importance of different factors. There are two kinds of critical speeds of interest for a rotating ring. One corresponds to the onset of instability of free vibrations, whereas the other corresponds to resonances of a rotating ring subjected to a stationary load of constant magnitude.

Rotation leads to axi-symmetric radial expansion of the ring. The expansion causes prestress in the ring in both circumferential and radial directions. There should be a threshold of the rotational speed to avoid the material failure caused by the rotation-induced prestress. As shown in Chapters 3-4, there are two kinds of prestress which should be examined beforehand, namely, the hoop prestress ${\sigma_\theta}^0$ and the radial prestress ${\sigma_r}^0$. One should always keep in mind that the model is valid when the material is in the linearly elastic range and therefore the principal stress caused by rotation is well below the yield stress of the material of the ring.

5.1.1. RESONANCE SPEEDS

Resonance speeds are defined as the speeds at which resonance of a rotating ring subjected to a stationary load occurs. These are the speeds which satisfy the condition $\bar{\omega} = 0$ [18, 19, 58, 88]. By substituting $\bar{\omega} = 0$ into the characteristic equation (4.39), one can solve for resonance speeds for each circumferential wavenumber. Note that these resonance speeds are altered in the presence of damping and resonances can disappear altogether provided the damping is sufficiently high.

MODELS CONSIDERED

In order to illustrate the importance of the boundary effects and through-thickness variation of stresses, predictions made by four models are compared. Table 5.1 shows the classical thin ring model and the meliorated models with different improvements considered. "R. stress variation" in the table means that the through-thickness variation of radial stress is considered. To achieve this, at least a quadratic polynomial for the radial displacement field is needed. "S. stress variation" stands for the consideration of the through-thickness variation of shear stress. Model 1 is the classical theory [9]; Model 4

Table 5.1: Classical and improved models.

Models	R. stress variation	S. stress variation	Shear deformation	Rotatory inertia	Displacement field	Static equilibrium
Model 1[9]	×	×	×	×	$N_1 = N_2 = 0$, i.e. Eq. (2.1)	Eq. (2.46)
Model 2[58]	✓	×	×	×	$N_1 = 2, N_1 = 0$, i.e. Eq. (3.2)	Eq. (3.30)
Model 3[27]	×	×	✓	✓	$N_1 = 0, N_2 = 1$ in Eq. (4.18)	Refer to [27]
Model 4 (Eqs. (4.28-4.29))	✓	✓	✓	✓	$N_1 = N_2 = 5$ in Eq. (4.18)	Eq. (4.25)

is the one developed in this paper. Model 2 [58] accounts for the through-thickness radial stress variation on the basis of the classical ring model. Model 3 is the one adopted from [27] in which the shear deformation and rotatory inertia are included, resulting in a Timoshenko-type model. In analogy to Timoshenko's beam theory, the shear coefficient in Model 3 is given by Eq. (4.40) for a rectangular cross-section.

PREDICTIONS OF THE VARIOUS MODELS

The critical speeds of a rotating ring are considered in this subsection. The three sets of parameters used to plot Fig. 2.8 in Chapter 2 will be adopted. In all figures hereafter, the letter "B" means bending-dominated motions, "E" stands for extension-dominated motions, and "S" represents shear-dominated motions. Note that only waves predicted by the lower order Model 1, Model 2 and Model 3 are distinguished in this way. The lower abscissa in each plot is the dimensionless wavenumber, whereas the upper abscissa is the corresponding discrete circumferential mode number. In Figs. 5.1(d), 5.2(d) and 5.3(d), the solid lines correspond to results from the proposed high-order Model 4. For the purpose of comparison, the curves in Figs. 5.1(d), 5.2(d) and 5.3(d) are replicated in Figs. 5.1(a)(b)(c), 5.2(a)(b)(c) and 5.3(a)(b)(c) in grey color.

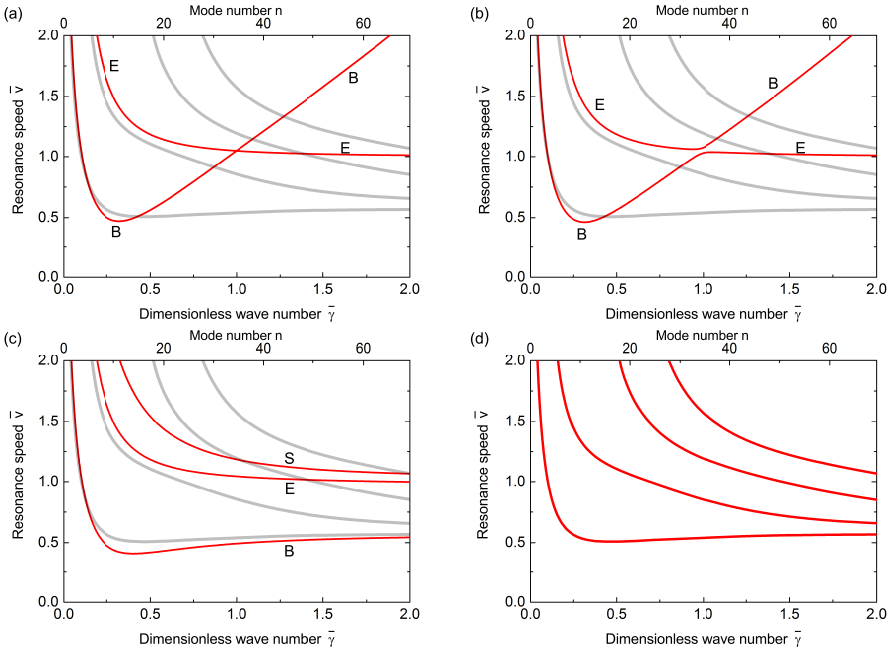

Figure 5.1: Resonance speeds for $h/R = 0.1, \bar{k}_c = 0.1, \bar{k}_r = 0.01$: (a) Model 1 (classical model [9]); (b) Model 2 [58]; (c) Model 3 (Timoshenko-type [27]); (d) Model 4 (the present model).

Figure 5.1 shows the resonance speeds for $\bar{k}_c = 0.1$ and $\bar{k}_r = 0.01$. Model 1 and Model 2 (Fig. 5.1(a)(b)) predict quite similar results, indicating that the through-thickness radial stress is not that important. The minimum resonance speed is similar but slightly higher than the minimum phase speed of the corresponding stationary ring case as approxi-

mated by Eq. (2.29) due to stiffening caused by the rotation-induced hoop stress. The applicable wavenumber range of Model 1 and Model 2 is lower than $\bar{\gamma} = 0.5$ when compared with the present model (the thick grey lines in Fig. 5.1(a)(b)) for the chosen parameters. Model 3 and Model 4 predict qualitatively similar resonance speeds for bending-dominated motions as shown in Fig. 5.1(c). The minimum resonance speeds predicted by Model 3 and Model 4 are similar to those predicted by Model 1 and Model 2. However, Model 4 predicts the highest minimum resonance speed. The resonance speeds of bending-dominated motions approach the Rayleigh wave speed at large wavenumbers. This convergence is reasonable since for the waves whose wavelengths are much shorter than the thickness of the ring the effect of the inner boundary disappears. The higher branches (S,E) are not predicted accurately by the Timoshenko-type theory.

To conclude, if the foundation is soft, one can use the classical model to compute the minimum resonance speed although the latter is slightly smaller than the minimum resonance speed predicted by the present model. However, for the resonance speeds of the bending-dominated motions with small wavelengths (high wavenumbers), the first order Timoshenko correction is needed should one be interested in meaningful results. Higher than Timoshenko-type theories are not needed since their predictions are very close to those of the Timoshenko-type theory.

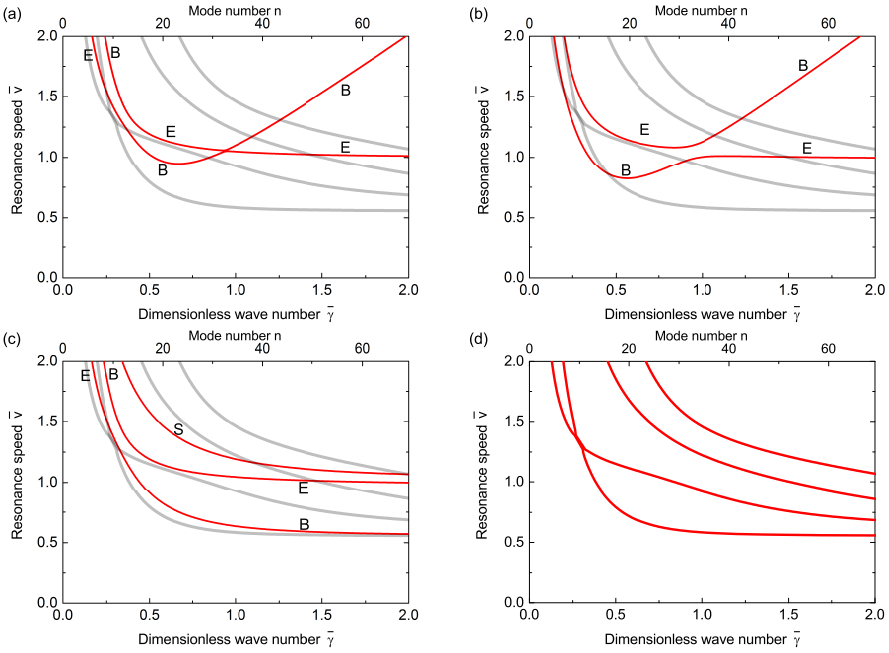

Figure 5.2: Resonance speeds for $h/R = 0.1$, $\bar{k}_c = 0.1$, $\bar{k}_r = 0.2$: (a) Model 1 (classical model [9]); (b) Model 2 [58]; (c) Model 3 (Timoshenko-type [27]); (d) Model 4 (the present model).

In Figure 5.2, the stiffness of radial springs is higher than that of the circumferential ones. For this set of parameters, the resonance speeds of bending-dominated motions are larger than those of other branches at low wavenumbers. As the wavenumber in-

creases, both the classical model and Model 2 predict curve veering twice: once at $\bar{\gamma} \approx 1$ and once at a smaller value of $\bar{\gamma}$. Although the classical model (Model 1) and Model 2 predict similar trends, the minimum resonance speed of Model 2 is lower than that of the classical theory. It is shown in Fig. 5.2(c) and (d) that the shear deformation and rotatory inertia play here a significant role; albeit the contribution of each component is not examined separately. Similar to Model 1 and Model 2, for low wavenumbers, bending-dominated motions have larger resonance speeds. Curves representing flexural and extensional motions veer once at the wavenumber at which the first curve veering occurs in Fig. 5.2(a) and (b) (the veering is not very obvious in Fig. 5.2(b) but the curves do veer). Beyond this point, in Fig. 5.2(c), resonances of shear-dominated motions occur at highest speeds, following by extension-dominated motions and bending-dominated motions. Similarly to Fig. 5.1(c) for the Timoshenko-type model, the Rayleigh surface wave speed is the limit of the bending-dominated motion as shown in Fig. 5.2(c). Also, for Model 4, resonance speeds of the lowest wave branch converge to the Rayleigh wave speed. Therefore, if a constant stationary load is applied to the ring and the rotational speed of the ring reaches the Rayleigh wave speed, Rayleigh wave resonance occurs. The Rayleigh wave resonance interpretation is first made by Rabier and Oden in [97] for the standing wave phenomenon in a spinning cylinder. Similar conclusions are made by Karttunen and von Hertzen in [98] who considered a viscoelastic cylinder cover under rolling contact. It is also shown that for low wavenumbers, the resonance speeds of Fig. 5.2(d) are different from those of Fig. 5.2(a)(c) but quite close to Fig. 5.2(b) in which the radial stress variation along the thickness is considered, implying that this variation is important for waves of relatively large wavelength. Comparing Fig. 5.2(a), (b), (c) and (d), one can conclude that the lower-order theories are completely inapplicable for medium stiff foundation ($\bar{k}_r = 0.2$).

In Figure 5.3 ($\bar{k}_r/\bar{k}_c = 5$), it is shown that the influence of stress variations increases with the increase of the foundation stiffness. The classical theory predicts higher resonance speeds of bending-dominated motions than the extension-dominated motions, and no curve veerings exist. However, when the through-thickness radial stress variation is included in Fig. 5.3(b), curves veer twice similarly to Fig. 5.2(b). From the classical theory, the minimum resonance speed corresponding to extensional motions converges to $\sqrt{E/\rho}$. Again, for the Timoshenko-type model in Fig. 5.3(c), the resonance speeds of the bending-dominated motion approach the Rayleigh surface wave speed at high wavenumbers. The quantitatively different resonance speeds predicted in Fig. 5.3(c) and (d) show the significance of boundary effects and through-thickness variation of stresses for the case of stiff foundation. By observing Fig. 5.3, it can be seen that the lower-order theories cannot predict the resonance speeds.

For all the three sets of parameters, one can conclude that high order corrections are needed to correctly predict the resonance speeds. For Case 1 in which $\bar{k}_r/\bar{k}_c = 0.1$, the minimum resonance speeds predicted from all models are close. However, when the stiffness of radial springs increases, the minimum resonance speeds predicted by different models are distinct. Shear deformation and rotatory inertia play an important role, as they ensure bending-dominated modes are the ones being always excited at lowest speeds. Although the individual contribution of shear deformation and rotatory inertia are not separately investigated, the observed differences are attributed largely

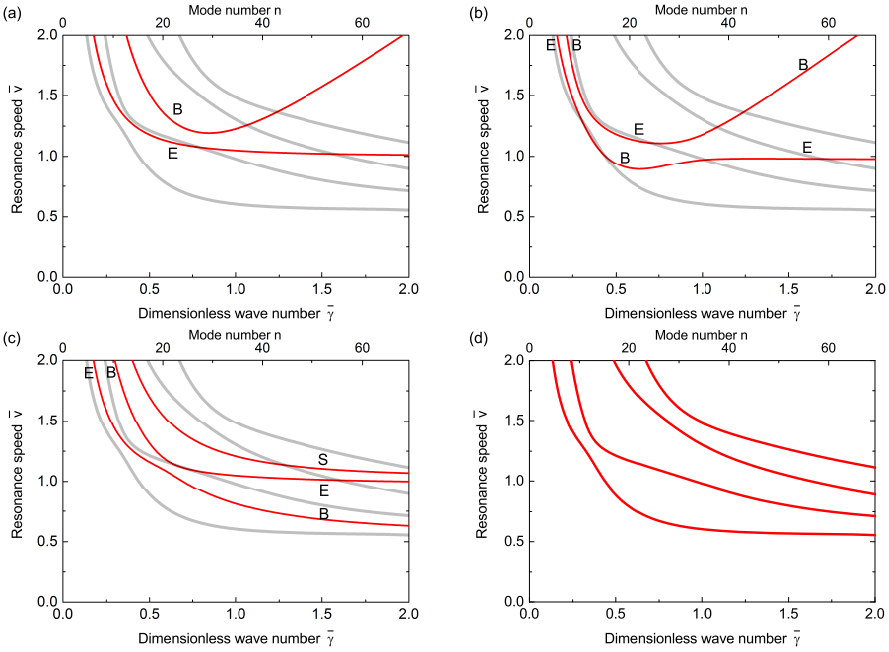

Figure 5.3: Resonance speeds for $h/R = 0.1$, $\bar{k}_c = 0.1$, $\bar{k}_r = 0.5$: (a) Model 1 (classical model [9]); (b) Model 2 [58]; (c) Model 3 (Timoshenko-type [27]); (d) Model 4 (the present model).

to the effect of shear deformation. The through-thickness variation of stresses and the consideration of boundary effects become significant when $\bar{k}_r/\bar{k}_c$ increases. The influence of boundary effects on dynamics of the ring is more important for waves with small wavenumbers (large wavelength) than waves with high wavenumbers. It is important to point out that for larger wavenumbers, the resonance speeds of the bending-dominated waves converge to the Rayleigh wave speed. By comparing Fig. 2.8(b), (d), (f) with Fig. 5.1(a), Fig. 5.2(a) and Fig. 5.3 (a), respectively, it is concluded that for a ring on foundation whose stiffness is of the same order or higher than the Young's modulus, the resonance speeds of a constant load moving circumferentially on the ring and the inverted problem, namely a rotating ring subjected to a constant stationary load, are similar according to the classical thin ring theory. However, due to stress-stiffening, the resonance speeds of rotating ring case are larger than those of the moving load case. In the comparison, the influence of the foundation stiffness in the circumferential direction is not examined since this is expected to be of importance for shear-dominated motion and thus it has limited influence on bending-dominated waves discussed here.

NECESSITY OF HIGH-ORDER THEORY FOR ROTATING RINGS

As can be concluded from Figs. 5.1-5.3, the use of high order theories is important for predicting resonance speeds. Even in the case of soft foundation, the predictions of waves generated are rather different. The predicted resonance speeds change significantly for increasing stiffness of radial springs. This statement holds also for thin rings.

For the case of a rotating ring, it is necessary to include high-order corrections, even in the case in which the ring is thin but attached to a stiff foundation. With increasing rotational speeds, the waves excited by a constant stationary load are completely different given the comparison of the predictions by the classical model and the proposed one. For example, comparing Fig. 5.3(a) and (d), if the ring rotates at $\bar{v} = 0.7$ and is subjected to a constant stationary load, no waves are generated according to the classical model whereas waves will be predicted by the present model.

5.1.2. CRITICAL SPEEDS ASSOCIATED WITH THE ONSET OF INSTABILITY

In [58], it has been concluded that the stiffness of the circumferential springs is a key factor influencing the critical speed corresponding to the onset of instability. Lower stiffness of circumferential springs results in lower critical speeds associated with the onset of instability. Here two sets of parameters are chosen; $\bar{k}_r = 0.28$, which corresponds to the stiffness of the radial springs $\bar{K}_r = 4 \times 10^5$ as in [58] and two values of $\bar{k}_c$.

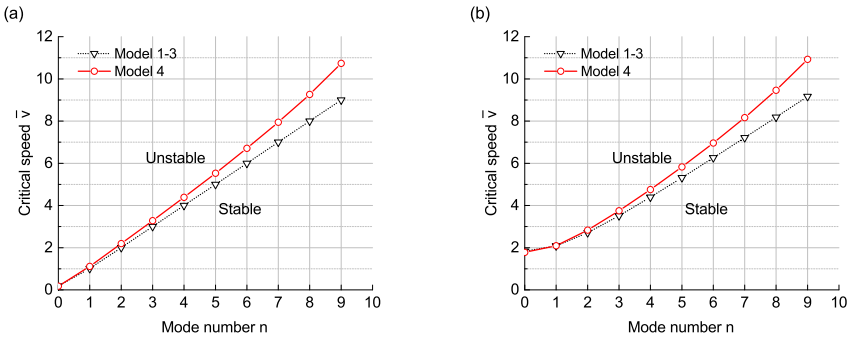

Figure 5.4: Stability boundaries predicted by different models for $h/R = 0.1, \bar{k}_r = 0.28$: (a) $\bar{k}_c/\bar{k}_r = 10^{-4}$; (b) $\bar{k}_c/\bar{k}_r = 10^{-2}$.

The critical speeds corresponding to the onset of instability for different modes (up to $n = 9$) are plotted in Fig. 5.4 using the models described previously. These speeds divide stable and unstable regions. In Fig. 5.4, it can be seen that divergence instability of the $n = 0$ rotational mode always occurs at lower rotational speeds compared to flutter of higher modes [58]. The critical speeds obtained from Model 1, Model 2 and Model 3 are quite similar whereas the present model predicts higher critical speeds for mode numbers $n \geq 1$. The differences become larger when the mode number increases. Nevertheless, it can be concluded that the lowest critical speed (corresponding to divergence of $n = 0$) is almost the same regardless of model. This conclusion is reasonable since higher order corrections influence modes in which elastic deformation dominates.

5.1.3. ON THE EXISTENCE OF CRITICAL SPEEDS

In the above analysis, the critical speeds calculated from different models are compared. However, it is worth mentioning that for a rotating ring on an elastic foundation, the critical speeds do not always exist. The existence of critical speeds depends on the contribution of the centrifugal softening and stiffening caused by rotation induced prestress.

It is argued in [58] that only for a certain combination of stiffnesses of the radial and circumferential springs instability may occur. The stiffness of circumferential springs plays a key role in critical speeds associated with instability. Relatively soft circumferential springs reduce the rotational speeds at which instability occurs. For resonances to occur, stiff radial springs are needed. On the one hand, stiff radial springs impose restrictions on the static expansion due to rotation, and therefore the stress-stiffening effect. The smaller the stiffening effect, the more likely resonances to occur. Meanwhile, if resonances can occur, larger stiffness of radial springs can confine the resonance speeds to those at which the material of the ring is still functioning in the linear elastic regime.

5.2. COMPARISON WITH MOVING LOAD CASE

The critical speeds corresponding to resonances for a constant point load moving circumferentially on an elastic ring are well known. The critical angular velocities satisfy [60, 61, 85, 99]

$$\Omega = \frac{\omega_n}{n} \tag{5.1}$$

for $n \geq 1$, and the minimum resonance speed is the lowest value of the above expression. This conclusion is relatively straightforward since the periodically applied moving load expressed by Dirac function $\delta(\theta - \Omega t)$ can be represented by a Fourier series as [100]

$$\delta(\theta - \Omega t) = \frac{1}{2\pi} + \frac{1}{\pi}\sum_{n=1}^{\infty} \cos n(\theta - \Omega t) = \frac{1}{2\pi} + \frac{1}{\pi}\sum_{n=1}^{\infty} \cos(n\theta - n\Omega t). \tag{5.2}$$

The loading has components with frequency being $n\Omega$. Therefore one expects resonance when $\omega_n = n\Omega$, which is the same to Eq. 5.1. The resonance speeds of each mode actually equal the phase speeds at discrete wavenumber which satisfy $\gamma = n/R$.

For a rotating ring subjected to a stationary point load with constant magnitude, one cannot assure resonances to always occur. It has been concluded that the stiffness of tangential springs plays a key role in the divergence instability [58]. Theoretically, zero stiffness of tangential springs results in divergence at zero rotational speed. Therefore, non-zero stiffness of tangential springs is chosen for comparison with moving load case. Fig. 5.5 and 5.6 show the comparisons of resonance speeds for moving load and rotating ring case with different stiffness of the foundation. For small stiffness of radial springs, no resonances will occur for rotating ring case. Therefore, the parameters in the figures all correspond to quite stiff foundation even for the case of $\bar{k}_r = 0.001$. Four values of $\bar{k}_r$ in Fig. 5.5 and 5.6 are chosen to plot. In Fig. 5.5(a)and 5.6(a) the upper limit of resonance speed is $\bar{v} = 1$ and therefore only the lowest branch of resonance speeds is shown. The reason is that at higher speeds, the predictions of other branches are not accurate since the static expansion is approaching unrealistically high value. Generally, rotation stiffens the ring, therefore, the resonance speeds of rotating ring case are larger than those in the moving load case as is shown in Fig. 5.5(a) and 5.6(a). With increasing $\bar{k}_r$, the resonance speeds for the two lower branches of both cases become close, except in the lower wavenumber ranges as Fig. 5.5(c)-(d) and Fig. 5.6(c)-(d) demonstrate. For the two higher branches of resonance speeds, the differences are still large.

The tangential stiffness $\bar{k}_c$ has more influence on the resonance speeds for lower mode (wave) numbers. For small tangential stiffness of the foundation, divergence in-

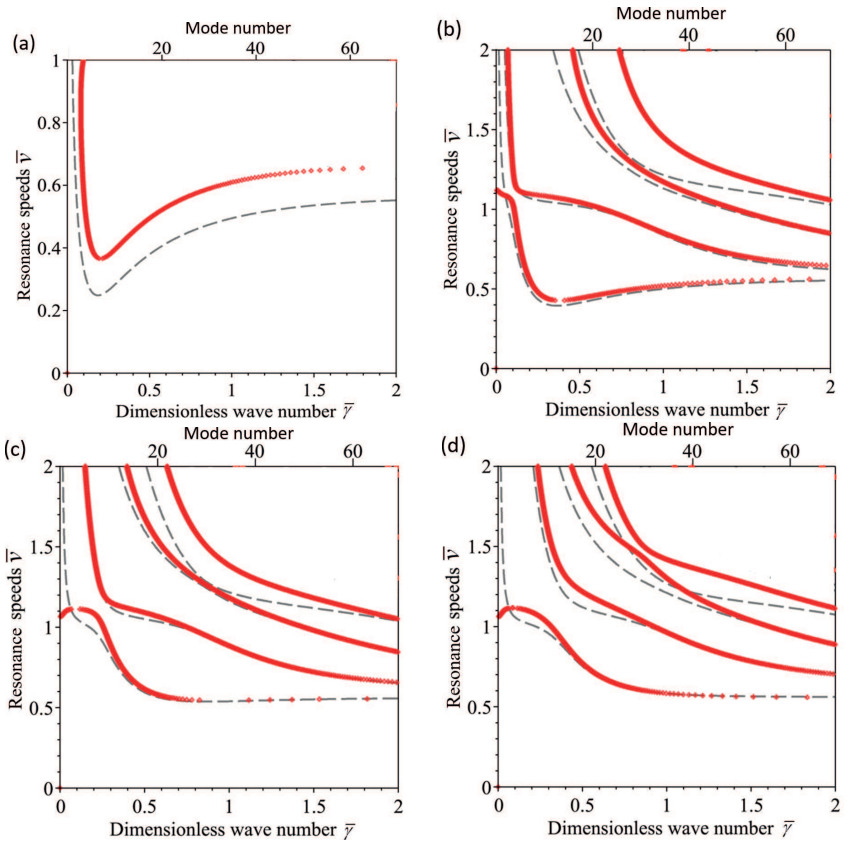

Figure 5.5: Comparison of resonance speeds, $h/R = 0.1, \bar{k}_c = 0.001$ using the high-order model. Grey dashed line for moving load case; Red dots for rotating ring case: (a) $\bar{k}_r = 0.001$; (b) $\bar{k}_r = 0.01$; (c) $\bar{k}_r = 0.1$; (d) $\bar{k}_r = 0.5$.

stability of mode $n = 0$ may happen for rotating rings as shown in Fig. 5.5(b-d). However, for larger $\bar{k}_c$ and $\bar{k}_r$ together, the moving load case and rotating ring case are almost equivalent even for lower mode numbers as shown in Fig. 5.6.

5.3. EFFECTS OF ROTATION ON CRITICAL SPEEDS

Rotating structures, as all gyroscopic systems, are subject to two fictitious forces besides the inertia force. The Coriolis force bifurcates the natural frequencies of the system whereas the centrifugal force generally softens the structures. Also, the rotation causes a pre-stress field, which stiffens the structures. The manifestation of softening effect is the existence of critical speeds at which instability is initiated or resonances occur. The stiffening effect tends to prevent them from happening. The dynamic behaviours of rotating rings depend on the net result of the stress stiffening and softening effects. The existence of critical speeds eventually is associated with the interplay between the stress stiffening and the centrifugal softening.

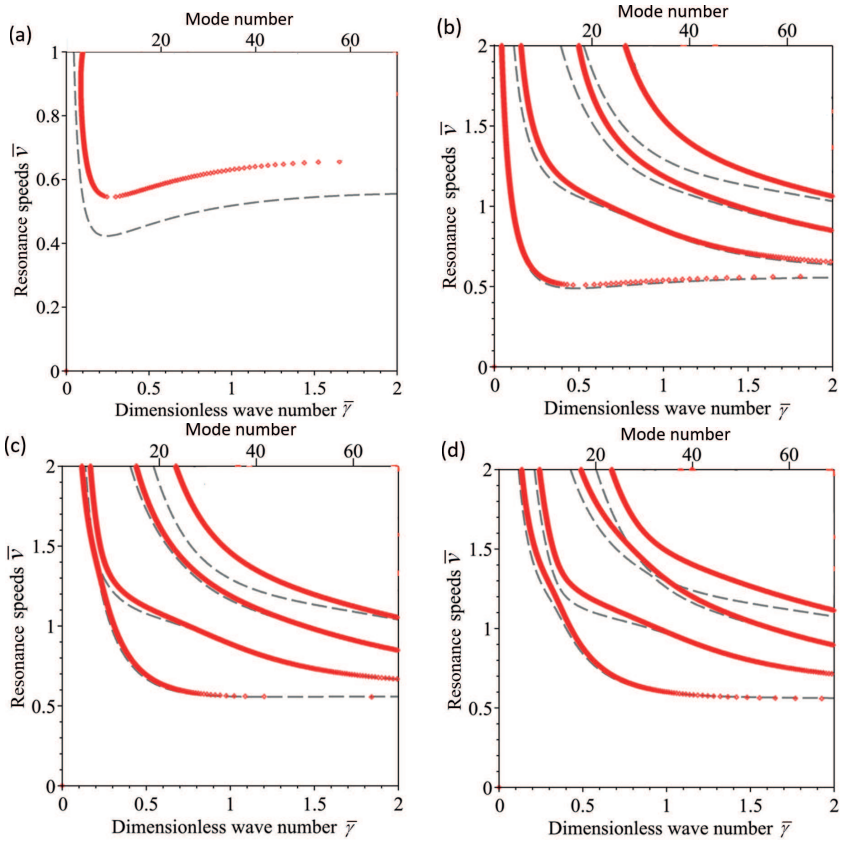

Figure 5.6: Comparison of resonance speeds, $h/R = 0.1$, $\bar{k}_c = 0.1$ using the high-order model. Grey dashed line for moving load case; Red dots for rotating ring case: (a) $\bar{k}_r = 0.001$; (b) $\bar{k}_r = 0.01$; (c) $\bar{k}_r = 0.1$; (d) $\bar{k}_r = 0.5$.

For a floating/free rotating ring, namely a rotating ring without foundation (this case is not realistic but it is a good example to start with), the stiffening caused by pretension seems always smaller than centrifugal softening. No critical speeds exist for this case. Critical speeds are found only when foundation is included, especially foundation with larger stiffnesses. It is shown that the stiffness of circumferential springs influences strongly the critical speed at which instability occurs. If the circumferential stiffness is absent, then for an infinitesimal rotating speed divergence will occur. However, the stiffness of radial springs is a destabilising factor since it constrains the radial expansion of the ring and thus the stiffening effect due to hoop tension decreases.

The effects of rotation is claimed to be of no importance in [101] for the study of the dynamic response of a cylinder cover under a moving load. In [101], the bending stiffness is totally neglected because the cover is made of soft polymer. This statement is only partially true for specific case such as the bending stiffness is zero, or the stiffness of the foundation is much larger than the bending stiffness of the ring.

5.4. CONCLUSIONS

In this chapter, two types of critical speeds of a rotating ring are investigated using the high-order model presented in Chapter 4. The first type corresponds to resonances of a rotating ring subjected to a stationary load. The second one is responsible for instability of the free vibration of a rotating ring. By analysing the critical speeds using different models, it is shown that higher order corrections of displacement are important even for thin rings which are elastically supported by stiff foundation. Based on the predictions of the new model, it is concluded that the bending-dominated motions always experience resonances at lower speeds than those of extensional and shear motions. For higher circumferential wavenumbers, the resonance speed converges to the Rayleigh wave speed. The influence of radial and shear stress boundary effects becomes significant when the foundation is stiff, especially for waves with large wavelength. The classical low-order models become inapplicable when the foundation is stiff or when the ring rotates at high speeds. The Timoshenko-type theory provides relatively good improvement on predictions of critical speeds, however, it is not accurate for rings rotating at high speed or rings supported by stiff foundation either. The reason is twofold. On the one hand, the static equilibrium of the Timoshenko-type theory is similar to the classical low-order theory. Therefore, the stiffening effect is not accurately included. On the other hand, the stress boundary conditions and through-thickness stress variations, which are of importance when the ring rotates at high speeds or supported by stiff springs, are not satisfied using the Timoshenko-type theory. In contrast, the model presented in Chapter 4 can be employed to study the dynamics of high-speed rotating rings since it is superior to all other models and also applicable for thick rings supported by stiff foundation.

The resonance speeds of a rotating ring subjected to stationary loads are compared with the resonance speeds of circumferentially moving load on a stationary ring. It is pointed out that there always exist resonance speeds for the moving load case (although these speeds are too large to be reached in practice), however, the existence of resonance speeds of rotating ring cases depends on the system parameters. Generally, resonance speeds may exist for soft rotating rings resting on stiff foundation. If resonance speeds exist for rotating rings, these speeds are close to those of moving load case if the foundation stiffness is relatively large comparing with the stiffness of the ring itself, namely when $\bar{k}_r$ and $\bar{k}_c$ are large. The minimum resonance speed of the moving load case is smaller than that of the rotating ring case. In Chapter 6, the existence of resonance speeds will be verified by examining the steady-state response of a rotating ring subjected to a stationary constant load.

6

STEADY-STATE RESPONSE OF A ROTATING RING SUBJECTED TO A STATIONARY LOAD

Despite the conflicting opinions in the literature on the existence of resonances of a rotating ring subjected to a stationary load with constant magnitude, resonance speeds are found in Chapter 3 and 5 using different models. Modes which are stationary in a space-fixed reference system, are excited by the load [19] when a ring rotates at its resonance speeds, resulting in a steady-state response which is time-invariant to a space-fixed observer. The experimental evidence of such a steady-state response is the occurrence of the so-called "standing waves" in rolling tires [87, 102]. Theoretically speaking, if the bending stiffness of the ring is small compared to the foundation stiffness so that the former can be altogether neglected, predictions of resonances are available in [101, 102].

In this chapter, the steady-state response of a rotating ring subjected to a stationary load is calculated using the high-order model developed in Chapter 4. It has been shown in Chapter 3 and 5 that the in-plane free vibrations can be unstable. In this Chapter, the parameters of the ring-foundation system are chosen such that the free vibrations are always stable at the rotational speeds which are of interest and therefore the steady-state response exists. The aim is to confirm the existence of resonance speeds and to show the differences in predicted displacements between the classical model presented in [9] and the high-order model developed in Chapter 4. The "Method of the Images" adopted from Ref. [60] is used to obtain the ring response. The influence of foundation stiffness is addressed.

The main original contribution of this chapter lies in the theoretical prediction of a wave-like stationary deformation pattern which occurs in a rotating ring subjected to a stationary load when the ring rotates at speeds higher than the minimum resonance speed. The deformation pattern predicted by the developed model is in agreement with the experimental observation for rolling tyres. To the author's knowledge, neither quan-

titative nor qualitative studies on this matter are reported using a *rotating ring model* with rotation effects properly considered.

6.1. GOVERNING EQUATIONS AND THE "METHOD OF THE IMAGES"

In this section, the high-order model developed in Chapter 4 is employed considering now the work done by external forcing. The technique of solving the governing equations is demonstrated in this section.

6.1.1. COMPLETE DESCRIPTION OF THE PROBLEM

To include loadings in the governing equations by the Hamilton's principle, the work done by the external loads needs to be formulated. A uniformly distributed along the ring width load $P(\theta,z,t)$ is applied to a rotating ring. The variation of the work done by the external load can be written as

$$b\int_{t_1}^{t_2}\int_{-h/2}^{h/2}\int_0^{2\pi}\delta W_{in}\,r\,\mathrm{d}\theta\,\mathrm{d}z\,\mathrm{d}t = b\int_{t_1}^{t_2}\int_{-h/2}^{h/2}\int_0^{2\pi}P(\theta,z,t)\,\delta w\,r\,\mathrm{d}\theta\,\mathrm{d}z\,\mathrm{d}t. \tag{6.1}$$

The same plane strain assumption holds as in Chapter 4. The load is assumed to be acting along the line $\theta=0$ on the outer ring surface and to be given as $P(\theta,z,t)=P(t)\delta(z-h/2)\delta((R+h/2)\theta)$ with $P(t)=P_0\exp(\mathrm{i}\Omega_f t)$ in Fig. 6.1. Note that θ is the polar coordinate of the non-rotating coordinate system whereas φ is the one in rotating coordinate reference system. It is also assumed that the ring rotates at a constant angular speed Ω and experiences a steady expansion before the load is applied. The radial displacement w is defined as positive when it points outward. The positive direction of the circumferential displacement u at an arbitrary point is the same to the linear velocity of this point. Then the variation of the work done by the load reads

$$\begin{aligned} b\int_{t_1}^{t_2}\int_{-h/2}^{h/2}\int_0^{2\pi}\delta W_{in}\,r\,\mathrm{d}\theta\,\mathrm{d}z\,\mathrm{d}t &= b\int_{t_1}^{t_2}\int_{-h/2}^{h/2}\int_0^{2\pi}\left(P(t)\delta(z-\frac{h}{2})\delta((R+\frac{h}{2})\theta)\right)\delta w\,r\,\mathrm{d}\theta\,\mathrm{d}z\,\mathrm{d}t \\ &\quad \text{variation} \\ &= b\int_{t_1}^{t_2}\int_0^{2\pi}\left(P(t)\underset{\text{Dirac function}}{\delta(\theta)}\overset{\text{variation}}{\delta}(w|_{z=h/2})\right)\mathrm{d}\theta\,\mathrm{d}t \end{aligned} \tag{6.2}$$

in which

$$\delta w|_{z=\pm h/2} = \sum_{l=0}^{l=N_1}\delta w_l\,(\pm h/2)^l, (l=0,1,2,3...N_1) \tag{6.3}$$

As shown in Eq. (4.20), the effect of the force will enter governing equations in the radial direction only.

The equations of motion that govern the small vibrations about the static equilib-

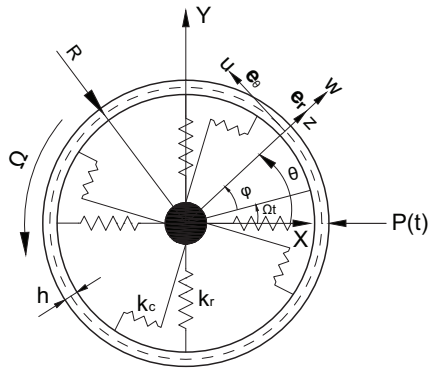

Figure 6.1: A rotating ring subjected to a stationary point load

rium in the radial direction are

$$\int_{\frac{-h}{2}}^{\frac{h}{2}} (\mathrm{I}_1^{lin} z^l)\,\mathrm{d}z + \rho \int_{\frac{-h}{2}}^{\frac{h}{2}} \left(r(\dot{v}_1 + \Omega\, v_1' - \Omega\, v_2) z^l\right)\mathrm{d}z + \left(f_1^{lin} - f_2^{lin}(-1)^l\right)\left(\frac{h}{2}\right)^l =$$
$$- p(\theta,t)(R+h/2)\left(\frac{h}{2}\right)^l = -\frac{R+h/2}{R+h/2}\left(\frac{h}{2}\right)^l P(t)\delta(\theta) = -\left(\frac{h}{2}\right)^l P(t)\delta(\theta), \tag{6.4}$$
$$(l = 0,1,2,3...N_1).$$

The dimension of $p(\theta,t)$ is N.m^{-2} whereas that of $P(t)$ is N.m^{-1}. δ is the Dirac delta function.

The linearised equations of motion in the circumferential direction are

$$\int_{\frac{-h}{2}}^{\frac{h}{2}} (\mathrm{I}_2^{lin} z^q)\,\mathrm{d}z + \rho \int_{\frac{-h}{2}}^{\frac{h}{2}} \left(r(\dot{v}_2 + \Omega\, v_2' + \Omega\, v_1) z^q\right)\mathrm{d}z + \left(f_3^{lin} - f_4^{lin}(-1)^q\right)\left(\frac{h}{2}\right)^q = 0, \tag{6.5}$$
$$(q = 0,1,2,3...N_2).$$

The details of the governing equations including all the coefficients and expressions, can be found in Eqs. (4.28-4.30). Due to the closeness of the ring, the load applies periodically with a spatial period of 2π. Therefore, the responses need to comply with the periodicity condition, i.e.:

$$w_d(z,0,t) = \sum_{l=0}^{l=N_1} w_{dl}(0,t)\, z^l = w_d(z,2\pi j,t) = \sum_{l=0}^{l=N_1} w_{dl}(2\pi j,t)\, z^l,$$
$$u_d(z,0,t) = \sum_{q=0}^{q=N_2} u_{dq}(0,t)\, z^q = u_d(z,2\pi j,t) = \sum_{q=0}^{q=N_2} u_{dq}(2\pi j,t)\, z^q, \tag{6.6}$$
$$(j = 1,2,3...\infty).$$

Furthermore, each component of the displacement expansion should satisfy the same periodicity condition:

$$w_{dl}(0,t) = w_{dl}(2\pi j,t), \quad u_{dq}(0,t) = u_{dq}(2\pi j,t), \quad (j = 1,2,3...\infty). \tag{6.7}$$

The subscript 'd' stands for dynamic displacements and is hereafter omitted for the sake of brevity.

The solutions will be sought for in dimensionless form. The dimensionless parameters adopted are the same as in Eq. (4.38). Introducing a dimensionless coordinate $\bar{z} = z/(h/2)$, the dimensionless displacements are defined as

$$\begin{aligned} W(\bar{z},\bar{\theta},\tau) &= w(z,\theta,t)/R, \\ U(\bar{z},\bar{\theta},\tau) &= u(z,\theta,t)/R \end{aligned} \tag{6.8}$$

and therefore

$$\begin{aligned} &W_l(\bar{\theta},\tau) = \left(\frac{h}{2}\right)^l w_l(\theta,t)/R, \quad U_q(\bar{\theta},\tau) = \left(\frac{h}{2}\right)^q u_q(\theta,t)/R, \\ &(l = 0,1,2,3...N_1, q = 0,1,2,3...N_2). \end{aligned} \tag{6.9}$$

in which the dimensionless form of the space-fixed coordinate is defined as $\{\bar{\theta} = \theta/\bar{k}, \tau = c_0 t/k\}$.

The equations that govern vibrations of a rotating ring subjected to a stationary point load from the classical theory in space-fixed coordinate are [9]

$$\begin{aligned} &\rho h\ddot{w} + 2\rho h\Omega(\dot{w}' - \dot{u}) - \rho h\Omega^2(w + 2u' - w'') + \frac{D}{R^4}(w'''' - u''') + \\ &\frac{K}{R^2}(w + u') + \frac{\sigma_\theta^0 h}{R^2}(u' - w'') + k_r w = -\frac{P(t)}{R}\delta(\theta), \\ &\rho h\ddot{u} + 2\rho h\Omega(\dot{u}' + \dot{w}) - \rho h\Omega^2(u - 2w' - u'') + \frac{D}{R^4}(w''' - u'') - \\ &\frac{K}{R^2}(w' + u'') + \frac{\sigma_\theta^0 h}{R^2}(u - w') + k_c u = 0. \end{aligned} \tag{6.10}$$

where $D = Eh^3/12$ is the bending stiffness, $K = Eh$ is the membrane stiffness, and $\sigma_\theta^0 = \rho R^2\Omega^2/(1 + k_r R^2/K - \rho R^2\Omega^2/E)$ is the initial hoop stress caused by rotation. The periodicity conditions must be satisfied:

$$w(0,t) = w(2\pi j, t), \quad u(0,t) = u(2\pi j, t). \tag{6.11}$$

Eqs. (6.10-6.11) complete the description of the problem using the classical thin ring model.

Eqs. (6.10) can be rewritten in dimensionless form as

$$\begin{aligned} &W_{\tau\tau} + W_{\bar{\theta}\bar{\theta}\bar{\theta}\bar{\theta}} + (\bar{N} + \bar{v}^2)W_{\bar{\theta}\bar{\theta}} + (\bar{k}^2 + \bar{k}_r - \bar{k}^2\bar{v}^2)W + 2\bar{v}W_{\bar{\theta}\bar{\tau}} - \bar{k}U_{\bar{\theta}\bar{\theta}\bar{\theta}} \\ &+ (\bar{k} + \bar{k}\bar{N} - 2\bar{k}\bar{v}^2)U_{\bar{\theta}} - 2\bar{k}\bar{v}U_\tau = -\bar{P}(\tau)\delta(\bar{\theta}) \\ &U_{\tau\tau} - (\bar{k}^2 + 1 - \bar{v}^2)U_{\bar{\theta}\bar{\theta}} + (\bar{k}_c - \bar{k}^2\bar{v}^2 + \bar{k}^2\bar{N})U + 2\bar{v}U_{\bar{\theta}\bar{\tau}} + \bar{k}W_{\bar{\theta}\bar{\theta}\bar{\theta}} \\ &- (\bar{k} + \bar{k}\bar{N} - 2\bar{k}\bar{v}^2)W_{\bar{\theta}} + 2\bar{k}\bar{v}W_\tau = 0 \end{aligned} \tag{6.12}$$

using the same dimensionless parameters introduced in Eq. (4.38). In Eq. (6.12) only low order terms remain, i.e.

$$W_0(\bar{\theta},\tau) = w_0(\theta,t)/R, \quad U_0(\bar{\theta},\tau) = u_0(\theta,t)/R. \tag{6.13}$$

6.1.2. METHOD OF THE IMAGES

The method of the images has been first applied to study the steady-state response of an elastic ring subjected to a moving load in [60]. The idea of this method is that the response of a bounded (in our case ring-like) system to a single load is equivalent to the response of a part of an infinitely long system (described by the same equations) subjected to an infinite set of loads in the linear framework. In other words, the method utilizes the fact that by introducing additional loads the periodicity boundary conditions are satisfied. These loads are called images since their locations are normally mirrored to the real load with respect to the boundaries. In the considered case, to satisfy the periodicity of the displacements, one should introduce infinitely many equivalent loads at a fixed distance 2π from each other.

The equations of motion that govern the small vibrations about the static equilibrium in the radial direction read

$$\begin{aligned}&\int_{\frac{-h}{2}}^{\frac{h}{2}} (\mathrm{I}_1^{lin} z^l)\,\mathrm{d}z + \rho \int_{\frac{-h}{2}}^{\frac{h}{2}} \left(r(\dot{v}_1 + \Omega\, v_1' - \Omega\, v_2) z^l\right)\mathrm{d}z + \left(f_1^{lin} - f_2^{lin}(-1)^l\right)\left(\frac{h}{2}\right)^l = \\ &- P(t)\left(\frac{h}{2}\right)^l \sum_{j=-\infty}^{\infty} \delta(\theta + 2\pi j), \\ &(l = 0, 1, 2, 3 \ldots N_1).\end{aligned} \tag{6.14}$$

The linearised equations of motion in the circumferential direction are given as

$$\begin{aligned}&\int_{\frac{-h}{2}}^{\frac{h}{2}} (\mathrm{I}_2^{lin} z^q)\,\mathrm{d}z + \rho \int_{\frac{-h}{2}}^{\frac{h}{2}} \left(r(\dot{v}_2 + \Omega\, v_2' + \Omega\, v_1) z^q\right)\mathrm{d}z + \left(f_3^{lin} - f_4^{lin}(-1)^q\right)\left(\frac{h}{2}\right)^q = 0, \\ &(q = 0, 1, 2, 3 \ldots N_2)\end{aligned} \tag{6.15}$$

in which the periodicity condition Eq. (6.6) is now captured by the summation of infinitely many equally-spaced point loads. The same holds for the classical model. The first equation in Eq. (6.12) becomes*

$$\begin{aligned}&W_{\tau\tau} + W_{\bar{\theta}\bar{\theta}\bar{\theta}\bar{\theta}} + (\bar{N} + \bar{v}^2) W_{\bar{\theta}\bar{\theta}} + (\bar{k}^2 + \bar{k}_r - \bar{k}^2 \bar{v}^2) W + 2\bar{v} W_{\bar{\theta}\bar{\tau}} - \bar{k} U_{\bar{\theta}\bar{\theta}\bar{\theta}} \\ &+ (\bar{k} + \bar{k}\bar{N} - 2\bar{k}\bar{v}^2) U_{\bar{\theta}} - 2\bar{k}\bar{v} U_{\tau} = -\bar{P}(\tau) \sum_{j=-\infty}^{\infty} \delta(\bar{\theta} + 2\pi j/\bar{k})\end{aligned} \tag{6.16}$$

when the periodicity condition is considered by a summation of infinitely many loads. The dimensionless force is expressed by

$$\bar{P} = \frac{P}{Eh}\bar{k}. \tag{6.17}$$

Since the problem is linear, the exact solution is the summation of the responses to all the individual loads and all the loads generate equivalent displacement fields but with spatial shift. More specifically, it suffices to obtain the response of the axially moving "extended ring" to a single load and then sum up this response infinitely many times

*Due to complexity, the dimensionless forms of Eqs. (6.14-6.15) from the high-order model are not explicitly given here.

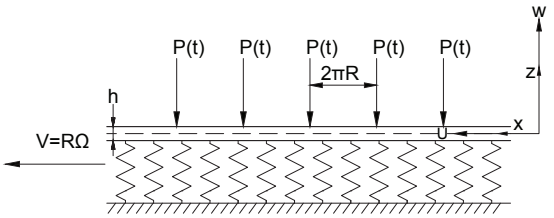

Figure 6.2: Method of the Images for an axially moving "extended ring"

accounting for the spatial shift 2π. One of the main advantages of the method of the images is that the aforementioned infinite summation can be computed analytically, using the formulae of an infinite geometric progression [60].

Considering a single load, the dimensionless form of equations (6.14-6.15) can be solved by means of application of the integral Fourier transform. Defining this transform as

$$\left\{ \begin{array}{c} \tilde{\tilde{W}}_l^{(\bar{\omega},\bar{\gamma})} \\ \tilde{\tilde{U}}_q^{(\bar{\omega},\bar{\gamma})} \end{array} \right\} = \int_{-\infty}^{+\infty} \int_{-\infty}^{+\infty} \left\{ \begin{array}{c} W_l \\ U_q \end{array} \right\} \exp(-\mathrm{i}\bar{\gamma}\bar{\theta} - \mathrm{i}\bar{\omega}\tau)\mathrm{d}\tau\mathrm{d}\bar{\theta} \tag{6.18}$$

where i is the imaginary unit and $\bar{\gamma} = n\bar{k}$ since it is defined that $\bar{\theta} = \theta/\bar{k}$. The definition of Eq. (6.18) is consistent with the assumed form of modes $\exp(\mathrm{i}n\theta + \mathrm{i}\omega t)$ in Chapters 2, 3 and 5. Applying the above transformation to the dimensionless form of equations (6.14-6.15), one obtains a set of algebraic equations

$$\mathbf{Ca} = \mathbf{f} \tag{6.19}$$

in which $\mathbf{C}$ is the coefficient matrix, $\mathbf{a}$ is the displacement vector and $\mathbf{f}$ is the force vector. The matrix and vectors are given in Appendix C.

All the unknown displacement components can be solved using the Cramer's rule. Each of them can be expressed in the form:

$$\begin{aligned} \tilde{\tilde{W}}_l^{(\bar{\omega},\bar{\gamma})} &= \frac{\det(\mathbf{C}_l)}{\det(\mathbf{C})} = \frac{2\pi\bar{P}_0\delta(\bar{\omega}-\bar{\Omega}_f)\Delta_{wl}}{\Delta} \\ \tilde{\tilde{U}}_q^{(\bar{\omega},\bar{\gamma})} &= \frac{\det(\mathbf{C}_{N_1+1+q})}{\det(\mathbf{C})} = \frac{2\pi\bar{P}_0\delta(\bar{\omega}-\bar{\Omega}_f)\Delta_{uq}}{\Delta} \end{aligned} \tag{6.20}$$

in which $\bar{\Omega}_f = \Omega_f k/c_0$ is the dimensionless frequency of the load and $\bar{P}_0 = P_0\,\bar{k}/(Eh)$ is the dimensionless load amplitude. Matrix $\mathbf{C}_l$ is formed by replacing the l-th column of $\mathbf{C}$ by the force vector $\mathbf{f}$ whereas $\mathbf{C}_{N_1+1+q}$ is the matrix $\mathbf{C}$ whose (N_1+1+q)-th column is replaced by $\mathbf{f}$.

The next step is to invert the obtained solutions Eq. (6.20) to the time and space domain by using the inverse Fourier transform. This can be done by following the pro-

cedure introduced in Ref. [60]:

$$\begin{aligned} W_l{}^s(\bar{\theta},\tau) &= \frac{\bar{P}_0}{2\pi}\exp\left(\mathrm{i}\bar{\Omega}_f\tau\right)\int_{-\infty}^{+\infty}\frac{\Delta_{wl}(\bar{\Omega}_f,\bar{\gamma})}{\Delta(\bar{\Omega}_f,\bar{\gamma})}\exp(\mathrm{i}\bar{\gamma}\bar{\theta})\mathrm{d}\bar{\gamma} \\ U_q{}^s(\bar{\theta},\tau) &= \frac{\bar{P}_0}{2\pi}\exp\left(\mathrm{i}\bar{\Omega}_f\tau\right)\int_{-\infty}^{+\infty}\frac{\Delta_{uq}(\bar{\Omega}_f,\bar{\gamma})}{\Delta(\bar{\Omega}_f,\bar{\gamma})}\exp(\mathrm{i}\bar{\gamma}\bar{\theta})\mathrm{d}\bar{\gamma} \end{aligned} \tag{6.21}$$

where $\bar{\theta}$ is the distance from the load. The integral in Eq. (6.21) can be evaluated by employing the residue theorem.

when $\bar{\theta} > 0$:

$$\left\{W_l{}^s;\ U_q{}^s\right\} = \mathrm{i}\bar{P}_0\exp\left(\mathrm{i}\bar{\Omega}_f\tau\right)\sum_p\left\{B_{wl}{}^p;\ B_{uq}{}^p\right\}\exp(\mathrm{i}\bar{\gamma}_p\bar{\theta}) \tag{6.22}$$

when $\bar{\theta} < 0$:

$$\left\{W_l{}^s;\ U_q{}^s\right\} = -\mathrm{i}\bar{P}_0\exp\left(\mathrm{i}\bar{\Omega}_f\tau\right)\sum_n\left\{B_{wl}{}^n;\ B_{uq}{}^n\right\}\exp(\mathrm{i}\bar{\gamma}_n\bar{\theta}) \tag{6.23}$$

where

$$\begin{aligned} \left\{B_{wl}{}^p;\ B_{uq}{}^p\right\} &= \left(\frac{\left\{\Delta_{wl}(\bar{\Omega}_f,\bar{\gamma}_p);\ \Delta_{uq}(\bar{\Omega}_f,\bar{\gamma}_p)\right\}}{\frac{\partial}{\partial\bar{\gamma}}\left(\Delta(\bar{\Omega}_f,\bar{\gamma})\right)|_{\bar{\gamma}=\bar{\gamma}_p}}\right), \\ \left\{B_{wl}{}^n;\ B_{uq}{}^n\right\} &= \left(\frac{\left\{\Delta_{wl}(\bar{\Omega}_f,\bar{\gamma}_n);\ \Delta_{uq}(\bar{\Omega}_f,\bar{\gamma}_n)\right\}}{\frac{\partial}{\partial\bar{\gamma}}\left(\Delta(\bar{\Omega}_f,\bar{\gamma})\right)|_{\bar{\gamma}=\bar{\gamma}_n}}\right). \end{aligned} \tag{6.24}$$

$\bar{\gamma}_n$ denotes the roots of equation $\Delta(\bar{\Omega}_f,\bar{\gamma}) = 0$ with negative imaginary part, whereas $\bar{\gamma}_p$ denotes the roots of $\Delta(\bar{\Omega}_f,\bar{\gamma}) = 0$ with positive imaginary part.

After obtaining the solutions in the time domain for the single load case, the exact solution can be found as an infinite summation of terms with the spatial shift 2π, namely

$$W_l(\bar{\theta},\tau) = \sum_{j=-\infty}^{\infty} W_l{}^s(\bar{\theta}+2\pi j/\bar{k},\tau),\ U_q(\bar{\theta},\tau) = \sum_{j=-\infty}^{\infty} U_q{}^s(\bar{\theta}+2\pi j/\bar{k},\tau). \tag{6.25}$$

After some manipulations, the analytical expressions of the displacements of the ring can be derived as [60]

for $\pi/\bar{k} > \bar{\theta} > 0$:

$$\begin{aligned} \left\{W_l;\ U_q\right\} =& \mathrm{i}\bar{P}_0\Big(\sum_p\left\{B_{wl}{}^p;\ B_{uq}{}^p\right\}\frac{\exp(\mathrm{i}\bar{\gamma}_p\bar{\theta})}{1-\exp(\mathrm{i}2\pi\bar{\gamma}_p/\bar{k})} \\ &-\sum_n\left\{B_{wl}{}^n;\ B_{uq}{}^n\right\}\frac{\exp\left(\mathrm{i}\bar{\gamma}_n(\bar{\theta}-2\pi/\bar{k})\right)}{1-\exp(-\mathrm{i}2\pi\bar{\gamma}_n/\bar{k})}\Big)\exp(\mathrm{i}\bar{\Omega}_f\tau) \end{aligned} \tag{6.26}$$

for $-\pi/\bar{k} < \bar{\theta} < 0$:

$$\begin{aligned}\{W_l;\, U_q\} =& \mathrm{i}\bar{P}_0\Big(\sum_p \{{B_{wl}}^p;\, {B_{uq}}^p\}\frac{\exp\left(\mathrm{i}\bar{\gamma}_p(\bar{\theta}+2\pi/\bar{k})\right)}{1-\exp(\mathrm{i}2\pi\bar{\gamma}_p/\bar{k})} \\ &-\sum_n \{{B_{wl}}^n;\, {B_{uq}}^n\}\frac{\exp(\mathrm{i}\bar{\gamma}_n\bar{\theta})}{1-\exp(-\mathrm{i}2\pi\bar{\gamma}_n/\bar{k})}\Big)\exp(\mathrm{i}\bar{\Omega}_f\tau)\end{aligned} \tag{6.27}$$

The real part of the above-given solution should be taken if the time signature of the load is given as $P(t) = P_0\cos(\Omega_f t)$, whereas the imaginary part corresponds to $P(t) = P_0\sin(\Omega_f t)$. $\bar{P}_0$ is the dimensionless load amplitude which equals $P_0\bar{k}/(Eh)$. The total dimensionless displacements are

$$W(\bar{z},\bar{\theta},\bar{\tau}) = \sum_{l=0}^{N_1}\left(\bar{z}^l\, W_l(\bar{\theta},\bar{\tau})\right),\;\; U(\bar{z},\bar{\theta},\bar{\tau}) = \sum_{q=0}^{N_2}\left(\bar{z}^q\, U_q(\bar{\theta},\bar{\tau})\right). \tag{6.28}$$

6.1.3. APPROXIMATION OF A POINT LOAD BY GAUSSIAN DISTRIBUTION

When a constant line load along the out-of-plane direction is applied to a two-dimensional medium, the assumptions of linear elasticity are invariably violated in the vicinity of the loading point for the elasticity theory [103], as well as for the high-order theory presented here. This is the intrinsic problem of this type of higher-order theories, not only rings, but also for shells, beams, etc. and for both static and dynamic loads. For stiff rings (soft foundation), such as rings made of steel, the sharp changes at the loading point of higher order terms are not obvious. This is due to the fact that the deformation caused by the concentrated force is balanced primarily by the foundation (the excitation of $n = 1$ mode). For soft rings (stiff foundation), the force causes much larger elastic deformations in the ring than the deformation of the foundation. Therefore, the violation becomes apparent. In order to circumvent this problem, one may realistically assume that a contact patch exists on the ring and thus distributed forces are applied on the ring. A Gaussian distribution can be used to specify the distribution of tractions within the contact patch. The displacements under the loading position become smooth if a distributed force is applied instead of a concentrated one. Using a normalized Gaussian distribution, the load represented by Dirac function can be replaced by a distributed load in the following manner:

$$P(t)\delta(\theta) = \frac{P_0\exp(\mathrm{i}\Omega_f t)}{\sqrt{2\pi\sigma^2}}\exp\left(-\frac{\theta^2}{2\sigma^2}\right). \tag{6.29}$$

The integrals of the left-hand side and right-hand side of Eq. (6.29) from $-\pi$ to π both equal to $P(t)$. Consequently, Eq. (6.21), namely the dynamic response of the ring under a single load, becomes

$$\begin{aligned}{W_l}^s(\bar{\theta},\tau) &= \frac{1}{2\pi}\exp\left(\mathrm{i}\bar{\Omega}_f\tau\right)\int_{-\infty}^{+\infty}\frac{\bar{P}(\bar{\gamma})\Delta_{wl}(\bar{\Omega}_f,\bar{\gamma})}{\Delta(\bar{\Omega}_f,\bar{\gamma})}\exp(\mathrm{i}\bar{\gamma}\bar{\theta})\mathrm{d}\bar{\gamma} \\ {U_q}^s(\bar{\theta},\tau) &= \frac{1}{2\pi}\exp\left(\mathrm{i}\bar{\Omega}_f\tau\right)\int_{-\infty}^{+\infty}\frac{\bar{P}(\bar{\gamma})\Delta_{uq}(\bar{\Omega}_f,\bar{\gamma})}{\Delta(\bar{\Omega}_f,\bar{\gamma})}\exp(\mathrm{i}\bar{\gamma}\bar{\theta})\mathrm{d}\bar{\gamma}\end{aligned} \tag{6.30}$$

where $\bar{P}(\bar{\gamma})$ is the dimensionless form of the Fourier transform of

$$\frac{P_0}{\sqrt{2\pi\sigma^2}}\exp\left(-\frac{\theta^2}{2\sigma^2}\right) \tag{6.31}$$

in the wave number domain. Eq. (6.30) can be evaluated by direct numerical integration. After obtaining the dynamic response of the ring under a single load, the total response is given by Eq. (6.25) together with Eq. (6.28) because of linearity of the system.

6.1.4. SOLUTION BY MEANS OF MODAL ANALYSIS

Modal analysis is commonly used in the literature to calculate the response of rotating rings under various loads [14, 20, 36]. It has been shown in Ref. [104] that the method of the images allows one to obtain an exact analytical expression for the ring response. The main advantage of the method of the images is that it allows to obtain the deformation field in the vicinity of the load with a very high accuracy.

6.1.5. CONSIDERATION OF DAMPING

The energy dissipation in the rotating ring can be considered in two ways. One way is to treat the foundation as Kelvin–Voigt elements with spring and dashpot in parallel. In this case, the damping force equals the damping coefficient times the relative velocities. The virtual work resulting from the damping force is

$$\int_{t_1}^{t_2}\delta W_c \mathrm{d}t = \int_{t_1}^{t_2}\int_0^{2\pi}\sigma_w v_1|_{-h/2}\,\delta w|_{-h/2}\,(R-h/2)\mathrm{d}\theta\mathrm{d}t \tag{6.32}$$

$$\int_{t_1}^{t_2}\delta W_{c2} \mathrm{d}t = \int_{t_1}^{t_2}\int_0^{2\pi}\sigma_u v_2|_{-h/2}\,\delta u|_{-h/2}\,(R-h/2)\mathrm{d}\theta\mathrm{d}t \tag{6.33}$$

or one can include the viscous damping of the foundation simply by replacing

$$\begin{aligned} k_r &\to k_r + \sigma_w\left(\frac{\partial}{\partial t}+\Omega\frac{\partial}{\partial\theta}\right),\\ k_c &\to k_c + \sigma_u\left(\frac{\partial}{\partial t}+\Omega\frac{\partial}{\partial\theta}\right). \end{aligned} \tag{6.34}$$

Note that in Eq. (6.33), in the expression for v_2, there is a constant component $R\Omega$. This component needs to be neglected when formulating the dashpots's reaction force.

Another dissipation mechanism is the internal damping of the ring material. When one considers large values of $\bar{k}_r$ (stiff foundation), one is equivalently considering soft materials like rubbers and polymers. Provided that, one needs to take into account their viscoelastic properties since the energy is dissipated mainly by the material itself. In this sense, the following complex moduli [105] can be used for the ring itself:

$$E^* = E_s + \mathrm{i}E_l\mathbf{sgn}(\omega),\ G^* = G_s + \mathrm{i}G_l\mathbf{sgn}(\omega) \tag{6.35}$$

where **sgn** is the signum function, E_s and G_s are the storage moduli, E_l and G_l are the loss moduli.

Another way to include the internal damping is to introduce

$$E^* = E(1+\zeta(\partial/\partial t + \Omega\partial/\partial\theta)) \tag{6.36}$$

where ζ is the hysteresis loss factor of the material. The shear modulus given by Eq. (4.5) changes accordingly to

$$G^* = \frac{E^*}{2(1+\nu)} = G(1+\zeta(\partial/\partial t + \Omega\partial/\partial\theta)). \tag{6.37}$$

The Lamé constants can be obtained accordingly.

6.2. STEADY-STATE RESPONSE OF A ROTATING RING UNDER A STATIONARY LOAD

The steady-state response of a rotating ring under a stationary point load is studied in this section for different dimensionless parameters. The dimensionless parameters $\bar{k}_r$ and $\bar{k}_c$ which represent the ratios of the stiffness of the foundation to the stiffness of the ring itself are of significant importance. Low values of $\bar{k}_r$ and $\bar{k}_c$ imply that the ring itself is stiff compared to the elastic foundation, for example, a steel ring. In contrast, high values of $\bar{k}_r$ and $\bar{k}_c$ indicate that the ring is soft in comparison with the elastic foundation, for example, a ring made of rubber-like material; or equivalently the radius of the ring is large. In the following calculations, $N_1 = N_2 = 5$ is chosen in Eq. (6.14-6.15) the same as Chapter 5.

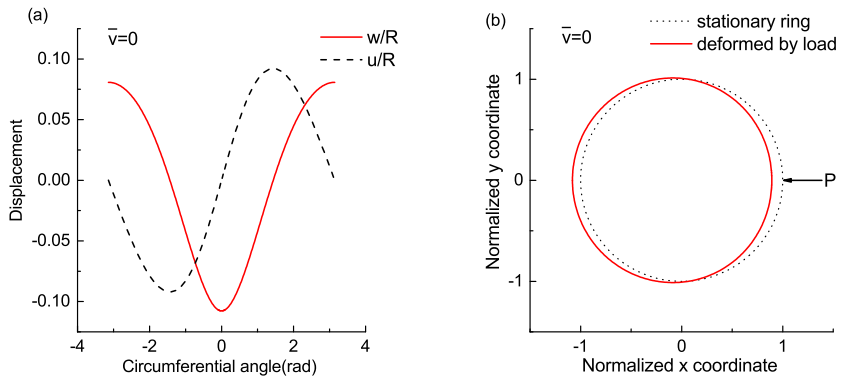

Figure 6.3: Classical model, $\bar{v} = 0$, $\bar{k}_r = 1\times10^{-6}$, $\bar{k}_c = 1\times10^{-9}$: (a) Displacements; (b) Ring deformation pattern.

6.2.1. SOFT FOUNDATION

A ring supported by soft springs can correspond to two cases: a) the foundation flexibility is large comparing to that of the ring; b) the ring has a small radius. The following dimensionless parameters are chosen: $\bar{k}_r = 1\times10^{-6}$ which stands for a soft foundation; the thickness-radius ratio $\kappa = h/R = 0.1$; the dimensionless force $\bar{P}_0 = 1\times10^{-5}$. The ring

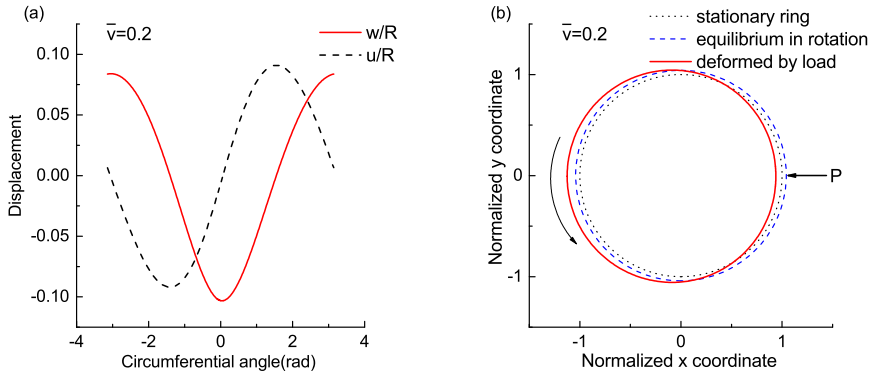

Figure 6.4: Classical model, $\bar{v} = 0.2$, $\bar{k}_r = 1 \times 10^{-6}$, $\bar{k}_c = 1 \times 10^{-9}$: (a) Displacements; (b) Ring deformation pattern.

is assumed to rest on a viscoelastic foundation. A coefficient ξ is introduced to represent the ratio of the viscous damping to the stiffness of the foundation. The ratios are defined as follows:

$$\xi_w = \frac{\sigma_w}{k_r}, \xi_u = \frac{\sigma_u}{k_c}. \tag{6.38}$$

For simplicity, the same ratio is applied in both the radial and circumferential directions, namely $\xi_w = \xi_u = \xi = 5 \times 10^{-3}$. The Poisson's ratio is chosen to be $\nu = 0.3$ which refers to a steel ring.

The steady-state response calculated from the classical model is first studied first. Fig. 6.3 shows the static response of a stationary ring subjected to a radial point load with constant magnitude according to the classical model Eq. (6.10). Fig. 6.4 shows the quasi-static response of the same ring subjected to the same load; but now the ring rotates at $\bar{v} = 0.2$. The classical model, Eq. (6.10), is used. From Fig. 6.3, it can be seen that the circumferential displacement is almost a perfect sinus, whereas the radial displacement is of a cosinusoidal shape with a translation in the direction of the applied force. The ring exhibits a translational rigid body-like motion in the direction of the applied force governed mainly by the $n = 1$ mode. As for $\bar{v} = 0.2$, the ring experiences a static radial expansion caused by rotation. The response is still mainly governed by the $n = 1$ mode. Damping starts to play a role when the ring rotates. It causes asymmetry of the ring deformation patterns with respect to the position of the applied load. The steady-state responses predicted from the high-order model are not plotted. It is because the responses calculated from the classical model and the high-order model are very similar; the responses predicted by the high-order model are just slightly smaller. When the applied load is varying harmonically, e.g. $\bar{P}(\tau) = \bar{P}_0 \cos(\bar{\Omega}_f \tau)$, many higher modes can be excited. The difference between the classical model and the high-order model are more obvious in this case but still marginal provided that the frequency of excitation is about or lower than the first cut-off frequency of the system.

The influence of circumferential springs can be assessed by comparing Figs. 6.3-6.4

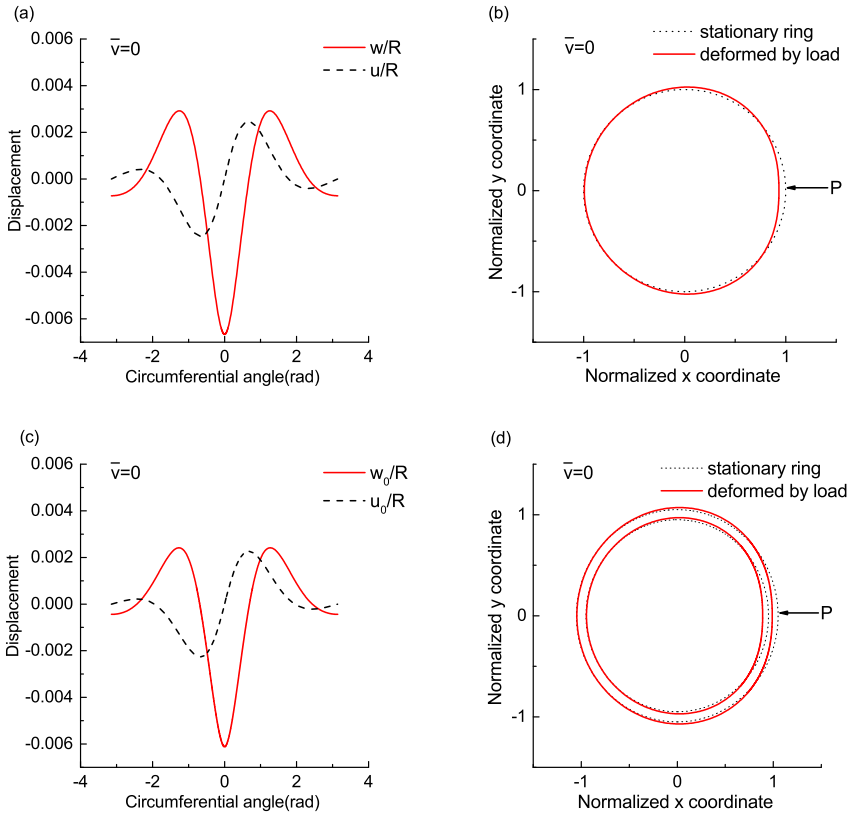

Figure 6.5: Displacements and deformation patterns of $\bar{k}_r = 1 \times 10^{-6}$, $\bar{k}_c = 1 \times 10^{-4}$, $\bar{v} = 0$: (a)(b) Classical model; (c)(d) High-order model. The ring deformation patterns are scaled by 10.

to Figs. 6.5-6.6. The presence of $\bar{k}_c$ suppresses the responses in both the radial and circumferential directions. As expected, the effect on circumferential displacement is more significant.

6.2.2. STIFF FOUNDATION

In this case, the material itself is soft or, equivalently, the ring has relatively large radius. Again $\kappa = h/R = 0.1$ is assumed. The Poisson's ratio is chosen to be $\nu = 0.4$ since the material is soft. As discussed in subsection 6.1.5, when soft materials like rubbers or polymers are considered, the viscoelastic properties are better captured by the loss factor of the material, e.g. Eq. (6.36). Here $\zeta = 0.002$ is employed. In addition, $\bar{k}_c = 0.1, \bar{k}_r = 0.01$ are chosen to represent a stiff foundation. The dimensionless force is selected to be $\bar{P}_0 = 0.002$. It has been shown in Chapter 5 that there exists a critical speed after which wave-like patterns occur for a rotating ring subjected to a stationary load with constant magnitude. It is the aim of this section to confirm the existence of critical speeds or,

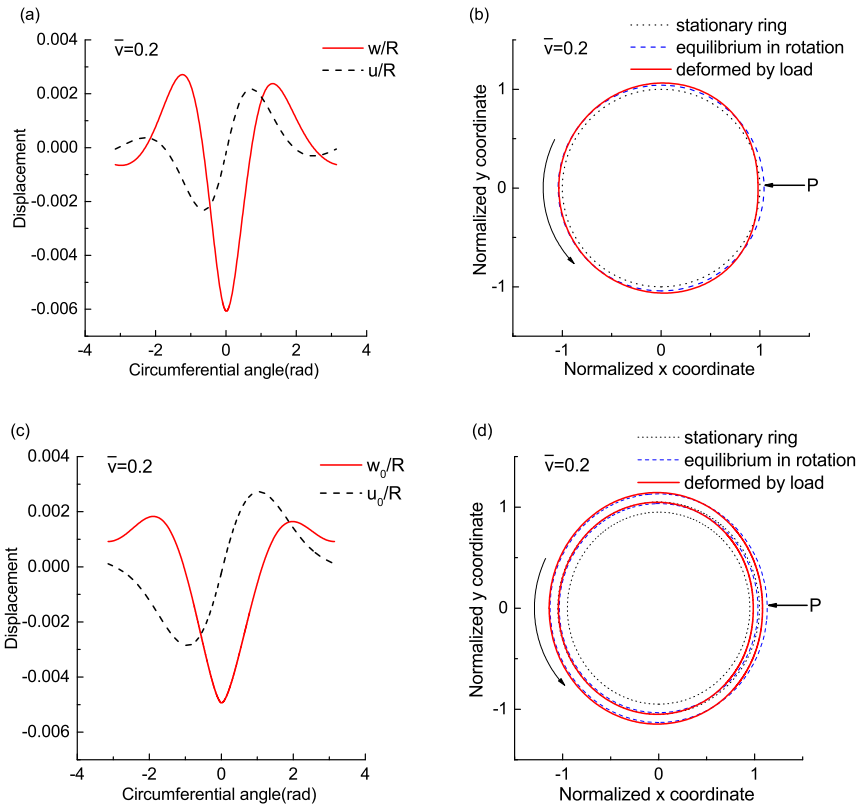

Figure 6.6: Displacements and deformation patterns of $\bar{k}_r = 1 \times 10^{-6}$, $\bar{k}_c = 1 \times 10^{-4}$, $\bar{v} = 0.2$: (a)(b) Classical model; (c)(d) High-order model. The ring deformation patterns are scaled by 10.

equivalently, the existence of stationary wave-like deformation.

DYNAMIC RESPONSE UNDER A CONSTANT LOAD

Fig. 6.7 presents the displacements and deformation patterns for $\bar{v} = 0$ (statics) using classical and the developed high-order model. For both the classical and the high-order model, the point load is approximated by Gaussian distribution Eq. (6.29) with $\sigma = 0.01$. Due to bending stiffness, the radial displacement using classical model has positive displacement around the loading point whereas it is not an apparent situation for radial displacement obtained using the high-order model. The high-order model predicts larger circumferential displacements than the classical model. It is interesting to see that the circumferential displacement at the outer surface has different phase comparing with components in middle and inner surfaces. The responses are localized and symmetric for a stationary ring as shown in Fig. 6.7(e)(f).

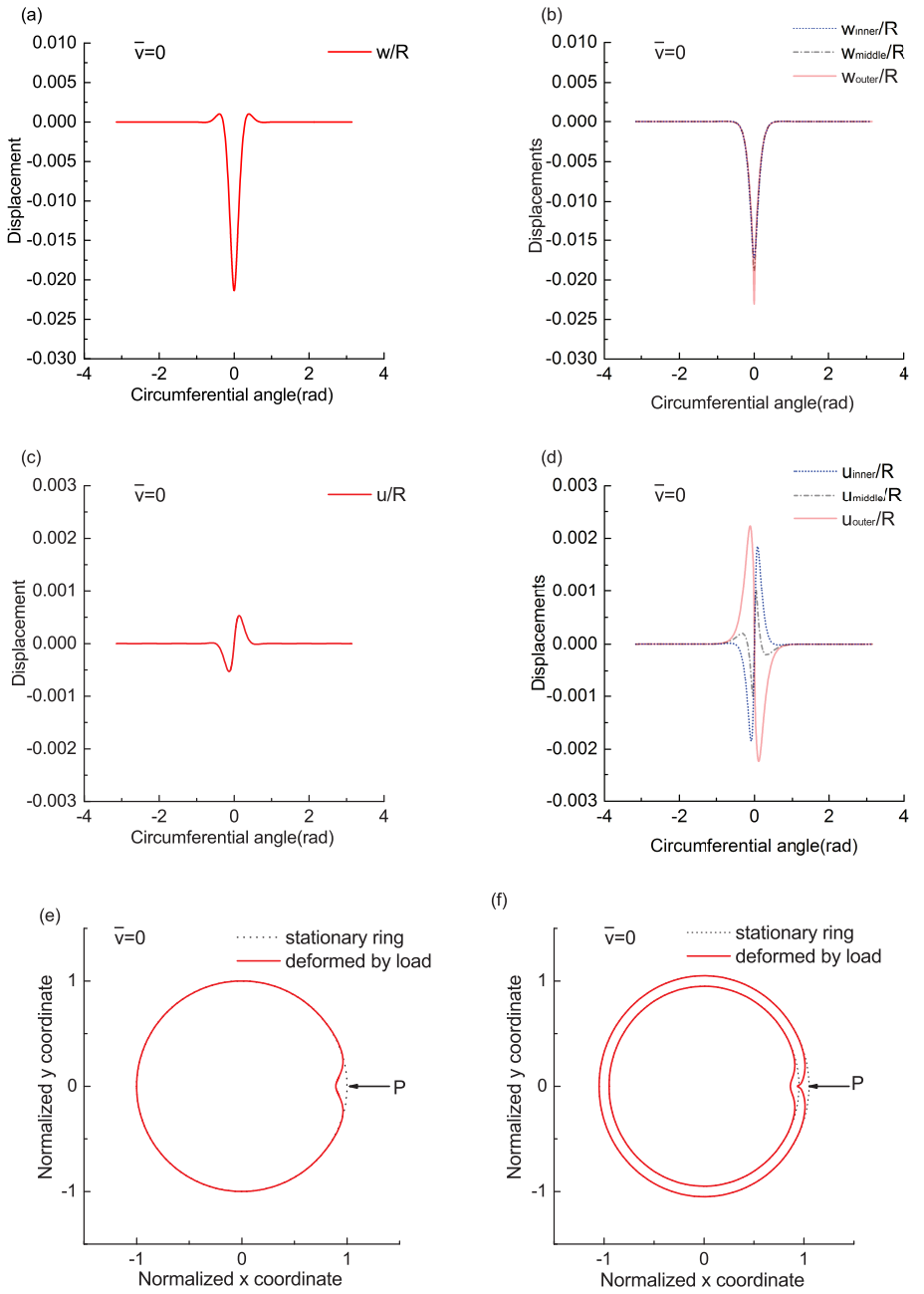

Figure 6.7: Responses predicted using classical (left) and high-order (right) models for $\bar{v} = 0$, $\bar{k}_r = 0.01$, $\bar{k}_c = 0.1$: (a)(b) Radial displacements; (c)(d) Circumferential displacements; (e)(f)Ring deformation pattern. The ring deformation patterns are scaled by 5.

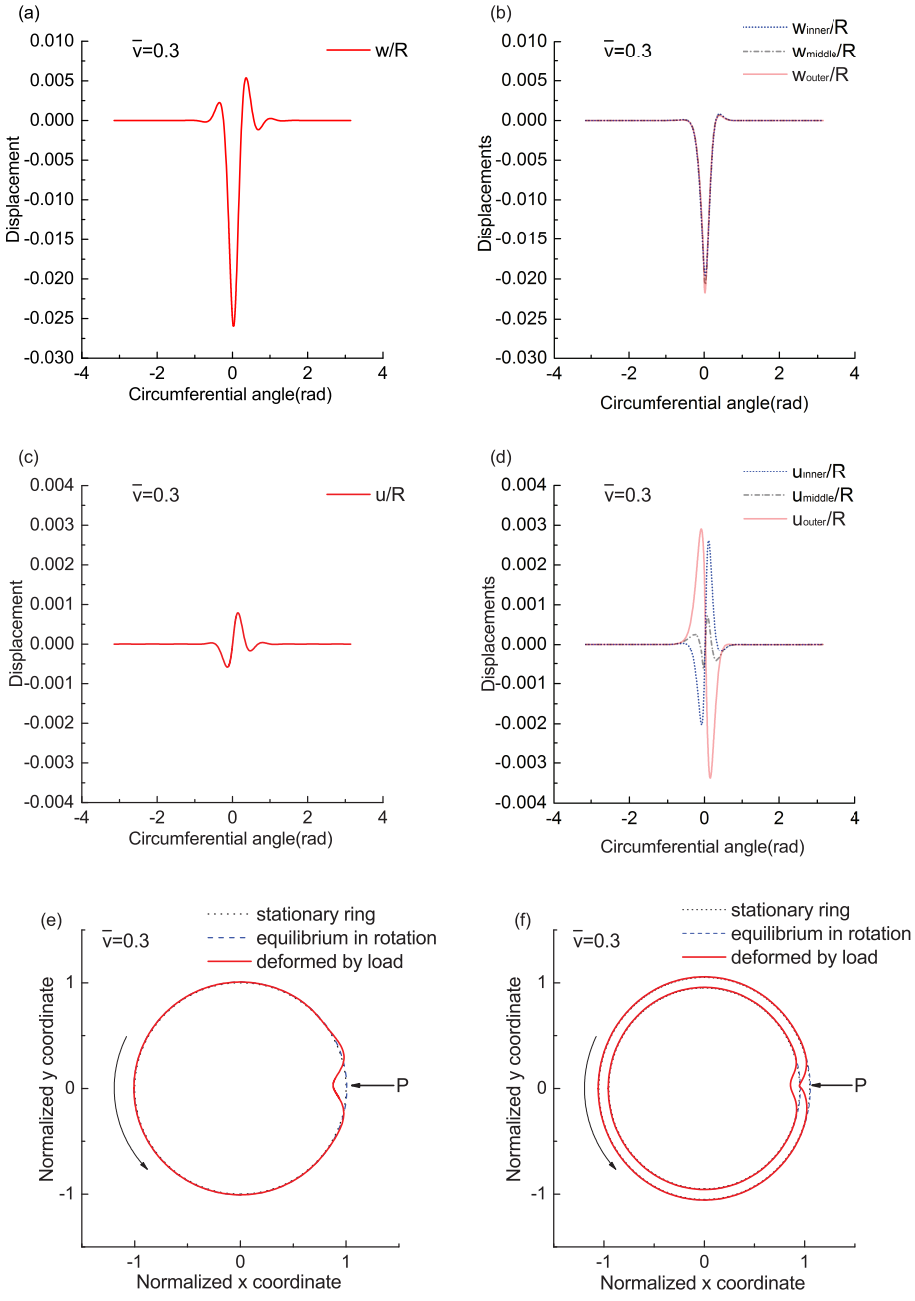

Figure 6.8: Responses predicted using classical (left) and high-order (right) models for $\bar{v} = 0.3$, $\bar{k}_r = 0.01$, $\bar{k}_c = 0.1$: (a)(b) Radial displacements; (c)(d) Circumferential displacements; (e)(f)Ring deformation pattern. The ring deformation patterns are scaled by 5.

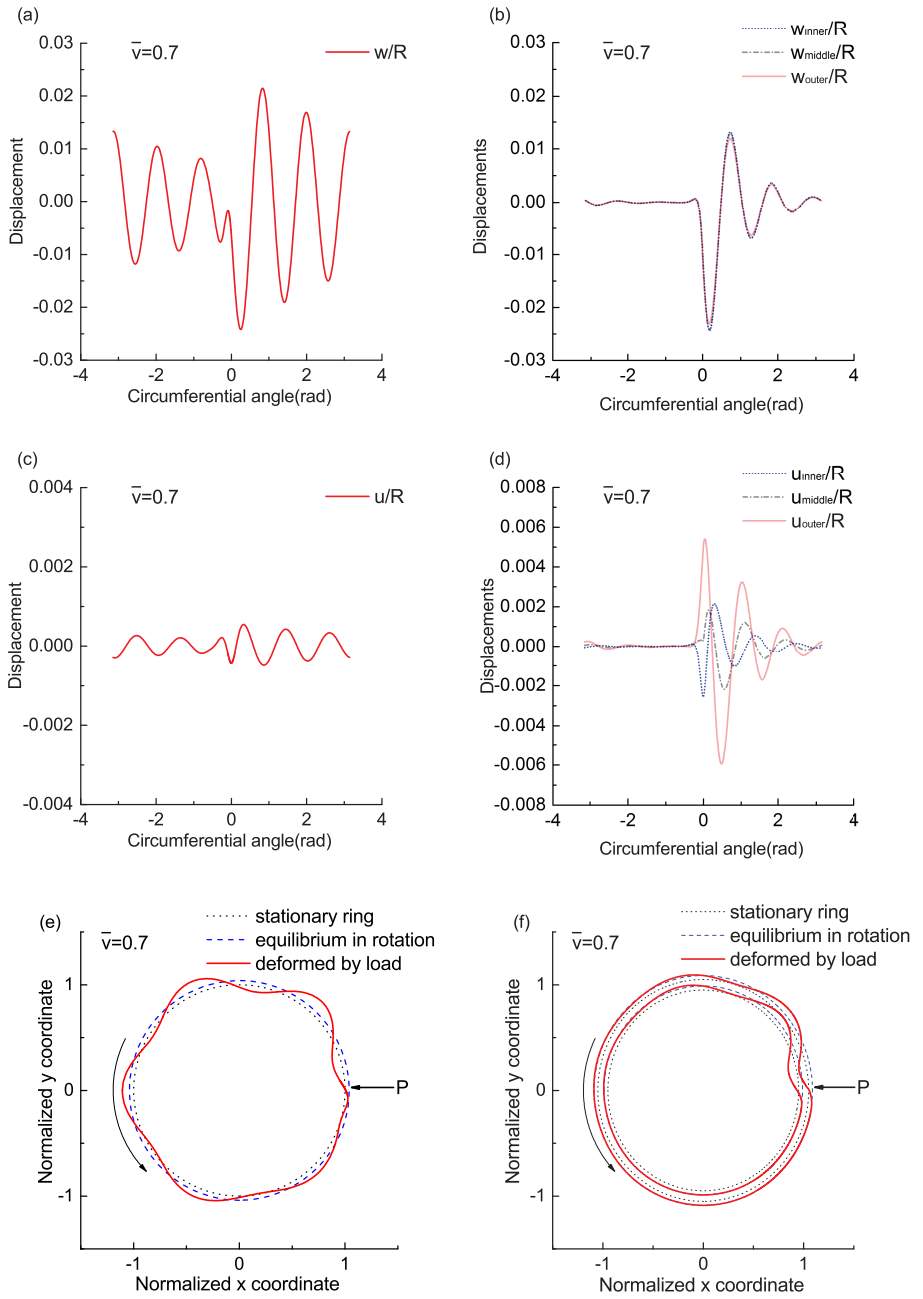

Figure 6.9: Responses predicted using classical (left) and high-order (right) models for $\bar{v} = 0.7$, $\bar{k}_r = 0.01$, $\bar{k}_c = 0.1$: (a)(b) Radial displacements; (c)(d) Circumferential displacements; (e)(f)Ring deformation pattern. The ring deformation patterns are scaled by 5.

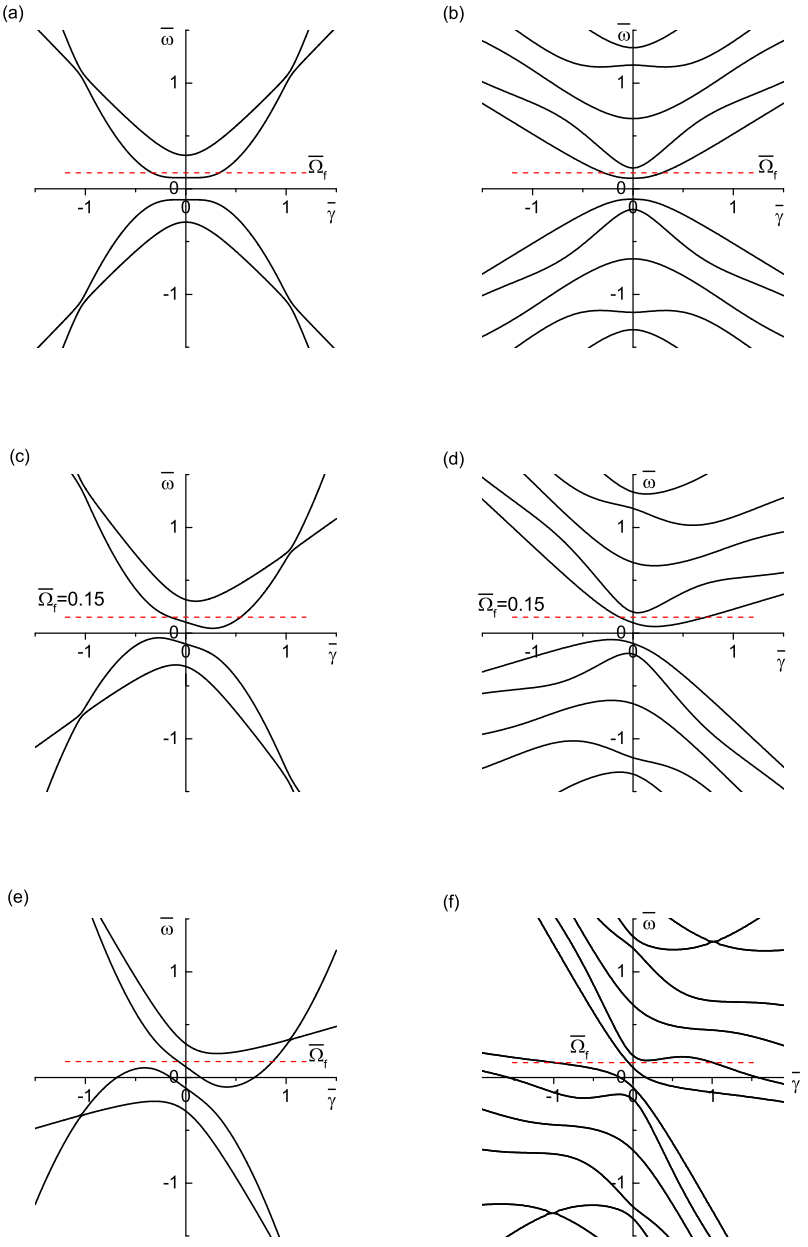

Figure 6.10: Dispersion curves, $\tilde{k}_r = 0.01$, $\tilde{k}_c = 0.1$: (a) $\bar{v} = 0$, Classical model; (b) $\bar{v} = 0$, High-order model; (c) $\bar{v} = 0.3$, Classical model; (d) $\bar{v} = 0.3$, High-order model; (e) $\bar{v} = 0.7$, Classical model; (f) $\bar{v} = 0.7$, High-order model.

Fig. 6.8 presents the displacements and deformations for $\bar{v} = 0.3$ based on the classical model, and the high-order model, respectively. The chosen rotational speed is lower than the critical speed related to resonances and thus no wave-like deformations are expected. The response of the ring rotating at $\bar{v} = 0.3$ is also localized, however it is not symmetric because of the effect of damping. The influence of higher order corrections is of significance now. As shown in Fig. 6.8(a)(b), high-order model results in smaller radial displacement. The circumferential displacement computed from high-order model is similar to the static case, however the outer circumferential displacement is not of the same magnitude as the inner one. Unlike the $\bar{v} = 0$ case, very small positive radial displacement appears for $\bar{v} = 0.3$ using high-order model.

According to Chapter 5, $\bar{v} = 0.7$ is larger than the minimum resonance speed predicted both by the classical model and the high-order model. The steady-state responses of $\bar{v} = 0.7$ calculated from the classical model are shown in Fig. 6.9. Waves are generated in the ring. From Fig. 6.9(a-d), it can be seen that in front of the contact patch (here "in front of the contact patch" corresponds to negative circumferential angle in Fig. 6.9, also called "leading edge" hereafter), the waves are shorter, whereas waves have larger wavelengths behind the contact patch (here "behind the contact patch" corresponds to positive circumferential angle in Figs. 6.9, also called "trailing edge" hereafter). When damping is small ($\zeta = 0.002$), the positive-travelling waves and the negative-travelling waves interfere as shown in (a)(c) of Fig. 6.9 as predicted using the classical model.

It is apparent from Fig. 6.9(a)(c) that higher order corrections play an important role in the steady-state response when the ring rotates at super-critical speeds [†] comparing to Fig 6.9(b)(d). The high-order model predicts much smaller wave-like radial displacement with larger wavelengths in the trailing edge. When projecting the displacements to the ring, unlike the prediction from the classical model in Fig. 6.9(e), it is clear that in Fig. 6.9(f) the response in the leading edge is almost washed out entirely. This is consistent with the experiments which were done for rolling tires. The "standing waves" exist only in the trailing edge [87, 102]. Note that for the chosen parameters, namely $\bar{k}_r = 0.01$, $\bar{k}_c = 0.1$, the steady-state responses predicted using the classical model and the high-order theory all show wave-like patterns although the deformation patterns are significantly different. However, if other parameters are chosen the responses from both models can also differ. For example, as shown in Chapter 5 the resonance speeds computed from the classical model and the high-order theory can be completely different.

DYNAMIC RESPONSE UNDER A HARMONIC LOAD

When considering the steady-state response of a rotating ring to a stationary point load with harmonic varying amplitude, insights can be gained by analysing the dispersion curves obtained from the governing equations derived in a space-fixed coordinate. Fig. 6.10 shows the dispersion curves of the same ring studied previously. The results are calculated for three rotational speeds: $\bar{v} = 0$ for stationary ring, $\bar{v} = 0.3$ corresponding to the sub-critically rotating case and $\bar{v} = 0.7$ elucidating the super-critically rotating case. The dashed horizontal lines $\bar{\Omega}_f$ in Fig. 6.10 stand for the excitation frequency of the load. The location of this line determines the deformation patterns of the ring. One crossing

[†] A ring rotating at a super-critical speed means that its rotational speed exceeds the minimum resonance speed (related to, in this case as critical) as defined in Chapter 5.

point between this line and the dispersion curves means one wave excited. The following observations can be made:

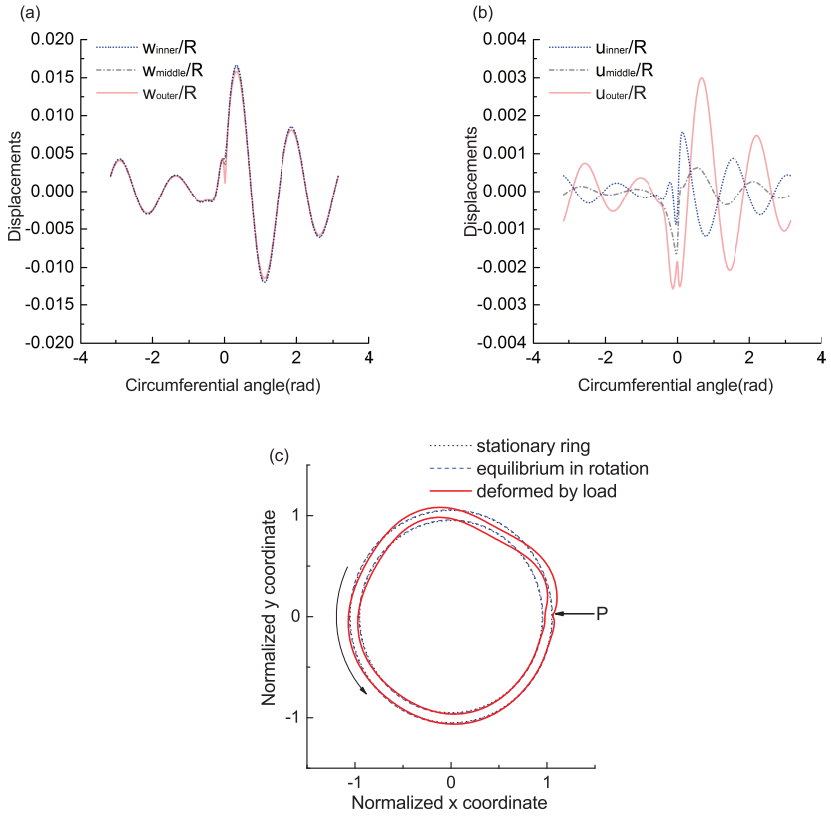

Figure 6.11: High-order model, displacements under a harmonic load, $\bar{\nu} = 0.3$, $\bar{k}_r = 0.01$, $\bar{k}_c = 0.1$, $\bar{\Omega}_f = 0.15$: (a) Radial displacement; (b) Circumferential displacement;(c) Ring deformation pattern. The ring deformation pattern is scaled by 5.

i) The dispersion curves are symmetric with respect to the frequency axis for a stationary ring whereas this symmetry is lost when the ring rotates.

ii) For the stationary and sub-critically rotating case, waves are generated only when the excitation frequency of the load exceeds a critical value. This critical frequency occurs when the horizontal line $\bar{\Omega}_f$ is tangent to the dispersion curve. For stationary ring case, the critical frequency is the first cut-off frequency. However, the critical frequency has a lower value than the first cut-off frequency of the corresponding stationary ring case when the ring is rotating sub-critically.

iii) For the stationary and sub-critically rotating case, similar steady-state responses are expected regardless of the choice of models if the excitation frequency is not too

high. Taking sub-critical speed $\bar{v} = 0.3$ as an example, if one assumes the frequency of the load is $\bar{\Omega}_f = 0.15$, two waves are excited since there are two intersections between the load frequency and the dispersion curves as shown in Fig. 6.10(c-d). The crossing points in Fig. 6.10(c) and (d) are located at similar places. Thus, the waves generated are expected to be similar. The displacements and ring deformation pattern of this case is shown in Fig. 6.11 using the developed high-order model.

iv) When the ring rotates super-critically (Fig. 6.10(e-f)), the intersections between the dispersion curves and the abscissa confirm that waves are excited for a stationary load at zero excitation frequency, namely $\bar{\Omega}_f = 0$. Unlike the stationary and sub-critically rotating case, the waves predicted by the classical and the high-order models are no longer similar for any frequency since the crossing points of the excitation frequency and the dispersion curves predicted by these models are distinct.

6.2.3. THE EFFECT OF CHOICE OF DAMPING

The choice of damping for different models has significant influence on the predicted dynamic response. If one chooses the same material damping value, the damping has larger effect on the high-order model. As shown in Fig. 6.9(b-d) that the waves are efficiently damped for the high-order model whereas for the classical model, $\zeta = 0.002$ has almost no effect. Another observation is that, if relatively high material damping is chosen, the point load does not need to be approximated by a distributed load since the damping will smooth the response around the loading point. If one chooses viscous damping, the effect of damping will be slightly larger for the classical model.

6.3. CONCLUSIONS

The steady-state response of a rotating ring on an elastic foundation subjected to a stationary point load is investigated in this chapter. The method of the images, which gives a semi-analytical solution to the problem, is applied to obtain the dynamic response. The predicted stationary deformation pattern of a super-critically rotating ring subjected to a constant stationary load confirms the experimentally observed "standing waves" in rolling tyres, not only qualitatively; also the characteristics of the predicted result and the experimental observation are in agreement.

The characteristics of the response to a point (line) load with constant magnitude are highly dependent on the ring parameters and the stiffness of the foundation. The dimensionless parameter $\bar{k}_r$, defined as the ratio of the stiffness of the elastic foundation to the bending stiffness of the ring, is found to dominate the behaviour of the response. For a stiff ring with soft foundation (low value of $\bar{k}_r$), the response is mainly governed by the modes with low mode numbers, especially the $n = 1$ mode. Thus, for a stiff ring subjected to a stationary constant load, both the classical model and the high-order model give similar predictions of the dynamic response since higher order corrections influence mostly higher modes deformation.

For soft ring on stiff foundation (namely large $\bar{k}_r$) subjected to a constant stationary load, resonance speeds exist as shown in Chapter 5. Physically speaking, high value of $\bar{k}_r$ means the ring is very flexible in comparison with the supporting elastic foundation, or equivalently, the ring's radius is so large that the ring itself acts as a straight structure

governed by the same equations. When the ring rotates sub-critically, the deformation is localised around the loading point. Viscosity of the foundation causes asymmetry of the ring deformation pattern with respect to the position of the loading. When the ring rotates super-critically, waves are generated in front of and behind the load. In the leading edge, waves have shorter wavelengths and higher frequencies. In the trailing edge, waves with longer wavelengths are excited. The amplitudes of them are also larger than the ones in the leading edge. Including some damping, the high frequency ones in the leading edge can be efficiently “washed out". This is exactly what is observed for rolling tyres. In the super-critically rotating case, the high-order model and the classical one give considerably different predictions of the response.

When a stationary harmonic load is applied, for the stationary ring and sub-critically rotating ring case, the classical model can be used in certain frequency range. However, waves predicted by the classical model and by the high-order model are different for all excitation frequencies in the case of a super-critically rotating ring.

7

STABILITY OF A STATIONARY OSCILLATOR INTERACTING WITH A ROTATING RING

Apart from the forced vibrations of a structure caused by moving loads/objects, the stability of the moving objects on the structure is one of the serious concerns in the field of moving load problems. It has been shown that a moving object can be unstable when it moves faster than a critical speed due to the generation of anomalous Doppler waves in the supporting structure [106]. In the past, the focus was placed on the stability analysis of objects moving along straight systems [107–111]. Recently, the stability of vibration of an oscillator moving uniformly along a circular thin ring supported by a viscoelastic foundation has been studied in [112] using the classical thin ring theory. The closeness of the ring introduces infinitely many resonance speeds [60, 61] which leads to rather complicated stable and unstable regions in the parameter plane. The reciprocal case, namely stability of a stationary oscillator interacting with a high-speed rotating ring, has not been studied. In the previous chapter, it is shown that waves can be excited in a super-critically rotating ring when a stationary point load is applied. Thus, it is reasonable to expect instability of the stationary oscillator as well.

In this chapter, a rotating elastic ring is considered as the structure supporting a stationary oscillator. The high-order model proposed in Chapter 4 is employed to describe vibrations of the ring. Compared to the problem of a moving oscillator on a stationary ring [112], the stability of a stationary oscillator in contact with a rotating ring is practically more important due to the wide application aear of interest, e.g. in gear dynamics, modelling of a train wheel, and calenders of paper machines [101]. It has been shown in Chapter 5 that critical speeds exist only for soft rings. Therefore, only oscillators which interact with a *soft* ring may become unstable when the ring rotates super-critically. In this chapter, a stationary oscillator in contact with a soft ring is considered as an illustrative example. The chapter is structured as follows. Section 7.1 establishes the mathematical model of the problem and its solution. The equivalent stiffness is analysed in

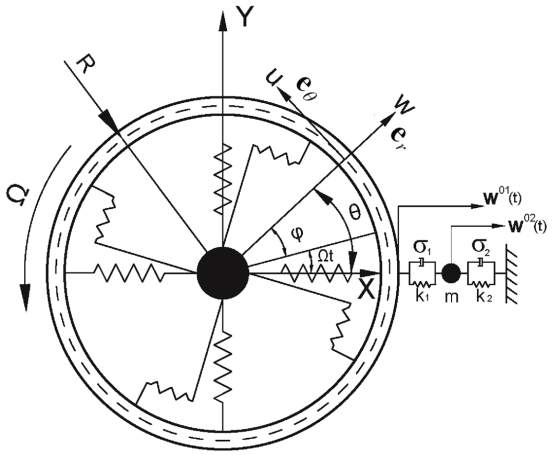

Figure 7.1: Rotating ring interacting with a stationary oscillator

section 7.2. Stability analysis using D-decomposition method is presented in section 7.3. Finally, conclusions are made in section 7.4. The main novelty of this chapter is the theoretical prediction of instability of a stationary oscillator-rotating ring system which has not been addressed in the past.

7.1. MODEL AND CHARACTERISTIC EQUATION

In this section, the mathematical model of a stationary oscillator interacting with a rotating ring is formulated. The study of a stationary oscillator-rotating ring system is motivated by modelling of an elastic train wheel interacting with railway tracks. It is assumed that the ring is rotating steadily and the static expansion is reached before the oscillator is applied. Clearly this is not the most realistic situation but it is acceptable to consider it given the lack of any prior studies on the matter. *

The ring properties are the same as the ones used in Chapter 4. As for the oscillator, m denotes its weight in kg/m. The contact between the mass and the ring is modelled by a spring k_1 and a dashpot σ_1. Furthermore, the mass is supported by a spring k_2 and a dashpot σ_2. The dimension of k_1 and k_2 is N/m^2. The viscosity parameters σ_1 and σ_2 have the unit of Ns/m^2. The ring is rotating at a constant angular speed Ω.

It is assumed that the static equilibrium is not influenced by the presence of the oscillator. For convenience, it is chosen to work in a space-fixed reference system $\theta = \varphi + \Omega t$.

*The realistic case is that before the ring starts to rotate, the oscillator is in contact with the ring. Then one needs to solve a new equilibrium using the nonlinear governing equations.

The equations that govern the vibrations of the ring in the radial direction read

$$\int_{\frac{-h}{2}}^{\frac{h}{2}} (\mathrm{I}_1^{lin} z^l)\,\mathrm{d}z + \rho \int_{\frac{-h}{2}}^{\frac{h}{2}} \left(r(\dot{v}_1 + \Omega\, v_1' - \Omega\, v_2) z^l\right)\mathrm{d}z + \left(f_1^{lin} - f_2^{lin}(-1)^l\right)\left(\frac{h}{2}\right)^l =$$
$$-\left(\frac{h}{2}\right)^l \sum_{j=-\infty}^{+\infty} \left(k_1(w^{01} - w^{02}) + \sigma_1(\frac{Dw^{02}}{Dt} - \frac{Dw^{01}}{Dt})\right)\delta(\theta + 2j\pi), \tag{7.1}$$
$(l = 0, 1, 2, 3...N_1)$.

The equations of motion in the circumferential direction are given as

$$\int_{\frac{-h}{2}}^{\frac{h}{2}} (\mathrm{I}_2^{lin} z^q)\,\mathrm{d}z + \rho \int_{\frac{-h}{2}}^{\frac{h}{2}} \left(r(\dot{v}_2 + \Omega\, v_2' + \Omega\, v_1) z^q\right)\mathrm{d}z + \left(f_3^{lin} - f_4^{lin}(-1)^q\right)\left(\frac{h}{2}\right)^q = 0, \tag{7.2}$$
$(q = 0, 1, 2, 3...N_2)$.

The details of the left hand sides of Eqs. (7.1-7.2) can be found in Eqs. (4.28-4.30) in Chapter 4.

Equation of motion of the oscillator reads:

$$m\frac{D^2 w^{02}}{Dt^2} + \sigma_2 \frac{Dw^{02}}{Dt} + \sigma_1(\frac{Dw^{02}}{Dt} - \frac{Dw^{01}}{Dt}) + k_2 w^{02} + k_1(w^{02} - w^{01}) = 0 \tag{7.3}$$

The continuous contact between the oscillator and the ring implies that:

$$w^{01}(t) = w|_{h/2}\ (\theta = 0, t) \tag{7.4}$$

where $w^{01}(t)$ and $w^{02}(t)$ denote the displacement of the ring at the contact point and the displacement of the mass, respectively. In Eqs. (7.1-7.2), prime stands for the spatial derivative with respective to the space-fixed coordinate θ and overdot represents time derivative. The system of Eqs. (7.1-7.4) governs vibrations of the ring-oscillator system.

At the contact point, Eq. (7.4) is rewritten as:

$$w^{01} = w|_{h/2} = \sum_{l=0}^{N_1} (w_l (h/2)^l). \tag{7.5}$$

For the sake of convenience, the problem will be analysed in dimensionless form. The same dimensionless parameters as in Chapter 2 are introduced. Additionally, the following dimensionless parameters reflecting the oscillator's properties are defined:

$$\varepsilon_{(1,2)} = \frac{\sigma_{(1,2)} c_0 \bar{k}}{Eh},\ K_{(1,2)} = \frac{k_{(1,2)} \bar{k} k}{Eh},\ W^{(01,02)} = \frac{w^{(01,02)}}{R},\ M = \frac{m}{\rho h R}. \tag{7.6}$$

The dimensionless form of the space-fixed reference system is $\{\bar{\theta} = \theta/\bar{k}, \tau = c_0 t/k\}$. The dimensionless form of Eq. (7.3) can be written as

$$M\frac{D^2 W^{02}}{D\tau^2} + \varepsilon_2 \frac{DW^{02}}{D\tau} + \varepsilon_1(\frac{DW^{02}}{D\tau} - \frac{DW^{01}}{D\tau}) + K_2 W^{02} + K_1(W^{02} - W^{01}) = 0. \tag{7.7}$$

The above equation (7.7) and the dimensionless form of Eqs. (7.1-7.2)† are the equations of motion of the ring-oscillator system in dimensionless form which will be solved in the sequel.

The following Fourier transform with respect to $\bar{\theta}$ and Laplace transform with respect to τ are defined:

$$\begin{aligned}
&\left\{ \begin{array}{c} \tilde{W}^{01}(s) \\ \tilde{W}^{02}(s) \end{array} \right\} = \int_0^{+\infty} \left\{ \begin{array}{c} W^{01}(\tau) \\ W^{02}(\tau) \end{array} \right\} \exp(-s\tau)\mathrm{d}\tau, \\
&\left\{ \begin{array}{c} \tilde{W}_l(\bar{\theta},s) \\ \tilde{U}_q(\bar{\theta},s) \end{array} \right\} = \int_0^{+\infty} \left\{ \begin{array}{c} W_l(\bar{\theta},\tau) \\ U_q(\bar{\theta},\tau) \end{array} \right\} \exp(-s\tau)\mathrm{d}\tau, \\
&\left\{ \begin{array}{c} \tilde{\tilde{W}}_l^{(\bar{\gamma},s)} \\ \tilde{\tilde{U}}_q^{(\bar{\gamma},s)} \end{array} \right\} = \int_{-\infty}^{+\infty} \left\{ \begin{array}{c} \tilde{W}_l(\bar{\theta},s) \\ \tilde{U}_q(\bar{\theta},s) \end{array} \right\} \exp(-\mathrm{i}\bar{\gamma}\bar{\theta})\mathrm{d}\bar{\theta}, \\
&(l = 0,1,2,3...N_1, q = 0,1,2,3...N_2).
\end{aligned} \tag{7.8}$$

in which $\bar{\gamma}$ is the dimensionless wave number, s is the dimensionless Laplace parameter and $\mathrm{i} = \sqrt{-1}$. Applying the above Fourier and Laplace transforms to the dimensionless forms of Eq. (7.1-7.2) and Eq. (7.7), one obtains (the initial conditions are taken as trivial since they have no effect on stability of linear systems):

$$\begin{aligned}
&\mathbf{C}_s\mathbf{a}_s = \mathbf{f}_s, \\
&(Ms^2 + K_2 + \varepsilon_2 s + K_1 + \varepsilon_1 s)\tilde{W}^{02}(s) - (K_1 + \varepsilon_1 s)\tilde{W}^{01}(s) = 0
\end{aligned} \tag{7.9}$$

in which $\mathbf{C}_s$ is the coefficient matrix whereas $\mathbf{a}_s$ is the displacement vector in the Laplace-wavenumber domain. The coefficient matrix can be obtained by replacing $\mathrm{i}\omega$ in $\mathbf{C}$ in Appendix C by the Laplace parameter s. The displacement vector is given as

$$\mathbf{a}_s = \left[\tilde{\tilde{W}}_0^{(\bar{\gamma},s)} \quad \tilde{\tilde{W}}_1^{(\bar{\gamma},s)} \quad \cdots \quad \tilde{\tilde{W}}_l^{(\bar{\gamma},s)} \quad \cdots \quad \tilde{\tilde{W}}_{N_1}^{(\bar{\gamma},s)} \quad \tilde{\tilde{U}}_0^{(\bar{\gamma},s)} \quad \tilde{\tilde{U}}_1^{(\bar{\gamma},s)} \quad \cdots \quad \tilde{\tilde{U}}_q^{(\bar{\gamma},s)} \quad \cdots \quad \tilde{\tilde{U}}_{N_2}^{(\bar{\gamma},s)} \right]^T. \tag{7.10}$$

The column vector accounting for the effect of the oscillator is expressed as

$$\mathbf{f}_s = \left[C_{\mathrm{w}0} \quad C_{\mathrm{w}1} \quad \cdots \quad C_{\mathrm{w}l} \quad \cdots \quad C_{\mathrm{w}N_1} \quad C_{\mathrm{u}0} \quad C_{\mathrm{u}1} \quad \cdots \quad C_{\mathrm{u}q} \quad \cdots \quad C_{\mathrm{u}N_2} \right]^T \tag{7.11}$$

in which

$$C_{\mathrm{w}l} = -(K_1 + \varepsilon_1 s)(\tilde{W}^{01}(s) - \tilde{W}^{02}(s)) \sum_{j=-\infty}^{+\infty} \exp(2\mathrm{i}\bar{\gamma} j\pi/\bar{k}), \quad (l = 0,1,2,3...N_1) \tag{7.12}$$

and

$$C_{\mathrm{u}q} = 0, \quad (q = 0,1,2,3...N_2). \tag{7.13}$$

†Due to complexity, the dimensionless forms of Eqs. (7.1-7.2) are not explicitly given here.

Evaluating Eqs. (7.9), each component of the displacement vector $\mathbf{a}_s$ can be expressed in the following form:

$$\tilde{\tilde{W}}_l^{(\bar{\gamma},s)} D_{wl}(\bar{\gamma},s) = -(K_1+\varepsilon_1 s)(\tilde{W}^{01}(s)-\tilde{W}^{02}(s)) \sum_{j=-\infty}^{+\infty} \exp(2\mathrm{i}\bar{\gamma} j\pi/\bar{k}), \tag{7.14a}$$

$$\tilde{\tilde{U}}_q^{(\bar{\gamma},s)} D_{uq}(\bar{\gamma},s) = -(K_1+\varepsilon_1 s)(\tilde{W}^{01}(s)-\tilde{W}^{02}(s)) \sum_{j=-\infty}^{+\infty} \exp(2\mathrm{i}\bar{\gamma} j\pi/\bar{k}) \tag{7.14b}$$

in which

$$D_{wl}(\bar{\gamma},s) = \frac{\bar{\Delta}(\bar{\gamma},s)}{\bar{\Delta}_{wl}(\bar{\gamma},s)},\ D_{uq}(\bar{\gamma},s) = \frac{\bar{\Delta}(\bar{\gamma},s)}{\bar{\Delta}_{uq}(\bar{\gamma},s)}. \tag{7.15}$$

The expressions of $\bar{\Delta}_{wl}$, $\bar{\Delta}_{uq}$, $\bar{\Delta}$ in Eq. (7.15) are not shown here for brevity. They can be obtained by means of any symbolic computation software.

Applying the inverse Fourier transform with respect to $\bar{\gamma}$ to Eq. (7.14)(a), the Laplace-displacement in the radial direction can be obtained in the following form:

$$\begin{aligned}\tilde{W}_l(\bar{\theta},s) &= -\frac{(K_1+\varepsilon_1 s)(\tilde{W}^{01}(s)-\tilde{W}^{02}(s))}{2\pi} \int_{-\infty}^{+\infty} \frac{\sum_{j=-\infty}^{+\infty} \exp(2\mathrm{i}\bar{\gamma} j\pi/\bar{k})}{D_{wl}(\bar{\gamma},s)} \exp(\mathrm{i}\bar{\gamma}\bar{\theta})\mathrm{d}\bar{\gamma}, \\ &= -\frac{(K_1+\varepsilon_1 s)(\tilde{W}^{01}(s)-\tilde{W}^{02}(s))}{2\pi} \sum_{j=-\infty}^{+\infty} \int_{-\infty}^{+\infty} \frac{\exp(\mathrm{i}\bar{\gamma}(\bar{\theta}+2j\pi/\bar{k}))}{D_{wl}(\bar{\gamma},s)} \mathrm{d}\bar{\gamma}.\end{aligned} \tag{7.16}$$

Substituting $\bar{\theta}=0$ into Eq. (7.16), one obtains

$$\tilde{W}_l(0,s) = -\frac{(K_1+\varepsilon_1 s)(\tilde{W}^{01}(s)-\tilde{W}^{02}(s))}{2\pi} \sum_{j=-\infty}^{+\infty} \int_{-\infty}^{+\infty} \frac{\exp(\mathrm{i}\bar{\gamma}(2j\pi/\bar{k}))}{D_{wl}(\bar{\gamma},s)} \mathrm{d}\bar{\gamma}. \tag{7.17}$$

Considering Eq. (7.5) together with Eq. (6.9), one obtains

$$\tilde{W}^{01}(s) = \sum_{l=0}^{N_1} \tilde{W}_l(0,s) = -\frac{(K_1+\varepsilon_1 s)(\tilde{W}^{01}(s)-\tilde{W}^{02}(s))}{2\pi} \sum_{l=0}^{N_1} (I_{wl}) \tag{7.18}$$

in which

$$I_{wl} = \sum_{j=-\infty}^{+\infty} \int_{-\infty}^{+\infty} \frac{\exp(\mathrm{i}\bar{\gamma}(2j\pi/\bar{k}))}{D_{wl}(\bar{\gamma},s)} \mathrm{d}\bar{\gamma}. \tag{7.19}$$

Rewriting Eq. (7.18) and combining with Eq. (7.9d), one obtains a system of equations with respect to $\tilde{W}_s^{01}$ and $\tilde{W}_s^{02}$:

$$\begin{aligned}&(K_1+\varepsilon_1 s+\chi_{eq})\tilde{W}_s^{01} - (K_1+\varepsilon_1 s)\tilde{W}_s^{02} = 0, \\ &(Ms^2+K_2+\varepsilon_2 s+K_1+\varepsilon_1 s)\tilde{W}_s^{02} - (K_1+\varepsilon_1 s)\tilde{W}_s^{01} = 0,\end{aligned} \tag{7.20}$$

with

$$\chi_{eq} = \left(\frac{\sum_{l=0}^{N_1} (I_{wl})}{2\pi} \right)^{-1}. \tag{7.21}$$

This function determines the radial reaction of the rotating ring to the stationary oscillator at the contact point and is called equivalent stiffness. There is a hidden assumption here. It should be noted that the point of the ring right under the oscillator displaces radially and circumferentially as well. Therefore, the dynamic stiffness should be extracted from the point under the oscillator after deformation by the contact with the oscillator. However, it is assumed that the circumferential displacement is small compared to the radial displacement since the oscillator is only allowed to move radially [‡]. Therefore, only the radial reaction from the ring to the oscillator is considered for the equivalent stiffness.

The expression of I_{wl} can be rewritten as

$$\begin{aligned} I_{wl} &= \sum_{j=-\infty}^{+\infty} \int_{-\infty}^{+\infty} \frac{\exp(2\mathrm{i}\bar{\gamma} j\pi/\bar{k})}{D_{wl}(\bar{\gamma}, s)} \mathrm{d}\bar{\gamma} \\ &= \left(\sum_{j=-\infty}^{-1} \int_{-\infty}^{+\infty} \frac{\exp(2\mathrm{i}\bar{\gamma} j\pi/\bar{k})}{D_{wl}(\bar{\gamma}, s)} \mathrm{d}\bar{\gamma} + \sum_{j=0}^{+\infty} \int_{-\infty}^{+\infty} \frac{\exp(2\mathrm{i}\bar{\gamma} j\pi/\bar{k})}{D_{wl}(\bar{\gamma}, s)} \mathrm{d}\bar{\gamma} \right) \\ &= \left(\sum_{j=1}^{+\infty} \int_{-\infty}^{+\infty} \frac{\exp(-2\mathrm{i}\bar{\gamma} j\pi/\bar{k})}{D_{wl}(\bar{\gamma}, s)} \mathrm{d}\bar{\gamma} + \sum_{j=0}^{+\infty} \int_{-\infty}^{+\infty} \frac{\exp(2\mathrm{i}\bar{\gamma} j\pi/\bar{k})}{D_{wl}(\bar{\gamma}, s)} \mathrm{d}\bar{\gamma} \right) \\ &= (I_{wl}^{-} + I_{wl}^{+}). \end{aligned} \tag{7.22}$$

According to the residue theorem,

$$\begin{aligned} I_{wl}^{-} &= \sum_{j=1}^{+\infty} \int_{-\infty}^{+\infty} \frac{\exp(-2\mathrm{i}\bar{\gamma} j\pi/\bar{k})}{D_{wl}(\bar{\gamma}, s)} \mathrm{d}\bar{\gamma} = -2\pi\mathrm{i} \sum_{j=1}^{+\infty} \sum_{n} B_{wl}^{n} \exp(-2\mathrm{i}\bar{\gamma}_n j\pi/\bar{k}) \\ &= -2\pi\mathrm{i} \sum_{n} B_{w}^{n} \frac{\exp(-2\mathrm{i}\bar{\gamma}_n \pi/\bar{k})}{1 - \exp(-2\mathrm{i}\bar{\gamma}_n \pi/\bar{k})}, \\ I_{wl}^{+} &= \sum_{j=0}^{+\infty} \int_{-\infty}^{+\infty} \frac{\exp(2\mathrm{i}\bar{\gamma} j\pi/\bar{k})}{D_{w}(\bar{\gamma}, s)} \mathrm{d}\bar{\gamma} = 2\pi\mathrm{i} \sum_{j=0}^{+\infty} \sum_{p} B_{w}^{p} \exp(2\mathrm{i}\bar{\gamma}_p j\pi/\bar{k}) \\ &= 2\pi\mathrm{i} \sum_{p} B_{w}^{p} \frac{1}{1 - \exp(2\mathrm{i}\bar{\gamma}_p \pi/\bar{k})}, \end{aligned} \tag{7.23}$$

in which

$$B_{wl}^{n} = \left(\frac{\bar{\Delta}_w(\bar{\gamma}_n, s)}{\frac{\partial}{\partial\bar{\gamma}} \bar{\Delta}(\bar{\gamma}, s)|_{\bar{\gamma}=\bar{\gamma}_n}} \right), \quad B_{wl}^{p} = \left(\frac{\bar{\Delta}_{wl}(\bar{\gamma}_p, s)}{\frac{\partial}{\partial\bar{\gamma}} \bar{\Delta}(\bar{\gamma}, s)|_{\bar{\gamma}=\bar{\gamma}_p}} \right). \tag{7.24}$$

[‡]For the chosen system parameters in the following Sections 7.2 and 7.3, this assumption is confirmed by Fig. 6.9(b)(d) in Chapter 6.

$\bar{\gamma}_n$ denotes the roots of equation $\bar{\Delta}(\bar{\gamma}, s) = 0$ with negative imaginary part, whereas $\bar{\gamma}_p$ denotes the roots of the same equation with positive imaginary part.

The characteristic equation of the oscillator vibration can be obtained by setting the determinant of the coefficient matrix of Eq. (7.20) to zero to give

$$(K_1 + \varepsilon_1 s + \chi_{eq})(Ms^2 + K_2 + \varepsilon_2 s + K_1 + \varepsilon_1 s) - (K_1 + \varepsilon_1 s)^2 = 0. \tag{7.25}$$

where χ_{eq} is given by Eq. (7.21). The system stability is determined by the roots of Eq. (7.25). The vibration of the oscillator is unstable if there is at least one root s with a positive real part, i.e. $\mathrm{Re}(s > 0)$. It is customary to replace s by $s = \mathrm{i}\omega$ in the following analysis.

7.2. THE EQUIVALENT (DYNAMIC) STIFFNESS UNDER THE OSCILLATOR

The equivalent stiffness χ_{eq} can be analogous to the driving-point dynamic stiffness of the ring. The only difference is that now this stiffness is not only a function of frequency, but also a function of the rotational speed. The equivalent stiffness of a structure reaches its minima at resonance frequencies. Similarly, the equivalent stiffness is minimum at resonance speeds. For an unbounded structure, e.g. an infinitely long Euler-Bernoulli beam, the critical speed after which instability may happen is the minimum phase speed of waves in the beam [107], which can be referred to as a resonance speed. Thus, for a closed ring, one may also expect that the instability of a stationary oscillator may occur when the rotational speed exceeds a critical speed at which resonances start to occur.

Hereafter, $\bar{k}_r = 0.01, \bar{k}_c = 0.1$ are used, which suggest a soft ring resting on a stiff foundation. $N_1 = N_2 = 5$ is employed in the governing equations (7.1-7.2). The critical speed for wave-like displacement patterns to be initiated is $\bar{v}_{cr} \approx 0.5$ as shown in Chapter 5 and here in Fig. 7.2. Three velocities of the ring rotation are considered: super-critical $\bar{v} = 0.7, 1.2$ and sub-critical $\bar{v} = 0.3$ as shown in Fig. 7.2. The real and imaginary parts of

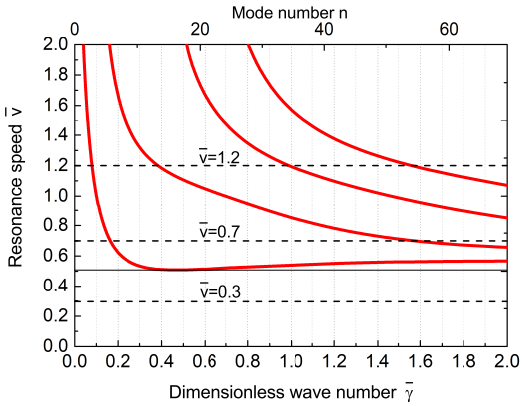

Figure 7.2: Resonance speeds of $\bar{k}_r = 0.01, \bar{k}_c = 0.1$.

the equivalent stiffness determine the elasto-inertial and viscous properties of the ring,

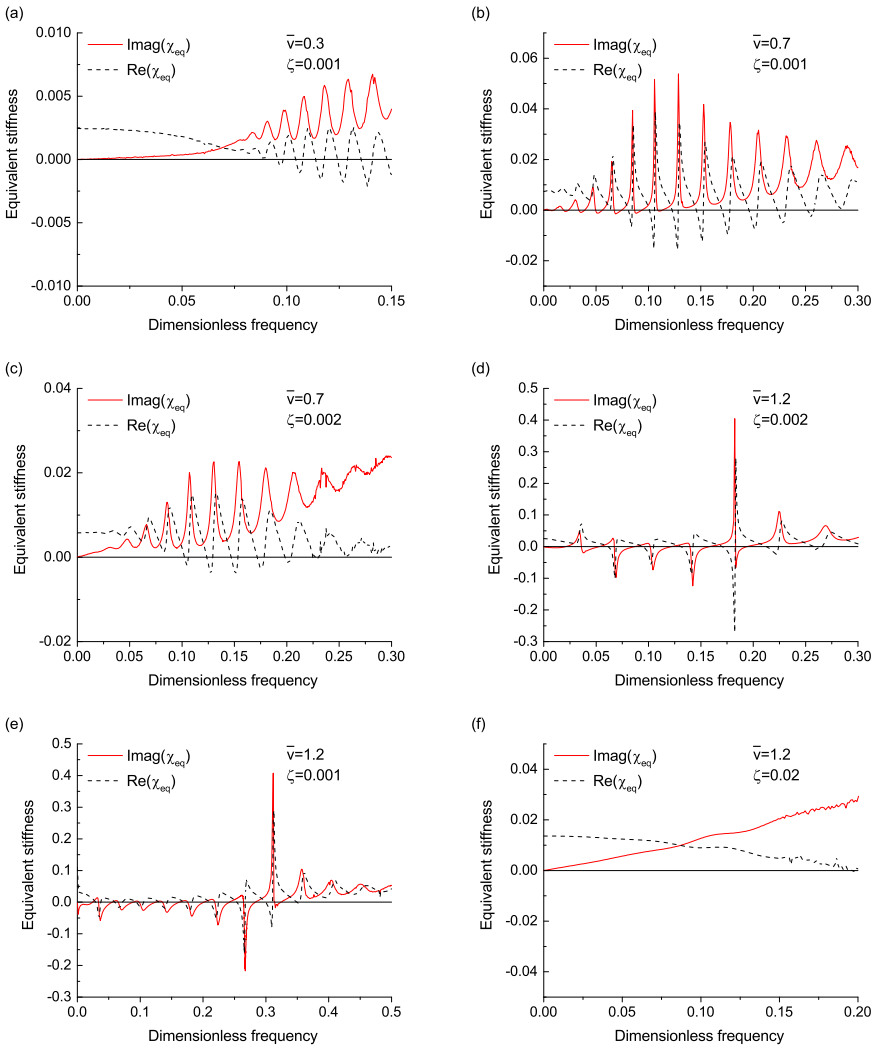

Figure 7.3: The equivalent stiffness χ_{eq} for varying speed $\bar{v}$ and material damping ζ.

respectively. For more details, one can refer to [113]. The equivalent viscosity can be negative when the object is moving super-critically [113]. It has been shown that a moving object might become unstable because of the "negative radiation damping" [107–109, 113–116]. For a rotating ring, the same conclusion holds. Unstable motions of a stationary oscillator may occur when the equivalent viscosity is negative. Note that the negative damping is only the necessary (not sufficient) condition for instability.

For a rotating ring interacting with a stationary oscillator, it is worth mentioning that if no damping is included in the model, the imaginary part of the equivalent stiffness is always zero regardless of the rotational speeds, i.e. sub-critical or super-critical. This is

in contrast to the case of a moving load on an infinitely long beam in which waves are generated in the infinitely long beam if the load moves with a super-critical speed. This implies that energy propagates away from the load and this energy loss occurs even in the case without damping. However, a ring is a closed system; there is no energy loss if no damping mechanism (physical/material damping) is considered in the model.

In Fig. (7.3) the equivalent stiffness at the contact point (at the outer surface) is plotted. The value of the rotational speed and the material damping are indicated in each plot. Fig. 7.3(a) shows the equivalent stiffness for the sub-critical case $\bar{v} = 0.3$ with rather small material damping. The imaginary part of the equivalent stiffness is always positive for all positive frequencies which indicates that no instability will occur in this case for a stationary oscillator interacting with the ring. In contrast, when $\bar{v} = 0.7$, there are multiple frequency regions (for $\bar{\omega} < 0.15$) in which the imaginary part of χ_{eq} is lower than zero, suggesting possible unstable motion of the oscillator. If one increases the value of ζ, no instability will occur as the imaginary part of χ_{eq} becomes positive (Fig. 7.3(c)). The same trends hold for $\bar{v} = 1.2$. It is clear that when the material damping increases, the frequency ranges in which $\mathrm{Im}(\chi_{eq})$<0 reduce and finally disappear.

7.3. STABILITY ANALYSIS

It has been shown in Chapters 3 and 5 that the free vibration can be unstable for certain parameters of a rotating ring. In this Chapter, the parameters chosen ensure that no instability of free vibrations of the ring will occur for any rotational speeds. Therefore, the stability analysis purely manifests the stability of the coupled oscillator-ring system.

7.3.1. DISSCUSSION ON THE CHARACTERISTIC EQUATION

The characteristic equation which governs vibrations of the oscillator is given by Eq. (7.25), After substituting $s = \mathrm{i}\omega$ into and rewriting it, one obtains

$$(K_1 + \mathrm{i}\varepsilon_1\omega + \chi_{eq})(-M\omega^2 + K_2 + \mathrm{i}\varepsilon_2\omega + K_1 + \mathrm{i}\varepsilon_1\omega) - (K_1 + \mathrm{i}\varepsilon_1\omega)^2 = 0. \tag{7.26}$$

As shown in Fig. 7.3, for a super-critically rotating ring, there are multiple frequency regions in which the system may be unstable. There is no universal rule that would allow to determine the number and distribution characteristics of these frequency regions. The principle of the argument can be employed to determine the unstable roots of the characteristic equation for specific oscillator-ring parameters [117]. An efficient alternative method to determine whether the system is stable is the D-decomposition method. It allows one to study influence of the change of a certain system parameter on stable and unstable regimes. The number of unstable roots is obtained without actually solving for the roots themselves (or solving for the roots only for one value of the parameter being examined). Therefore, the stable and unstable regions are determined in the chosen parameter plane.

In engineering practice, the stiffness k_2 is likely to change. For example, in application to railway engineering, the train wheel can be modelled as a rotating ring, whereas the track mass vibrates as an oscillator which is connected to the wheel by a Hertz contact spring. The support of the track mass by the substructure can be treated as a spring. To ensure vibrational stability, the most reasonable way is to adjust the stiffness of the

soil, namely k_2 in our model. Thus, k_2 is chosen as the varying parameter to be studied. According to Eq. (7.26), the dimensionless parameter K_2 can be expressed as

$$K_2 = M\omega^2 - \frac{\chi_{eq}(K_1 + \mathrm{i}\varepsilon_1\omega)}{\chi_{eq} + K_1 + \mathrm{i}\varepsilon_1\omega} - \mathrm{i}\varepsilon_2\omega. \tag{7.27}$$

For convenience, one can introduce a new equivalent dynamic stiffness as

$$\chi'_{eq} = \frac{\chi_{eq}(K_1 + \mathrm{i}\varepsilon_1\omega)}{\chi_{eq} + K_1 + \mathrm{i}\varepsilon_1\omega}. \tag{7.28}$$

Now Eq. (7.27) can be reduced to

$$K_2 = M\omega^2 - \chi'_{eq} - \mathrm{i}\varepsilon_2\omega. \tag{7.29}$$

It can be seen from Eq. (7.28) that the equivalent stiffness χ_{eq} and K_1 act as two springs connected in series. Assigning that

$$\chi_{eq} = a(\omega) + \mathrm{i}b(\omega) \text{ with } a = \mathrm{Re}(\chi_{eq}),\ b = \mathrm{Im}(\chi_{eq}), \tag{7.30}$$

one obtains

$$\begin{aligned} \chi'_{eq} &= \frac{\chi_{eq}(K_1 + \mathrm{i}\varepsilon_1\omega)}{\chi_{eq} + K_1 + \mathrm{i}\varepsilon_1\omega} = \frac{\big(a + b\mathrm{i}\big)(K_1 + \mathrm{i}\varepsilon_1\omega)}{a + b\mathrm{i} + (K_1 + \mathrm{i}\varepsilon_1\omega)} \\ &= \frac{a\omega^2{\varepsilon_1}^2 + K_1(a^2 + aK_1 + b^2) + \mathrm{i}\big(a^2\omega\varepsilon_1 + b(\omega^2{\varepsilon_1}^2 + b\omega\varepsilon_1 + {K_1}^2)\big)}{(a + K_1)^2 + (b + \varepsilon_1\omega)^2}. \end{aligned} \tag{7.31}$$

If one assumes $\varepsilon_1 = 0$, then Eq. (7.31) becomes

$$\chi'_{eq} = \frac{K_1(a^2 + aK_1 + b^2) + \mathrm{i}b{K_1}^2}{(a + K_1)^2 + b^2}. \tag{7.32}$$

It is observed from Eq. (7.32) that the frequencies corresponding to $\mathrm{Im}(\chi_{eq}(\mathrm{i}\omega)) = 0$ are also the roots of $\mathrm{Im}(\chi'_{eq}(\mathrm{i}\omega)) = 0$ when $\varepsilon_1 = 0$.

7.3.2. AN ILLUSTRATIVE EXAMPLE USING D-DECOMPOSITION

As an example, K_2 is chosen as the varying parameter to be investigated as shown in Eq. (7.29). Assuming K_2 is a complex value momentarily, the idea of D-decomposition method is to map the complex ω-plane following Eq. (7.29) onto the complex K_2-plane using ω as the parameter for the curve. The mapped line will divide the K_2-plane into domains with different numbers of roots with a positive real part. After the mapping, since physically K_2 must be real, the crossing points on the real axis are the points which divide domains with different number N of unstable roots. The values of ω corresponding to the crossing points are given by

$$\mathrm{Im}(\chi'_{eq}(\mathrm{i}\omega)) + \varepsilon_2\omega = 0. \tag{7.33}$$

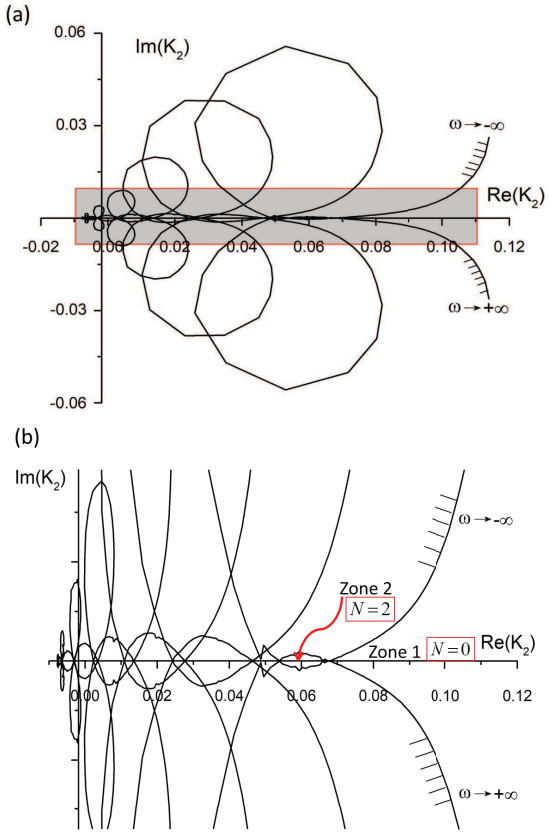

Figure 7.4: D-decomposition curves, $\bar{v} = 0.7$, $\zeta = 0.001$, $\varepsilon_1 = \varepsilon_2 = 0$, $K_1 = 0$, $M = 6$: (a) Re(K_2) vs Im(K_2); (b) Enlarged view of the real axis.

The D-decomposition curves Re(K_2) versus Im(K_2) according to Eq. (7.29) for a supercritical case $\bar{v} = 0.7$ is plotted in Fig. 7.4. The following parameters are chosen: $K_1 = 0$, $M = 6.0$, and $\zeta = 0.001$. For simplicity, the damping values of the oscillator are $\varepsilon_1 = \varepsilon_2 = 0$. From Fig. 7.3(b) one sees the equivalent stiffness of this case. There are multiple frequency ranges of negative imaginary part of the equivalent stiffness, which means instability may occur and there are multiple crossing points on the real axis of K_2. This is indeed the case as shown in Fig. 7.4(a). Several crossing points exist, separating multiple stable and unstable regions. The side of shading of the D-decomposition curves corresponds to the right-hand side of the imaginary axis of the ω plane. Note that the shading is only done partially for $\omega \to \pm\infty$ for the sake of visual clarity. However, it can be extended easily for all the curves. The real axis of K_2 is enlarged for a better view. Recall that K_2 must be positive and real, hence only the number of unstable roots in the domain $K_2 \in \{\text{Re}(K_2) > 0, \text{Im}(K_2) = 0\}$ is considered, namely the positive real axis in the K_2-plane. The crossing points (critical K_2, namely K_2^*) on the real axis are the points which divide domains with different number of unstable roots. The values of ω corresponding to the

crossing points are given by Eq. (7.33). Crossing the D-decomposition line one time in the shading direction means that the number of unstable roots increases by one. The number of unstable roots for the two rightmost frequency regions Zone 1 and Zone 2 are listed. In Zone 1 where $K_2 \approx> 0.7$ the oscillator is always stable. The number of unstable roots is found to be zero using the Cauchy's argument principle. Once the number of unstable roots is known for any region of the K_2 plane, the D-decomposition method allows to determine the number of unstable roots for any other value of K_2 by counting crossings of the D-Decomposition curve and the real axis. In the Zone 2, namely $0.054 <\approx K_2 <\approx 0.07$, the D-Decomposition curve crosses the real axis twice, suggesting there are two more unstable roots than in Zone 1, making it in total 2 unstable roots in this region. The motion of the oscillator with K_2 in this range is unstable. The number of unstable roots in other regions can be obtained accordingly be examining the number of crossings and the shading direction.

7.4. CONCLUSIONS

In this chapter, the instability of a stationary oscillator on a rotating elastic ring on foundation has been discussed. To describe the ring, the high-order theory proposed in Chapter 4 is employed. A soft ring on stiff foundation is considered as an example.

The equivalent (dynamic) stiffness at the contact point is investigated for speeds lower and higher than the minimum resonance speed. The equivalent stiffness at the contact point calculated from the developed high-order theory can have a negative imaginary part for rings which rotate super-critically. Thus, instability may occur for certain system parameters. However, the vibration of the stationary oscillator-rotating ring system is always stable if the ring is rotating sub-critically. The material damping serves as a stabilising factor for the whole system and it has a significant influence on the frequency ranges in which the imaginary part of the equivalent stiffness is negative.

8

CONCLUSIONS

Though rings are geometrically simple structures, the dynamic phenomena a ring can exhibit are rather rich. A ring can be treated as a shell structure once the axial dimension is omitted. The closeness of the ring introduces a periodicity of 2π in terms of circumferential angle. When a ring rotates, it becomes essentially a gyroscopic system. The dynamics of a rotating ring belongs to the class of the moving load problems when a load is in contact with the ring. In other words, the dynamics of high-speed rotating rings considered in this thesis can be labelled as shell-type, periodic, gyroscopic and moving load problems.

A plethora of rotating ring models are available in the literature. The majority of them deal with in-plane vibrations of rotating thin rings which consider only the displacements at the middle surface and utilise the Euler-Bernoulli hypothesis. Among existing rotating thin ring models, different governing equations considering the rotation effects are present in the literature based on different assumptions and derivation procedures. Some assumptions and derivation procedures are questionable and resulting erroneous predictions of the dynamic behaviour of thin rings rotating at high speeds. The main reason for such predictions is that these assumptions and approximations result in different static equilibria which has significant effect at high rotational speeds. Another limitation of thin ring models is associated with the possible presence of a stiff elastic foundation. In this case, thin ring models predict, at high wavenumbers, a convergence of the minimum resonance speed to the longitudinal wave speed of the material the ring is made. This prediction violates the physics as it is the Rayleigh wave speed the resonance speed has to converge to [97].

The Timoshenko-type models which account for the shear deformation and rotatory inertia are also available in the literature even though less frequently. The improved models give better predictions, e.g. of the critical speeds. However, an intrinsic problem holds for all low-order models existing, regardless of whether the classical thin ring models or the improved Timoshenko-type models are considered. These models were derived assuming the inner and outer surfaces of the ring to be traction-free. However, when one considers a ring whose inner surface is elastically restrained by distributed

springs, this assumption is violated. The traction force (both static and dynamic components) at the inner surface can significantly influence the stress distribution in the ring and affect its dynamics. This is especially important in the case of rings rotating at high speeds and supported by stiff foundation.

8.1. NOVEL CONTRIBUTIONS OF THE MODEL

A new high-order model which can properly address all the issues mentioned previously is developed in this thesis. The novel contributions of the thesis in terms of new models developed are:

i) **Proper consideration of the rotation effects;**
The fictitious forces (centrifugal force and Coriolis force) induced by the rotation give rise to two counteracting effects: stress-stiffening and spin-softening (centrifugal softening). The softening effect, which is associated with the kinetic energy, decreases the stiffness of the ring with increasing rotation speed and eventually destabilises the rotating equilibrium. In contrast, the initial hoop tension in the ring caused by rotation stiffens the ring and acts as a stabilising factor. The total effect of rotation is determined eventually by the dominance of either the softening or the stiffening component. It is concluded that in most of the previous studies, the softening effect has been considered. In contrast, the stiffening effect is not always properly accounted for and this may lead to erroneous results, especially when the rotational speed is large.

   The stiffening is only captured by employing a nonlinear strain measure in the strain energy. Consequently, the choice of the nonlinear strain-displacement relation is of importance. The reason is that different strain-displacement relations result in different static equilibria at high speeds of rotation. In this work, the quadratic truncation of the geometrically exact strain-displacement relation is used.

ii) **Through-thickness correction of the displacement fields;**
Generally speaking, the classical ring theory based on Love's approximation [19] and the Timoshenko type of models suffice to describe the dynamics of stationary thin/moderately thick rings in most cases. However, when the inner surface of a ring is connected to a hub via stiff springs (namely a stiff foundation), higher order terms are needed in the displacement fields for the following reasons: a) The stresses (both the rotation-induced static stress and the dynamic stress) at the inner surface are non-zero whereas the outer surface is still stress-free. To account for the variation of stresses along the thickness, higher than Timoshenko-type order terms need to be included in both the radial and circumferential displacement fields; b) Large stiffness of the foundation leads to high cut-off frequencies, and consequently high natural frequencies of the elastic modes. The low-order models will give erroneous predictions of wave characteristics at high wavenumber ranges. The same conclusion holds for stationary rings on stiff foundation.

iii) **Influence of the boundary effects;**
As mentioned before, the inner surface of the ring is not traction-free due to the presence of elastic foundation. Thus, when formulating governing equations, the

boundary effects should be accounted for to meet the true physics. The influence of the boundary effects is of importance when the ring is supported by stiff foundation.

8.2. MAIN FINDINGS

Having the aspects above considered, the following conclusions, as well as clarifications of some open issues are obtained:

1) **Instability of in-plane free vibration of high-speed rotating rings;**
   The occurrence of instability of the in-plane free vibration of high-speed rotating rings is an open issue in the literature. In a few references where instability is mentioned, its occurrence is related to the rotational speed at which one of the natural frequencies considered in the rotating reference system becomes zero. In fact, this speed corresponds to resonance of a rotating ring subjected to a co-rotating load. The misconception between resonance and instability is dispelled in this thesis. Instability has been predicted for high-speed rotating thin rings. Divergence instability of the 0th mode always occurs before flutter of higher modes.

   The influences of ring parameters on the stability of rotating rings have been conducted. It is shown that the stiffness of circumferential springs influences strongly the critical speed at which instability occurs. If the circumferential stiffness is absent, then for an infinitesimal rotating speed divergence will occur. However, the stiffness of radial springs is a destabilising factor since it constrains the radial expansion of the ring and thus the stiffening effect due to hoop tension decreases. More interestingly, if the stiffness of radial springs is smaller than a certain value for a fixed value of the stiffness of circumferential springs, instability will never occur. This observation may be useful in engineering design. The extensional stiffness of the ring helps to avoid instability.

2) **Existence of resonance speeds and “standing wave" phenomenon in forced vibrations of rotating rings;**
   Resonance speeds at which resonances of a rotating ring subjected to a stationary load occur are found using the developed high-order model. The higher order corrections of the displacement fields are proved to be important even for thin rings which are elastically supported by stiff foundation. It is concluded that for higher wavenumbers, the resonance speeds of the lowest branch converge to the Rayleigh wave speed of the material. The influence of radial and shear stress boundary effects becomes significant when the foundation is relatively stiff.

   Having found the resonance speeds, it is natural that wave-like deformation is predicted for a super-critically rotating ring subjected to stationary loads. This deformation pattern is stationary to a space-fixed observer. This has been observed experimentally for rolling tires and is termed as “standing wave" phenomenon.

3) **Instability of a stationary oscillator interacting with a ring rotating at a high speed.**
   Instability of objects interacting with infinite elastic continua is associated with anomalous Doppler waves generated in the continua and the resulting "negative damping" (negative imaginary part of the equivalent stiffness of the supporting medium).

Therefore, the necessary condition for instability to occur is that the objects move faster than a critical speed of waves in the continua. Using the developed high-order model, it is shown that for the case of stationary oscillator interacting with a rotating ring, the oscillator can be unstable when the ring rotates at speeds higher than the minimum resonance speed.

4) **Importance of proper consideration of the geometrical nonlinearity;**
It is, in fact, true that there exist different nonlinear strain-displacement relations accounting for the geometric nonlinearity. The choice of nonlinear-strain displacement relations may lead to differences in the predictions of the dynamic behaviour of a ring rotating at high speeds. Two nonlinear strain-displacement relations are widely used in the literature. These are: (i) the Green-Lagrange strain, and (ii) the engineering strain which is the second order truncation of geometrically exact strain-displacement relation. Whatever the choice, however, the stress and strain measures need to be conjugate to comply with considerations of internal elastic energy. It is known that the work-conjugate of the Green-Lagrange strain is the 2nd Piola-Kirchhoff stress. Thus, if one would use the Green-Lagrange strain relation, the material constants need to be derived by experiments using 2nd Piola-Kirchhoff stress and Green-Lagrange strain. The material constant (the Young's modulus) is obtained from experiments using engineering stress and strain measures which are widely adopted in the literature. Therefore, the engineering stress and strain measures are used in this work to be consistent with the experiments upon which the derivation of the Young's modulus is based.

A

NONLINEAR STRAIN-DISPLACEMENT RELATIONS

According to [24], for a circular cylinder, the exact strain-displacement relations are

$$\begin{aligned}
\varepsilon_x &= \sqrt{(1+v_{,x})^2+(u_{,x})^2+(w_{,x})^2}-1 \\
\varepsilon_\theta &= \sqrt{\left(\frac{v_{,\theta}}{r}\right)^2+\left(1+\frac{u_{,\theta}}{r}+\frac{w}{r}\right)^2+\left(\frac{w_{,\theta}}{r}-\frac{u}{r}\right)^2}-1 \\
\varepsilon_r &= \sqrt{{v_{,r}}^2+{u_{,r}}^2+(1+w_{,r})^2}-1
\end{aligned} \tag{A.1}$$

where w, u, v are the radial, circumferential and longitudinal displacements, respectively. The subscripts x, r, θ represent the coordinates in longitudinal, radial and circumferential directions, respectively. The term $u_{,\theta}$ denotes $u_{,\theta} = \partial u/\partial\theta$; similar definitions hold for other terms.

When a thin ring is considered, the axial displacement v drops. Assuming one deals with the displacements in the middle surface only, then only the circumferential strain retains

$$\varepsilon_\theta = \sqrt{(1+\varepsilon_0)^2+\beta^2}-1 \tag{A.2}$$

where

$$\varepsilon_0 = \frac{u_{,\theta}}{r}+\frac{w}{r},\ \beta = \frac{u}{r}-\frac{w_{,\theta}}{r}. \tag{A.3}$$

Eq. (A.2) can be rewritten as

$$\varepsilon_\theta = \sqrt{1+\eta}-1 \tag{A.4}$$

where

$$\eta = 2\varepsilon_0+(\varepsilon_0)^2+(\beta)^2. \tag{A.5}$$

By application of Taylor series expansion to the second order of η, Eq. (A.4) yields

$$\varepsilon_\theta = \frac{1}{2}\eta+O(\eta^2) = \varepsilon_0+\frac{1}{2}(\varepsilon_0)^2+\frac{1}{2}(\beta)^2+O(\eta^2) \tag{A.6}$$

whereas Eq. (A.4) becomes

$$\varepsilon_\theta = \frac{1}{2}\eta - \frac{1}{8}\eta^2 + O(\eta^3) = \varepsilon_0 + \frac{1}{2}(\beta)^2 - \frac{1}{8}\big((\varepsilon_0)^2 + (\beta)^2\big)^2 - \frac{1}{2}\varepsilon_0\big((\varepsilon_0)^2 + (\beta)^2\big) + O(\eta^3) \quad \text{(A.7)}$$

when it is truncated till the third order of η.

Retaining terms with respect to the middle surface displacements up to the second degree, Eq. (A.6) yields the Green-Lagrange strain-displacement relation

$$\varepsilon_\theta = \varepsilon_0 + \frac{1}{2}(\varepsilon_0)^2 + \frac{1}{2}(\beta)^2 = \frac{u_{,\theta}}{r} + \frac{w}{r} + \frac{1}{2}\big(\frac{u_{,\theta}}{r} + \frac{w}{r}\big)^2 + \frac{1}{2}\big(\frac{u}{r} - \frac{w_{,\theta}}{r}\big)^2, \quad \text{(A.8)}$$

whereas Eq. (A.7) yields

$$\varepsilon_\theta = \varepsilon_0 + \frac{1}{2}(\beta)^2 = \frac{u_{,\theta}}{r} + \frac{w}{r} + \frac{1}{2}\big(\frac{u}{r} - \frac{w_{,\theta}}{r}\big)^2, \quad \text{(A.9)}$$

which is the Engineering strain.

B

EXACT SOLUTION FOR NATURAL FREQUENCIES OF ELASTICALLY RESTRAINED RINGS

A stationary (non-rotating) ring can be considered as a circular annulus. Either plane strain [118] or plane stress [119] assumption can be made according to the practical problem for the in-plane vibrations of the ring. Assume steady-state time-harmonic waves in the ring, after dropping the time signature $e^{i\omega t}$, the governing equations in polar coordinate (r,θ) are

$$\begin{aligned} &\frac{\partial \sigma_r}{\partial r}+\frac{\sigma_r-\sigma_\theta}{r}+\frac{1}{r}\frac{\partial \tau_{\theta r}}{\partial \theta}+\rho\omega^2 w=0,\\ &\frac{\partial \tau_{\theta r}}{\partial r}+\frac{1}{r}\frac{\partial \sigma_\theta}{\partial \theta}+\frac{2\tau_{\theta r}}{r}+\rho\omega^2 u=0 \end{aligned} \tag{B.1}$$

where $w=w(r,\theta)$, $u=u(r,\theta)$ are the radial and circumferential displacement, respectively. Considering a linear relation between stress and strain, i.e. the Hooke's law Eq. (4.3), one obtains

$$\begin{aligned} \sigma_r &= 2\mu\varepsilon_r+\bar{\lambda}(\varepsilon_r+\varepsilon_\theta)=2\mu\frac{\partial w}{\partial r}+\bar{\lambda}\left(\frac{\partial w}{\partial r}+\frac{w}{r}+\frac{1}{r}\frac{\partial u}{\partial \theta}\right),\\ \sigma_\theta &= 2\mu\varepsilon_\theta+\bar{\lambda}(\varepsilon_r+\varepsilon_\theta)=2\mu\left(\frac{w}{r}+\frac{1}{r}\frac{\partial u}{\partial \theta}\right)+\bar{\lambda}\left(\frac{\partial w}{\partial r}+\frac{w}{r}+\frac{1}{r}\frac{\partial u}{\partial \theta}\right),\\ \tau_{\theta r} &= \mu\gamma_{\theta r}=\mu\left(\frac{\partial u}{\partial r}-\frac{u}{r}+\frac{1}{r}\frac{\partial w}{\partial \theta}\right). \end{aligned} \tag{B.2}$$

Expression of $\bar{\lambda}$ can be found in Eq. (4.4).

The Helmholtz decomposition is used to obtain two decoupled governing equations:

$$\nabla^2\hat{\Phi}+\frac{\omega^2}{{c_L}^2}\hat{\Phi}=0,\ \ \nabla^2\hat{H}_z+\frac{\omega^2}{{c_T}^2}\hat{H}_z=0 \tag{B.3}$$

where $c_L = \sqrt{(\bar{\lambda}+2\mu)/\rho}$ and $c_T = \sqrt{\mu/\rho}$. The displacements can be expressed as

$$w = \frac{\partial \hat{\Phi}}{\partial r} + \frac{1}{r}\frac{\partial \hat{H}_z}{\partial \theta},\ u = \frac{1}{r}\frac{\partial \hat{\Phi}}{\partial \theta} - \frac{\partial \hat{H}_z}{\partial r}. \tag{B.4}$$

Applying the separation of variables on Eq. (B.3), yields

$$\begin{aligned} \hat{\Phi}(r,\theta) &= \left(A_n J_n(k_p\, r) + B_n\, Y_n(k_p\, r)\right)\cos(n\theta), \\ \hat{H}_z(r,\theta) &= (C_n\, J_n(k_s\, r) + D_n\, Y_n(k_s\, r))\sin(n\theta) \end{aligned} \tag{B.5}$$

where $k_p = \omega/\, c_L$ and $k_s = \omega/\, c_T$; J_n and Y_n are the Bessel functions of the first and second kind, respectively.

The boundary conditions are

$$\sigma_r\,|_{-h/2} = k_r\, w\,|_{-h/2}\ ,\ \ \tau_{\theta r}\,|_{-h/2} = k_c\, u\,|_{-h/2} \tag{B.6}$$

at the inner surface and

$$\sigma_r\,|_{h/2} = 0,\ \ \tau_{\theta r}\,|_{h/2} = 0 \tag{B.7}$$

at the outer surface.

The frequency equation can be obtained by substituting Eq. (B.5) into the boundary conditions (B.6-B.7) and by setting subsequently the determinant of the coefficient matrix to zero.

C

THE COEFFICIENT MATRIX, DISPLACEMENT AND FORCE VECTORS FOR CHAPTER 6

The coefficient matrix **C** is of the order $(N_1 + N_2 + 2) \times (N_1 + N_2 + 2)$. The displacement vector **a** and the force vector **f** are of the order $(N_1 + N_2 + 2) \times 1$.

$$\mathbf{C}=\begin{bmatrix}
\Delta_{w00} & \Delta_{w01} & \cdots & \Delta_{w0l} & \cdots & \Delta_{w0N_1} & \Delta_{u00} & \Delta_{u01} & \cdots & \Delta_{u0q} & \cdots & \Delta_{u0N_2}\\
\Delta_{w10} & \Delta_{w11} & \cdots & \Delta_{w1l} & \cdots & \Delta_{w1N_1} & \Delta_{u10} & \Delta_{u11} & \cdots & \Delta_{u1q} & \cdots & \Delta_{u1N_2}\\
\vdots & \vdots & \cdots & \vdots & \cdots & \vdots & \vdots & \vdots & \cdots & \vdots & \cdots & \vdots\\
\Delta_{wl0} & \Delta_{wl1} & \cdots & \Delta_{wll} & \cdots & \Delta_{wlN_1} & \Delta_{ul0} & \Delta_{ul1} & \cdots & \Delta_{ulq} & \cdots & \Delta_{ulN_2}\\
\cdots & \vdots & \cdots & \vdots & \cdots & \vdots & \vdots & \vdots & \cdots & \vdots & \cdots & \vdots\\
\Delta_{wN_10} & \Delta_{wN_11} & \cdots & \Delta_{wN_1l} & \cdots & \Delta_{wN_1N_1} & \Delta_{uN_10} & \Delta_{uN_11} & \cdots & \Delta_{uN_1q} & \cdots & \Delta_{uN_1N_2}\\
\Delta_{w(N_1+1)0} & \Delta_{w(N_1+1)1} & \cdots & \Delta_{w(N_1+1)l} & \cdots & \Delta_{w(N_1+1)N_1} & \Delta_{u(N_1+1)0} & \Delta_{u(N_1+1)1} & \cdots & \Delta_{u(N_1+1)q} & \cdots & \Delta_{u(N_1+1)N_2}\\
\Delta_{w(N_1+2)0} & \Delta_{w(N_1+2)1} & \cdots & \Delta_{w(N_1+2)l} & \cdots & \Delta_{w(N_1+2)N_1} & \Delta_{u(N_1+2)0} & \Delta_{u(N_1+2)1} & \cdots & \Delta_{u(N_1+2)q} & \cdots & \Delta_{u(N_1+2)N_2}\\
\vdots & \vdots & \cdots & \vdots & \cdots & \vdots & \vdots & \vdots & \cdots & \vdots & \cdots & \vdots\\
\Delta_{w(N_1+q+1)0} & \Delta_{w(N_1+q+1)1} & \cdots & \Delta_{w(N_1+q+1)l} & \cdots & \Delta_{w(N_1+q+1)N_1} & \Delta_{u(N_1+q+1)0} & \Delta_{u(N_1+q+1)1} & \cdots & \Delta_{u(N_1+q+1)q} & \cdots & \Delta_{u(N_1+q+1)N_2}\\
\vdots & \vdots & \cdots & \vdots & \cdots & \vdots & \vdots & \vdots & \cdots & \vdots & \cdots & \vdots\\
\Delta_{w(N_1+N_2+1)0} & \Delta_{w(N_1+N_2+1)1} & \cdots & \Delta_{w(N_1+N_2+1)l} & \cdots & \Delta_{w(N_1+N_2+1)N_1} & \Delta_{u(N_1+N_2+1)0} & \Delta_{u(N_1+N_2+1)1} & \cdots & \Delta_{u(N_1+N_2+1)q} & \cdots & \Delta_{u(N_1+N_2+1)N_2}
\end{bmatrix}. \tag{C.1}$$

All the entries can be obtained by any symbolic computation software. The displacement vector in frequency-wavenumber domain is given as

$$\mathbf{a}=\begin{bmatrix}\tilde{\tilde{W}}_0^{(\bar{\omega},\bar{\gamma})} & \tilde{\tilde{W}}_1^{(\bar{\omega},\bar{\gamma})} & \cdots & \tilde{\tilde{W}}_l^{(\bar{\omega},\bar{\gamma})} & \cdots & \tilde{\tilde{W}}_{N_1}^{(\bar{\omega},\bar{\gamma})} & \tilde{\tilde{U}}_0^{(\bar{\omega},\bar{\gamma})} & \tilde{\tilde{U}}_1^{(\bar{\omega},\bar{\gamma})} & \cdots & \tilde{\tilde{U}}_q^{(\bar{\omega},\bar{\gamma})} & \cdots & \tilde{\tilde{U}}_{N_2}^{(\bar{\omega},\bar{\gamma})}\end{bmatrix}^T. \tag{C.2}$$

The force vector is given by

$$\mathbf{f}=\begin{bmatrix}P_{\mathrm{w}0} & P_{\mathrm{w}1} & \cdots & P_{\mathrm{w}l} & \cdots & P_{\mathrm{w}N_1} & P_{\mathrm{u}0} & P_{\mathrm{u}1} & \cdots & P_{\mathrm{u}q} & \cdots & P_{\mathrm{u}N_2}\end{bmatrix}^T. \tag{C.3}$$

Since the load is only applied on the radial direction, thus

$$P_{\mathrm{w}l}=-2\pi\bar{P}_0\delta(\bar{\omega}-\bar{\Omega}_f),(l=0,1,2,3...N_1) \tag{C.4}$$

whereas the components acting on the circumferential direction are

$$P_{\mathrm{u}q}=0,(q=0,1,2,3...N_2). \tag{C.5}$$

REFERENCES

[1] P. Chidamparam and A. W. Leissa, *Vibrations of planar curved beams, rings, and arches,* Applied Mechanics Reviews **46**, 467 (1993).

[2] G. Bryan, *On the beats in the vibrations of a revolving cylinder or bell,* Proceedings of the Cambridge Philosophical Society **7**, 101 (1890).

[3] S. Gong, *Tire ring model-literature review*, Tech. Rep. (Delft University of Technology, 1989).

[4] M. Matsubara, D. Tajiri, T. Ise, and S. Kawamura, *Vibrational response analysis of tires using a three-dimensional flexible ring-based model,* Journal of Sound and Vibration **408**, 368 (2017).

[5] A. Gasmi, P. F. Joseph, T. B. Rhyne, and S. M. Cron, *Development of a two-dimensional model of a compliant non-pneumatic tire,* International Journal of Solids and Structures **49**, 1723 (2012).

[6] S. Yoon, U. Park, J. Rhim, and S. S. Yang, *Tactical grade MEMS vibrating ring gyroscope with high shock reliability,* Microelectronic Engineering **142**, 22 (2015).

[7] C. Bert and T. Chen, *On vibration of a thick flexible ring rotating at high speed,* Journal of Sound and Vibration **61**, 517 (1978).

[8] S. Noga, R. Bogacz, and T. Markowski, *Vibration analysis of a wheel composed of a ring and a wheel-plate modelled as a three-parameter elastic foundation,* Journal of Sound and Vibration **333**, 6706 (2014).

[9] C. G. Cooley and R. G. Parker, *Vibration of high-speed rotating rings coupled to space-fixed stiffnesses,* Journal of Sound and Vibration **333**, 2631 (2014).

[10] H. Lu, T. Chai, and C. G. Cooley, *Vibration properties of a rotating piezoelectric energy harvesting device that experiences gyroscopic effects,* Journal of Sound and Vibration **416**, 258 (2018).

[11] J. Padovan, *On standing waves in tires,* Tire Science and Technology **5**, 83 (1977).

[12] G. Potts, C. Bell, L. Charek, and T. Roy, *Tire vibrations,* Tire Science and Technology **5**, 202 (1977).

[13] M. Endo, K. Hatamura, M. Sakata, and O. Taniguchi, *Flexural vibration of a thin rotating ring,* Journal of Sound and Vibration **92**, 261 (1984).

[14] S. Huang and W. Soedel, *Effects of Coriolis acceleration on the free and forced in-plane vibrations of rotating rings on elastic foundation,* Journal of Sound and Vibration **115**, 253 (1987).

[15] S. Huang and W. Soedel, *Response of rotating rings to harmonic and periodic loading and comparison with the inverted problem,* Journal of Sound and Vibration **118**, 253 (1987).

[16] S. Huang and W. Soedel, *Effects of Coriolis acceleration on the forced vibration of rotating cylindrical shells,* Journal of Applied Mechanics **55**, 231 (1988).

[17] J. Lin and W. Soedel, *On general in-plane vibrations of rotating thick and thin rings,* Journal of Sound and Vibration **122**, 547 (1988).

[18] J. Lin and W. Soedel, *On the critical speeds of rotating thick or thin rings,* Mechanics of Structures and Machines **16**, 439 (1988).

[19] W. Soedel, *Vibrations of Shells and Plates* (CRC Press, 2004).

[20] S. Gong, *A study of in-plane dynamics of tires*, Ph.D. thesis, Delft University of Technology (1993).

[21] Y.-J. Kim and J. S. Bolton, *Effects of rotation on the dynamics of a circular cylindrical shell with application to tire vibration,* Journal of Sound and Vibration **275**, 605 (2004).

[22] K. Saeedi, *Influence of Rotating Tire Dynamics on Vehicle System Vibrations*, Ph.D. thesis, Concordia University (2012).

[23] R. Zadoks and C. Krousgrill, *Complex dynamics in the quadratically non-linear response of a rotating ring with elastic hub,* Journal of Sound and Vibration **165**, 385 (1993).

[24] M. Stein, *Nonlinear theory for plates and shells including the effects of transverse shearing,* AIAA journal **24**, 1537 (1986).

[25] W. Kim and J. Chung, *Free non-linear vibration of a rotating thin ring with the in-plane and out-of-plane motions,* Journal of Sound and Vibration **258**, 167 (2002).

[26] C. G. Cooley and R. G. Parker, *Limitations of an inextensible model for the vibration of high-speed rotating elastic rings with attached space-fixed discrete stiffnesses,* European Journal of Mechanics-A/Solids **54**, 187 (2015).

[27] H. Ding, M. Zhu, Z. Zhang, Y.-W. Zhang, and L.-Q. Chen, *Free vibration of a rotating ring on an elastic foundation,* International Journal of Applied Mechanics **9**, 1750051 (2017).

[28] J. T. Tielking, *Plane vibration characteristics of a pneumatic tire model,* SAE Technical Paper 650492 (1965), 10.4271/650492.

[29] W. Bickford and E. Reddy, *On the in-plane vibrations of rotating rings,* Journal of Sound and Vibration **101**, 13 (1985).

[30] R. Eley, C. Fox, and S. McWilliam, *Coriolis coupling effects on the vibration of rotating rings,* Journal of Sound and Vibration **238**, 459 (2000).

[31] U. Nackenhorst and M. Brinkmeier, *On the dynamics of rotating and rolling structures,* Archive of Applied Mechanics **78**, 477 (2008).

[32] D. Huang, L. Tang, and R. Cao, *Free vibration analysis of planar rotating rings by wave propagation,* Journal of Sound and Vibration **332**, 4979 (2013).

[33] D. Beli, P. B. Silva, and J. R. de França Arruda, *Vibration analysis of flexible rotating rings using a spectral element formulation,* Journal of Vibration and Acoustics **137**, 041003 (2015).

[34] B. Koff and Y. El-Aini, *A simple frequency expression for the in-plane vibrations of rotating rings,* in *ASME 1991 International Gas Turbine and Aeroengine Congress and Exposition* (American Society of Mechanical Engineers, 1991) pp. V005T14A007–V005T14A007.

[35] J. Padovan, *On viscoelasticity and standing waves in tires,* Tire Science and Technology **4**, 233 (1976).

[36] J. Lin and W. Soedel, *Dynamic response of a rotating thick ring to force or displacement excitation,* Journal of Sound and Vibration **121**, 317 (1988).

[37] Y. Wei, L. Nasdala, and H. Rothert, *Analysis of forced transient response for rotating tires using REF models,* Journal of Sound and Vibration **320**, 145 (2009).

[38] L. Meirovitch, *A new method of solution of the eigenvalue problem for gyroscopic systems,* AIAA Journal **12**, 1337 (1974).

[39] L. Meirovitch, *A modal analysis for the response of linear gyroscopic systems,* ASME Transactions Series E Journal of Applied Mechanics **42**, 446 (1975).

[40] J.-L. Lin, *Vibrations of Rotating Thick Or Thin Rings*, Ph.D. thesis, Purde University (1987).

[41] W. Bickford and S. Maganty, *On the out-of-plane vibrations of thick rings,* Journal of Sound and Vibration **108**, 503 (1986).

[42] F. R. Hogan and J. R. Forbes, *Modeling of a rolling flexible circular ring,* Journal of Applied Mechanics **82**, 111003 (2015).

[43] D. Huang and H. He, *Analyzing out-of-plane vibration of a rotating ring with wave propagation.* Key Engineering Materials **693**, 31 (2016).

[44] J. Padovan, *Coriolis effects on nonlinear oscillations of rotating cylinders and rings,* in *Advances in Engineering Science*, Vol. 2 (1976).

[45] A. Maewal, *Nonlinear harmonic oscillations of gyroscopic structural systems and the case of a rotating ring,* Journal of Applied Mechanics **48**, 627 (1981).

[46] C. Glynn, *On the resonant nonlinear traveling waves in a thin rotating ring,* International Journal of Non-Linear Mechanics **17**, 327 (1982).

[47] S. Natsiavas, *Dynamics and stability of non-linear free vibration of thin rotating rings,* International Journal of Non-Linear Mechanics **29**, 31 (1994).

[48] S. Natsiavas, *Non-linear parametric resonance of spinning rings,* Journal of Sound and Vibration **184**, 93 (1995).

[49] S. Natsiavas and S. Theodossiades, *Regular and chaotic forced vibration of thin rotating rings,* International Journal of Non-Linear Mechanics **33**, 843 (1998).

[50] J.-T. Jeong, S.-G. Kim, and S.-I. Lee, *Nonlinear vibration analysis of a rotating ring,* Transactions of the Korean Society of Mechanical Engineers A **25**, 1119 (2001).

[51] S. Natsiavas, *On the dynamics of rings rotating with variable spin speed,* Nonlinear Dynamics **7**, 345 (1995).

[52] S. V. Canchi and R. G. Parker, *Parametric instability of a rotating circular ring with moving, time-varying springs,* Journal of Vibration and Acoustics **128**, 231 (2006).

[53] C. Wang, *Stability of a rotating ring under external pressure,* Journal of Applied Mechanics **51**, 439 (1984).

[54] C. Pelchen and J. Wauer, *Small vibrations of rotating ring segments and full rings under external or internal pressure,* Journal of Applied Mechanics **59**, 1038 (1992).

[55] K. Singh and B. pal Singh, *In-plane vibrations of rotating sectors and rings with and without radial supports by finite element method,* Computers & Structures **19**, 545 (1984).

[56] E. Reddy and W. Rickford, *On the in-plane vibrations of a rotating ring with equi-spaced spokes,* Journal of Sound and Vibration **103**, 533 (1985).

[57] A. Karimzadeh, M. T. Ahmadian, K. Firoozbakhsh, and M. Rahaeifard, *Vibrational analysis of size-dependent rotating micro-rings,* International Journal of Structural Stability and Dynamics , 1771012 (2017).

[58] T. Lu, A. Tsouvalas, and A. V. Metrikine, *The in-plane free vibration of an elastically supported thin ring rotating at high speeds revisited,* Journal of Sound and Vibration **402**, 203 (2017).

[59] A. Arena and W. Lacarbonara, *On the stability of magnetically levitated rotating rings,* International Journal of Mechanical Sciences **131–132**, 286 (2017).

[60] A. V. Metrikine and M. Tochilin, *Steady-state vibrations of an elastic ring under a moving load,* Journal of Sound and Vibration **232**, 511 (2000).

[61] G. Forbes and R. Randall, *Resonance phenomena of an elastic ring under a moving load,* Journal of Sound and Vibration **318**, 991 (2008).

[62] V. V. Krylov and O. Gilbert, *On the theory of standing waves in tyres at high vehicle speeds,* Journal of Sound and Vibration **329**, 4398 (2010).

[63] W. Graham, *Discussion of 'On the theory of standing waves in tyres at high vehicle speeds' by V.V. Krylov and O. Gilbert, Journal of Sound and Vibration 329 (2010) 4398–4408,* Journal of Sound and Vibration **332**, 6029 (2013).

[64] V. V. Krylov, *Commentary on Discussion of 'On the theory of standing waves in tyres at high vehicle speeds' by V.V. Krylov and O. Gilbert, Journal of Sound and Vibration 329 (2010) 4398–4408,* Journal of Sound and Vibration **332**, 7290 (2013).

[65] S. Huang and B. Hsu, *Resonant phenomena of a rotating cylindrical shell subjected to a harmonic moving load,* Journal of Sound and Vibration **136**, 215 (1990).

[66] H. Li, K.-Y. Lam, and T.-Y. Ng, *Rotating Shell Dynamics* (Elsevier, 2005).

[67] A. Tsotras, *On the interaction between modal behaviour and contact force development of a pneumatic tyre*, Ph.D. thesis, Loughborough University (2010).

[68] B. Kang, C. Riedel, and C. Tan, *Free vibration analysis of planar curved beams by wave propagation,* Journal of Sound and Vibration **260**, 19 (2003).

[69] S.-K. Lee, B. Mace, and M. Brennan, *Wave propagation, reflection and transmission in curved beams,* Journal of Sound and Vibration **306**, 636 (2007).

[70] F. J. Fahy and P. Gardonio, *Sound and Structural Vibration: Radiation, Transmission and Response* (Academic press, 2007).

[71] K. Graff, *Wave Motion in Elastic Solids* (Dover Publications, Inc., 1975).

[72] B. R. Mace and E. Manconi, *Wave motion and dispersion phenomena: Veering, locking and strong coupling effects,* The Journal of the Acoustical Society of America **131**, 1015 (2012).

[73] N. Perkins and C. Mote, *Comments on curve veering in eigenvalue problems,* Journal of Sound and Vibration **106**, 451 (1986).

[74] S. J. Walsh and R. White, *Vibrational power transmission in curved beams,* Journal of Sound and Vibration **233**, 455 (2000).

[75] A. D. Kerr, *The continuously supported rail subjected to an axial force and a moving load,* International Journal of Mechanical Sciences **14**, 71 (1972).

[76] A. W. Leissa, *Vibration of Shells* (Scientific and Technical Information Office, National Aeronautics and Space Administration, 1973).

[77] M. Amabili, *Nonlinear vibrations and stability of shells and plates* (Cambridge University Press, 2008).

[78] P. Kindt, P. Sas, and W. Desmet, *Development and validation of a three-dimensional ring-based structural tyre model,* Journal of Sound and Vibration **326**, 852 (2009).

[79] M. Deshpande and C. Mote, *In-plane vibrations of a thin rotating disk,* Journal of Vibration and Acoustics **125**, 68 (2003).

[80] H. Macke, *Traveling-wave vibration of gas-turbine engine shells,* Journal of Engineering for Power **88**, 179 (1966).

[81] J. Wickert, *Non-linear vibration of a traveling tensioned beam,* International Journal of Non-Linear Mechanics **27**, 503 (1992).

[82] F. Pellicano and F. Vestroni, *Nonlinear dynamics and bifurcations of an axially moving beam,* Journal of Vibration and Acoustics **122**, 21 (2000).

[83] L. E. Penzes and H. Kraus, *Free vibration of prestressed cylindrical shells having arbitrary homogeneous boundary conditions,* AIAA Journal **10**, 1309 (1972).

[84] J. Padovan, *Natural frequencies of rotating prestressed cylinders,* Journal of Sound and Vibration **31**, 469 (1973).

[85] W. Soedel, *On the dynamic response of rolling tires according to thin shell approximations,* Journal of Sound and Vibration **41**, 233 (1975).

[86] R. Panneton, A. Berry, and F. Laville, *Vibration and sound radiation of a cylindrical shell under a circumferentially moving load,* The Journal of the Acoustical Society of America **98**, 2165 (1995).

[87] J. Cho, K. Kim, and H. Jeong, *Numerical investigation of tire standing wave using 3-D patterned tire model,* Journal of Sound and Vibration **305**, 795 (2007).

[88] T. Lu and A. Metrikine, *On the existence of a critical speed of a rotating ring under a stationary point load,* in *Proceedings of XLIII International Summer School-Conference APM 2015* (SPBSPU/IPME RAS, St. Petersburg, Russia, June 2015) pp. 22–27.

[89] T. Lu, A. Tsouvalas, and A. V. Metrikine, *Stability of in-plane vibration of an elastically supported rotating thin ring, revisited,* in *Proceedings of the 11th International Symposium on Vibrations of Continuous Systems* (2017) pp. 46–48.

[90] T. Lu, A. Tsouvalas, and A. V. Metrikine, *A high-order model for in-plane vibrations of rotating rings on elastic foundation,* Journal of Sound and Vibration **455**, 118 (2019).

[91] H. Matsunaga, *Effects of higher-order deformations on in-plane vibration and stability of thick circular rings,* Acta Mechanica **124**, 47 (1997).

[92] E. Carrera, *Theories and finite elements for multilayered plates and shells: a unified compact formulation with numerical assessment and benchmarking,* Archives of Computational Methods in Engineering **10**, 215 (2003).

[93] E. Carrera and A. Pagani, *Analysis of reinforced and thin-walled structures by multiline refined 1d/beam models,* International Journal of Mechanical Sciences **75**, 278 (2013).

[94] E. Carrera, M. Filippi, and E. Zappino, *Laminated beam analysis by polynomial, trigonometric, exponential and zig-zag theories,* European Journal of Mechanics-A/Solids **41**, 58 (2013).

[95] A. Pagani, M. Boscolo, J. Banerjee, and E. Carrera, *Exact dynamic stiffness elements based on one-dimensional higher-order theories for free vibration analysis of solid and thin-walled structures,* Journal of Sound and Vibration **332**, 6104 (2013).

[96] G. Cowper, *The shear coefficient in Timoshenko's beam theory,* Journal of Applied Mechanics **33**, 335 (1966).

[97] P. J. Rabier and J. T. Oden, *Bifurcation in rotating bodies*, Vol. 11 (Springer Verlag, 1989).

[98] A. T. Karttunen and R. von Hertzen, *A numerical study of traveling waves in a viscoelastic cylinder cover under rolling contact,* International Journal of Mechanical Sciences **66**, 180 (2013).

[99] D. Bogy, H. Greenberg, and F. Talke, *Steady solution for circumferentially moving loads on cylindrical shells,* IBM Journal of Research and Development **18**, 395 (1974).

[100] R. Leung and R. Pinnington, *Vibration of a rotating disc subjected to an in-plane force at its rim, or at its centre,* Journal of Sound and Vibration **114**, 281 (1987).

[101] A. T. Karttunen and R. von Hertzen, *Dynamic response of a cylinder cover under a moving load,* International Journal of Mechanical Sciences **82**, 170 (2014).

[102] A. Chatterjee, J. P. Cusumano, and J. D. Zolock, *On contact-induced standing waves in rotating tires: experiment and theory,* Journal of Sound and Vibration **227**, 1049 (1999).

[103] Y. Murakami, *Theory of elasticity and stress concentration* (John Wiley & Sons, 2016).

[104] T. Lu and A. Metrikine, *A rotating ring in contact with a stationary load as a model for a flexible train wheel,* in *Proceedings of the IX International Conference on Structural Dynamics, EURODYN2014*, edited by A. Cunha, E. Caetano, P. Ribeiro, and G. Müller (Faculty of Engineering of University of Porto, Porto, Portugal, 2014) pp. 3769–3773.

[105] A. T. Karttunen and R. von Hertzen, *Steady-state vibration of a viscoelastic cylinder cover subjected to moving loads,* European Journal of Mechanics-A/Solids **58**, 202 (2016).

[106] A. Metrikin, *Unstable lateral oscillations of an object moving uniformly along an elastic guide as a result of an anomalous Doppler effect,* Acoustical Physics **40**, 85 (1994).

[107] A. V. Metrikine and H. Dieterman, *Instability of vibrations of a mass moving uniformly along an axially compressed beam on a viscoelastic foundation,* Journal of Sound and Vibration **201**, 567 (1997).

[108] A. Wolfert, H. Dieterman, and A. V. Metrikine, *Stability of vibrations of two oscillators moving uniformly along a beam on a viscoelastic foundation,* Journal of Sound and Vibration **211**, 829 (1998).

[109] A. V. Metrikine, S. Verichev, and J. Blaauwendraad, *Stability of a two-mass oscillator moving on a beam supported by a visco-elastic half-space,* International Journal of Solids and Structures **42**, 1187 (2005).

[110] T. Mazilu, *Instability of a train of oscillators moving along a beam on a viscoelastic foundation,* Journal of Sound and Vibration **332**, 4597 (2013).

[111] K. Abe, Y. Chida, P. E. Balde Quinay, and K. Koro, *Dynamic instability of a wheel moving on a discretely supported infinite rail,* Journal of Sound and Vibration **333**, 3413 (2014).

[112] T. Lu and A. V. Metrikine, *Instability of an oscillator moving circumferentially along a thin ring on a viscoelastic foundation, Proceedings of the X International Conference on Structural Dynamics, EURODYN2017*, Procedia Engineering **199**, 2555 (2017).

[113] S. Verichev and A. V. Metrikine, *Dynamic rigidity of a beam in a moving contact,* Journal of Applied Mechanics and Technical Physics **41**, 1111 (2000).

[114] A. V. Metrikine and K. Popp, *Instability of vibrations of an oscillator moving along a beam on an elastic half-space,* European Journal of Mechanics-A/Solids **18**, 331 (1999).

[115] A. V. Metrikine and S. Verichev, *Instability of vibrations of a moving two-mass oscillator on a flexibly supported Timoshenko beam,* Archive of Applied Mechanics **71**, 613 (2001).

[116] S. Verichev and A. V. Metrikine, *Instability of a bogie moving on a flexibly supported Timoshenko beam,* Journal of Sound and Vibration **253**, 653 (2002).

[117] X. Ying and I. N. Katz, *A reliable argument principle algorithm to find the number of zeros of an analytic function in a bounded domain,* Numerische Mathematik **53**, 143 (1988).

[118] G. Liu and J. Qu, *Guided circumferential waves in a circular annulus,* Journal of Applied Mechanics **65**, 424 (1998).

[119] S. Bashmal, R. Bhat, and S. Rakheja, *Frequency equations for the in-plane vibration of circular annular disks,* Advances in Acoustics and Vibration **2010** (2010), 10.1155/2010/501902.

ACKNOWLEDGEMENTS

The choice to pursue a PhD study was an easy decision for me. In September 2012 I arrived in the Netherlands to start my PhD study under the supervision of Prof. Andrei Metrikine. Back then I just had received my BSc degree and neither did I have any concrete training on research nor any knowledge of what I present in this thesis. Recalling this fact, I realise what a "risk-taker" Andrei was by accepting me as his student and moreover, as his first Chinese PhD student. Now I have to say that I feel grateful for this. Before I arrived in the Netherlands, I did my work to read Andrei's papers but that did not help. For example, when I saw the term "transition radiation" in Andrei's paper, I recalled this term from my high school textbook of physics, but I could not relate it by any mean to mechanics. Of course this is not the only question I had at the beginning of my PhD study and fortunately for most of the questions I had back then, I have answers now with Andrei and Apostolos' guidance through these years. However, during the PhD process, you start with the purpose of reducing questions and doubts but instead, you end up by gathering more of them. This is research, right? After all these years, things have changed a lot but there is still one thing that remains the same: research is still what I would like to do.

I always think I am fortunate to be in Delft, and especially to have Andrei as my supervisor. Andrei, you are much more than a supervisor to me. Without you, I would not be here in Delft, I would not be the person I am. You are always enthusiastic and patient to explain your ideas and you almost always have answers to my questions immediately. I feel like you sit on the top floor of a high-rise building and thus you can see the global picture of the problem. There are so many excellent scientific ideas in your mind. Every meeting we had together I learnt things. After meetings, quite often I could also receive extra jokes (I consider them as bonuses without answering your bonus questions) based on your specific sense of humour which always amazed me. I mentioned to you quite a long time ago that I became emotional when I read the part of your former PhD student Stas's acknowledgements about you in his dissertation. I found "resonance" between words I would like to say to you and the words he has said to you already. Thank you Andrei, for lighting me the research path, for teaching me analytical methods, for backing me up during my conference presentations, for helping me improve my writing skills, for sharing with me your history knowledge... I would like to also thank you for the financial arrangement at the late stage of my PhD study and your recommendation with regard to the Post-doc position in the railway engineering group. I believe I am "growing" constantly under your supervision and with your care.

I would like to deeply thank my co-promotor Dr. Apostolos Tsouvalas. Apostolos, I am proud and happy to work with such an intelligent scientist like you. A long time ago when I just started my research and you were still carrying on your own PhD research, one day you dropped by my office and we started talking about my PhD topic. At some point you started talking about dispersion curves of shells and plates. You talked about

infinite many branches of dispersion curves. I only knew that my thin ring structure has just two of them and I had no idea where these infinite many others come from. However, what you said stayed in my mind. One year later, when I read the book "Wave Motion in Elastic Solids", I suddenly recalled what you had said. Come on, you were a PhD student one year ahead of me and you managed to know that much! You kept amazed me to be such an intelligent person. I am grateful that you have been involved in my research. You always came up with good ideas and gave me constructive feedbacks in different perspectives. I learnt so much from you, beyond the knowledge itself. I will never forget these discussions either at TU or on the way back to the railway station after work. Thank you also for the financial arrangement at the late stage of my PhD study. I am glad to have you as both co-promotor and good friend.

I am proud to be part of the dynamic group with such a pleasant working environment. The group is strong scientifically, but more importantly, everyone is so kind to each other. Thank you Karel, your enthusiasm about science inspires me a lot. Scientific discussions with you help me know more knowledge about moving load and ordinary talks with you encourage me to be a better person. I will not forget the misinterpretation about the relation between me and Hayo due to cultural difference. Hayo, thank you for making the parties end with so much fun. Chris and João, thank you for the joyous movie nights together and for sharing your programming skills, Kodo, thank you for driving me home many times after the group parties. My colleagues Yaxi, Maxim, Peter, Yue Song, Andrei Faragau, Pim, William, Eliz-Mari, Antonio, Marnix, Nikos, Dominik, Renate, Jeroen, Sergio, Alessandro, Mamin, Francesca, Valentina, Cody, Thanasis, Evangelos, Frank Renting, Frank Sliggers, Federico, Jiangyi, Ger, Timo, Tim, Faraz, André, Marco, Arvind, I appreciate the useful discussions and your sharing of knowledge. And the amusing group outings, the well organized Christmas dinners, the nice coffee breaks made an unforgettable memory in me. I would like to express my sincere gratitude to Anneke Meijer who was the section secretary of the group and always gave me immediate help. I wish that you are enjoying your retirement time. I also thank Marysa from offshore engineering and Jacqueline from railway engineering for their amazing support all these years.

Living in a completely different country would be tough without my wonderful compatriots. I would like to thank Yang and Mingjuan for great company for almost the whole journey of my PhD study. We are not just colleagues but also close friends who share joys and sadness. Weiwei, thank you for always being like a family member to me, listening to my complaints and giving me useful advice. I am amazed by your ability to deal with things and your ability to learn. Zilong, I forget how many times you helped me repair my bike and after repairing the bike it was not me to treat you a dinner but the opposite. So many memories about you and Yan are in my mind and a "thank you" is not enough. Kai, I am grateful for these coffee breaks we had together to encourage each other, talk about our future plans. Now you are in China but Shulan is here helping us a lot. Thank you both. Chenjie, many thanks for sharing your drone with me, playing games and watching these Marvel movies together. You let me know that life can have different colors. Daniel, I am glad that we were room mates and later became friends with common hobbies. I am thankful to Jincheng, a friend from the same University in Beijing. I would not be abroad to pursue a PhD degree without your encouragement. I would like to convey

my special thanks to Dr. Zhiwei Qian who always gives me valuable suggestions which makes my living in the Netherlands easier. I am lucky to know Xiaowei, Wuyuan, Feifei Wang, Xiaochen, Zhen Yang, Lin Xiao, Manxia, Yuewei, Lizuo, Tao Zou, Yu Sun, Likun Ma, Qi Wang, Peng Lu, Xu Ma, Haoyu Wang, Kai Zhang, Xiangming Liu, Chen Shen, Lei Xu, Pan Zhang, Yunlong Guo, Peng Wei, Wenjuan Lyu, Jinhu Wang, Xin Tian, Yue Zhao, Jian Fang, Tiantian Du, Jiayi Chen, Qujiang Lei, Ming Li, Xin Li, Shanshan Ren, Yixin Lyu, Bowei Huang, Zhebin Hu, Tianchi Tang, Fei Yan, Tianshi Lu. Thank you all for making my stay in the Netherlands enjoyable. I am thankful to Wuyuan, Cheng Yi, Shuai Tang, Huifang Lan, Jiao Chen, Yan Zhang, Xiaoka for the after-school actives for kids, for sharing experiences of raising the little ones.

I am very grateful to Sayeda and Zahid. Sayeda, our friendship started with being officemates but it did not end after your graduation. I am glad to know Zahid later on. You are such a nice couple. We learn from you how to be better parents and we know more about the Bengali culture. Thanks a lot for your hospitality as well. And many thanks to Zahid for designing the nice cover of this book. Deniz, although we had not been office mates for long, your and Seda's kindness made me feel so warm, like the warm wine we had in the city center in that cold winter. Samira, thank you for being such a wonderful office mate to share your knowledge and culture. Marina, thank you for arranging the karting. It was fun although I felt car sick during the racing. I would like to thank my work neighbours and friends Alieh, Anupam, Cor, Dr. Xueyan, Ruxing, Peng Lin, Yi Zhang, Hong Zhang, Rita, Yaolu, Mingzhao Zhuo, Zhaojie Sun in the neighbouring offices. Thanks for the talks, jokes and coffee breaks which drove away boring days. I thank Prashanth for inviting me to join these weekend beers which always marked a perfect ending of the busy week.

I would like to acknowledge the financial support of Chinese Scholarship Council (CSC). I thank Prof. Qingchao Wei from Beijing Jiaotong University (BJTU) for encouraging me to continue my study abroad. I am thankful to Prof. Qinghuai Liang and Dr. Haoye Wang from BJTU who helped me with the application of the scholarship. Many thanks to Prof. Jin Shi, Dr. Yangjie Wang and Dr. Meng Ma from BJTU, Dr. Qingjun Chen from South China University of Technology, Prof. Shiyu Wang from Tianjin University for the advice on my career. I am grateful to Prof. Zili Li from railway engineering group in TUD for his suggestions on research and giving me an useful book. I am thankful to my Post-doc supervisor Dr. Steenbergen for the valuable discussions, support and appreciation for the work. I thank Prof. Masami Ishikawa from Tohoku Gakuin University. It was a pleasure to discuss culture similarities and to visit the Japanese garden together.

I owe the biggest "Thank you" to my family. I thank my dear parents Shirong and Juying. Although thousands kilometres apart, I can always feel your endless and unconditional support. Pale words cannot express my gratitude for everything you have done for me. My dear sister Li, thank you so much for your care and for always believing in me. I deeply thank my mother-in-law Min Pu for the trust, support and care. And finally, Diye, I cannot thank you enough. Without your love, support and patience, I would never managed to go this far. Thank you for your enormous devotion to our family and for bringing me Shudi, which makes my life much more complete.

Tao LU
Delft, June 2019

CURRICULUM VITÆ

Tao LU

01-07-1987	Born in Sichuan, China.

EDUCATION

Sep. 2007–Jun. 2011	Bachelor in Civil Engineering Beijing Jiaotong University
Sep. 2011–Jun. 2012	Ph.D. candidate in Railway Engineering Beijing Jiaotong University
Sep. 2012–Nov. 2017	Ph.D. Research Delft University of Technology Faculty of Civil Engineering and Geosciences Dynamics of Solids and Structures
Dec. 2017–present	Post-doc researcher Railway Engineering Delft University of Technology

LIST OF PUBLICATIONS

JOURNAL ARTICLES

1. **T. Lu**, A. Tsouvalas, A.V. Metrikine, *The steady-state response of a rotating ring subjected to a stationary load*, under review.

2. M. Sadri, **T. Lu**, M. Steenbergen, *Railway track degradation: The contribution of a spatially variant support stiffness - Global variation*, Journal of Sound and Vibration, 114992 (2020).

3. M. Sadri, **T. Lu**, M. Steenbergen, *Railway track degradation: The contribution of a spatially variant support stiffness - Local variation*, Journal of Sound and Vibration **455**, 203 (2019).

4. **T. Lu**, A. Tsouvalas, A.V. Metrikine, *A high-order model for in-plane vibrations of rotating rings on elastic foundation*, Journal of Sound and Vibration **455**, 118 (2019).

5. **T. Lu**, A. Tsouvalas, A.V. Metrikine, *The in-plane free vibration of an elastically supported thin ring rotating at high speeds revisited*, Journal of Sound and Vibration **402**, 203 (2017).

CONFERENCE ARTICLES

1. **T. Lu**, M. Sadri, A. Zoeteman, M. Steenbergen, *Influences of the support stiffness non-uniformity on expected track degradation, The Sixteenth International Conference on Civil, Structural & Environmental Engineering Computing, Riva del Garda, Italy, 16-19 September 2019.*

2. **T. Lu**, A. Tsouvalas, A. Metrikine, *In-plane vibration of rotating rings using a high order theory*, MATEC Web of Conferences **211**, (2018).

3. M. Sadri, **T. Lu**, A. Zoeteman, M. Steenbergen, *Railway track design & degradation*, MATEC Web of Conferences **211**, (2018).

4. **T. Lu**, A.V. Metrikine, *Instability of an oscillator moving circumferentially along a thin ring on a viscoelastic foundation*, Procedia Engineering **199**, 2555 (2017).

5. **T. Lu**, A. Tsouvalas, A. Metrikine, *Stability of in-plane vibration of an elastically supported rotating thin ring, revisited, ISVCS11, 11th International Symposium on Vibrations of Continuous Systems, Royal Victoria Hotel, Llanberis, Snowdonia, Wales, UK, July 16-22, 2017.*

6. **T. Lu**, A. Metrikine, *On the existence of a critical speed of a rotating ring under a stationary point load, in: Proceedings of 43th International Summer School-Conference Advanced Problems in Mechanics (APM); St. Petersburg (Russia), 22-27 June 2015.*

7. **T. Lu**, A. Metrikine, *A rotating ring in contact with a stationary load as a model for a flexible train wheel. EURODYN 2014: Proceedings of the 9th International Conference on Structural Dynamics, Porto, Portugal, 30 June-2 July 2014.*